Stony Brook University

Untangling the interactions: Structural basis of nitric oxide regulated cyclic-di-GMP metabolism in bacteria

A Dissertation Presented

by

Tanaya Lahiri

to

The Graduate School

in Partial Fulfillment of the

Requirements

for the Degree of

Doctor of Philosophy

in

Chemistry

(Concentration – Chemical Biology)

Stony Brook University

December 2013

Stony Brook University

The Graduate School

Tanaya Lahiri

We, the dissertation committee for the above candidate for the

Doctor of Philosophy degree, hereby recommend

acceptance of this dissertation.

Elizabeth M. Boon, PhD – Dissertation Advisor
Associate Professor, Department of Chemistry

Peter J. Tonge, PhD - Chairperson of Defense
Professor, Department of Chemistry

Robert C. Rizzo, PhD – Third Committee Member of Defense
Associate Professor, Department of Applied Mathematics and Statistics

David G. Thanassi, PhD – Outside Committee Member of Defense
Professor, Department of Molecular Genetics and Microbiology

This dissertation is accepted by the Graduate School

Charles Taber
Dean of the Graduate School

Abstract of the Dissertation

Untangling the interactions: Structural basis of nitric oxide regulated cyclic-di-GMP metabolism in bacteria

by

Tanaya Lahiri

Doctor of Philosophy

in

Chemistry

(Concentration – Chemical Biology)

Stony Brook University

2013

Bacteria use numerous small molecules for cellular signaling. These primary and secondary messengers act within the cell to relay signal transduction and regulate distinct pathways. Among these the diatomic gas molecule nitric oxide (NO) and the nucleotide cyclic-di-GMP play central role in virulence, quorum sensing, and biofilm formation. In this dissertation, we have focused on the H–NOX (heme–nitric oxide/oxygen binding) protein in the biofilm–dwelling bacterium *Shewanella woodyi (Sw)*, which mediates NO-induced biofilm dispersal by modulating the activity of a dual–functioning diguanylate cyclase/phosphodiesterase enzyme that we have named HaCE, (H-NOX–associated cyclic-di-GMP enzyme). These enzymes tightly regulate the intracellular spatio-temporal concentrations of cyclic-di-GMP which is synthesized from 2 molecules of GTP by enzymes called Diguanylate Cyclases (DGC), and gets

hydrolyzed to pGpG by enzymes called Phosphodiesterases (PDE), in turn controlling biofilm formation. Thus, H-NOX/HaCE represents a potential drug target for regulating biofilm formation. This is the first biophysical and structural study of an NO–bound *Sw*H-NOX/*Sw*HaCE complex. We have shown that *Sw*H-NOX/*Sw*HaCE associate in a $\alpha_2\beta_2$ (heterotetramer) stoichiometry. The *Sw*H-NOX surface residues critical for binding to *Sw*HaCE have been identified using NMR studies. Fluorescent quenching binding studies, co-immunoprecipitation and enzyme assays confirm this protein-protein interface and its importance for H-NOX/HaCE function.

Also described is the role of charged residues that are required for substrate binding and divalent metal ion coordination in the hydrolysis of cyclic-di-GMP by PDE domains found in bi-functional enzymes with an N-terminal DGC domain. Previously published crystal structures of active PDE enzymes indicate a TIM-barrel type of fold for the catalytic domain. The catalytic pocket, situated towards the C-terminus, contains an unstructured loop, called “loop 6”, which is conserved in this family of enzymes. In this work, the role of these conserved residues has been elucidated using mutational studies combined with biophysical studies and enzymatic analysis to show how structure affects enzyme function.

Dedication Page

This thesis is dedicated to my parents;

Father, Late Mr. Tarun Kumar Lahiri, and Mother, Mrs. Ivanova Lahiri.

Hope he is watching me from the stars above, and is proud of me.

Thank you for everything.

Table of Contents

List of Figures/Tables/Illustrations

List of Abbreviations

5'–pGpG	5'→3' phosphoguanylyl phosphate
AUC	Analytical ultra centrifugation
BDSF	*Burkholderia* diffusible signal factor, cis-2-dodecenoic acid
BME	B Mercapto ethanol
CD	Circular dichroism
CSP	Chemical shift perturbation
Cyclic-di-GMP	Cyclic diguanosine monophosphate
DGC	Diguanylate cyclase
DSF	Diffusible signal factor, cis-2-decenoic acid
EAL	Phosphodiesterase motif
FPLC	Fast pressure liquid chromatography
GGDEF	Diguanylate cyclase motif
GTP	Guanosine triphosphate
H-NOX	Heme nitric oxide/oxygen binding domain
HaCE	H-NOX associated cyclic-di-GMP processing enzymes
HPLC	High pressure liquid chromatography
ITC	Isothermal titration calorimetry
MG	Malachite green
NMR	Nuclear magnetic resonance
NO	Nitric oxide
PAS	Per/Ant/Sim

PDE	Phosphodiesterase
PMSF	p-methyl sulfonyl fluoride
PPI	Protein-protein interactions
REC	Receiver domain
SAXS	Small angle x-ray scattering
SEC	Size exclusion chromatography
TBAOH	Tetra butyl ammonium hydroxide
$\alpha_2\beta_2$	Heterotetramer protein complex

Acknowledgments

-- ॐ --

ज्ञानशक्तिसमारूढः तत्त्वमालाविभूषितः ।
भुक्तिमुक्तिप्रदाता च तस्मै श्रीगुरवे नमः ॥

dnyaanashaktisamsasuuDhaH tattvamaalavibhuuShitaH
bhuktimuktipradaataa cha tasmai shriigurave namaH

Salutation to that noble Guru, who is established in the power of knowledge, adorned with the garland of various principles and is the bestower of prospority and liberation.

-- ॐ --

I would like to first and foremost thank, the Almighty, who made everything possible, who gave me strength and determination to be where I am today.

I would like to thank my advisor, Prof. Elizabeth M. Boon, who has been a guru and a mentor, guiding me through the path of scientific curiosity. She has been patient with my scientific naivety, letting me learn through my mistakes, and always being there to hold my hand when needed. I am grateful for the scientific independence she granted me to make informed choices and decisions, helping me grow as a scientist, while always pushing me to do my best.

I would also like to thank my committee, Prof. Peter Tonge and Prof. Robert Rizzo, for the scientific discussions and valuable advice. I would also like to thank my outside member, Prof. David Thanassi, for being part of my committee.

I would like to thank my collaborators, Bowu Luan and Prof Daniel P. Raleigh, who have been extremely supportive and generous with the scientific discussions, experiments, and data analysis.

I am grateful to the NYSBC facility, especially the scientists, Dr. Kaushik Dutta and Dr. Shibani Bhattacharya, who have taught me everything about experimental NMR, and provided invaluable advice.

I am grateful to Prof. Johnson for the delightful conversation, scientific inputs and suggestions for science and life.

I would like to thank Dr. Sandhya and Dr. Natasha for watching over, and pulling me through whenever I felt lost. They have been immensely supportive as colleagues and friends, teaching me to see the big picture, and never be disappointed.

I would like to thank all the past and present Boon lab members, who have been brilliant colleagues and friends. All of them have helped me grow up and mature as a person and as a scientist as part of the group. I would also like to thank the Carrico lab (past and present lab members), as I have found great friends in this lab across the hall.

I would like to pay my gratitude to my parents, my father, Late Mr. Tarun Kumar Lahiri, and my mother, Mrs. Ivanova Lahiri. I owe them everything for who I am today. Their biggest gift to me was the ability to dream. It is this dream that I fulfill today, and I hope they are proud.

I would like to thank Ashish, for being there. You have, with your calm and collect, helped me deal with situations, and are a wonderful companion.

Friends are a very important part of my existence, and there are many faces behind this thesis, Divneet for her patient ears, Dr. Partha, a great friend and mentor, Sreyoshi, for her balance approach towards life, Saathyaki & Sujatha, for the wonderful vacations, Dr. Debasis, forever reminding me to be competitive and ambitious, Dr. Dhruv and Yueming for the coffee breaks, Dr. Lakshmi for making me laugh so hard I cried, Dr. Avik & Dr. Anindita for teaching me how to snowshoe on a snowy mountain, Shivam, Aradhana, Deblina, Divya, Soumya, Dr. Kunal and so many other names. Thank you all for being patient with my crazy talk, my quirkiness and just making me happy.

Thank you to Katherine, Charmine and all the main office staff for being so nice and patient with my endless queries.

Vita, Publications and/or Fields of Study

1. Structural basis of the regulation of *Sw*HaCE by NO-bound *Sw*H-NOX. *Tanaya Lahiri, Bowu Luan, Daniel P. Raleigh and Elizabeth M. Boon* (submitted, Biochemistry, 2013)

2. Structural-function studies of the catalytic residues and loop6 from the PDE domain of a bi-functional enzyme *Sw*HaCE. *Tanaya Lahiri, Natasha M. Nesbitt and Elizabeth M. Boon* (2013), *in preparation.*

3. Investigating the synergistic role of NO and DSF as biofilm dispersal agents. *Tanaya Lahiri, Dhruv P. Arora and Elizabeth M. Boon; in preparation.*

4. SAXS and co-immunoprecipitation studies reveal domain–domain contacts in the bi-functional enzyme *Sw*HaCE. *Sajjad Hossain, Patrick Zelinsky, Tanaya Lahiri, Bowu Luan, Daniel P. Raleigh and Elizabeth M. Boon; in preparation.*

CHAPTER 1: INTRODUCTION

1.1 Signaling in bacteria via protein-protein interactions and role of gasotransmitters

Signaling networks in all organisms are composed of modular proteins that function in a cohesive, signal-dependent manner. At the molecular level, this behavior can include conformational changes, interactions with other modular units, change in enzyme function and changes at the genomic level. In other words, signal transduction relays can reflect at the transcriptional, translational as well as post-translational level. Gas molecules have been known to play important roles as signaling molecules in both mammals and bacteria. Nitric oxide (NO) signaling is well established in mammals, where it plays functional roles in physiological processes such as vasodilation, smooth muscle relaxation and neuronal signaling[1]. Soluble guanylyl cyclase (sGC) is the only known mammalian sensor of NO, with biochemical studies showing that the alpha-subunit of sGC binds NO at picomolar concentrations[2].

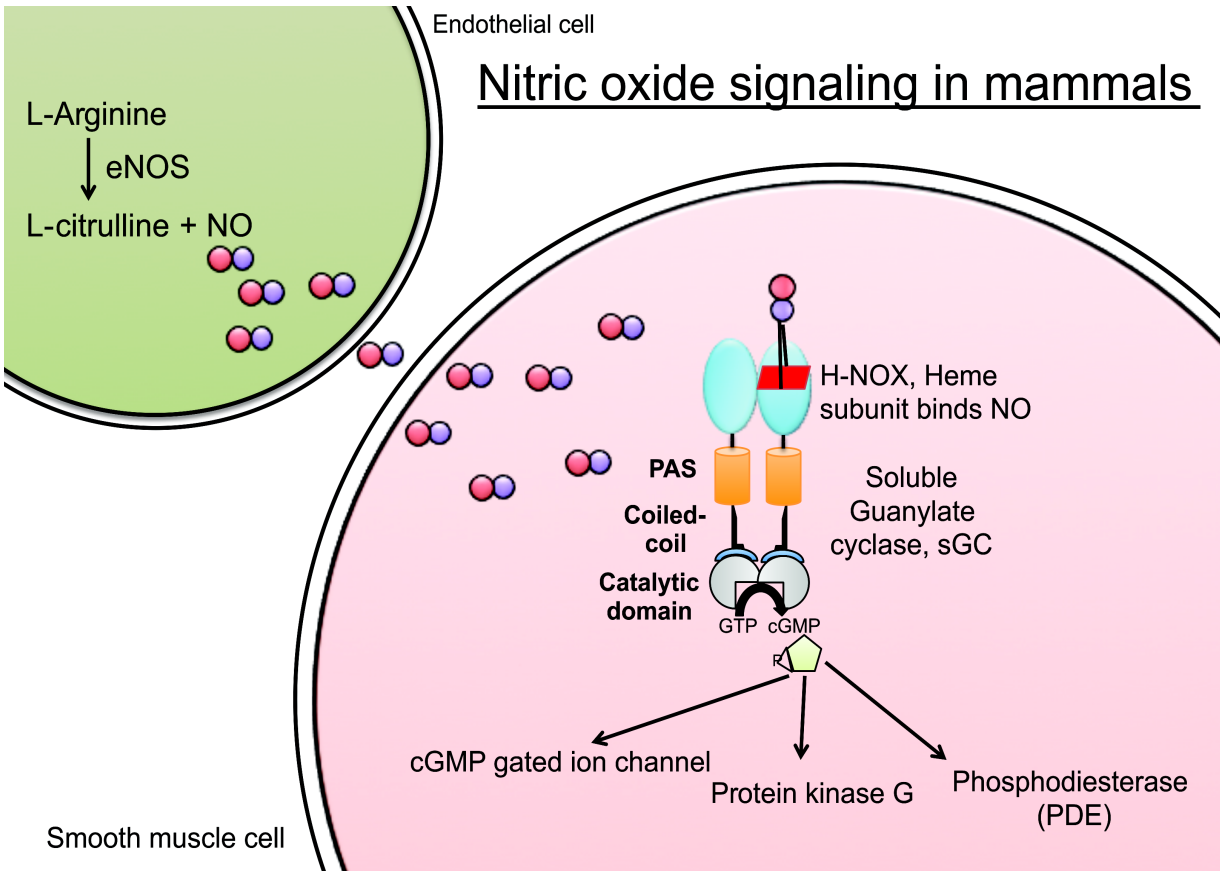

Figure 1-1: Schematic of NO production and diffusion in mammalian cells. NO synthesized by endothelial NOS diffuses out to neighboring cells, where it can bind to the mammalian NO sensor, sGC, which has a heme subunit in the β subunit.

sGC contains 4 domains in each monomeric subunit (α, β) – HNOB domain (heme nitric oxide binding), PAS domain (Per/Art/Sim), CC domain (coiled-coil) and catalytic cyclase domain (catalyzes cyclization of GTP to cGMP). The HNOB domain in the β subunit binds a heme (heme B) cofactor, known as H-NOX (heme nitric oxide/oxygen binding domain); this can bind gas molecules (NO, CO, O_2) as ligands[2]. The α and β monomer subunits function as heterodimers to catalyze the cyclization of GTP to cGMP, an intracellular secondary messenger molecule in mammals. NO-binding to the β heme subunit results in an upregulation in the activity of the cyclase domain, which is mediated via interactions through the coiled-coil domain and the PAS domain[3, 4] (fig 1-1).

Interestingly, homologs of the N-terminal heme containing H-NOX domain that binds NO were found in bacterial genomes[5, 6]. Since then, many bacterial genomes have been characterized and found to encode an H-NOX gene, often as a stand-alone protein or fused to output domains (fig 1-2).

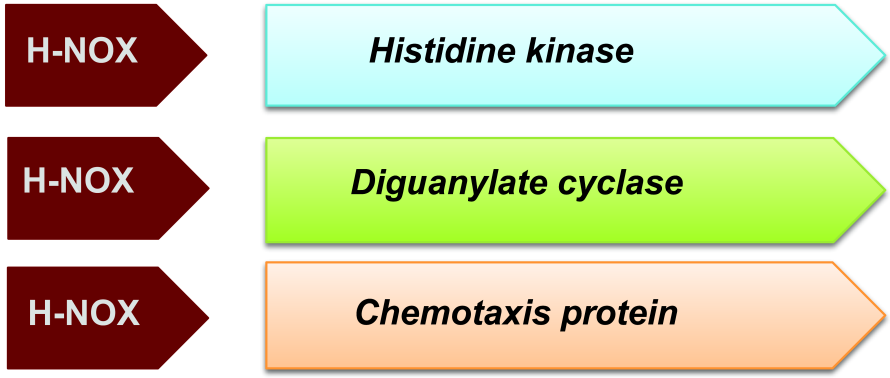

Figure 1-2: Genomic arrangement of bacterial H-NOX domains. Many H-NOX proteins are co-cistronic with enzymes such as diguanylate cyclases, phosphodiesterases, histidine kinases and response regulators.

1.2 Bacterial H-NOX and association with co-cistronic enzymes

Many bacterial genomes have annotated genes encoding the H-NOX domain containing protein[6]. This domain, which senses NO in mammals, was predicted to have a similar function in bacteria. The characterized bacterial H-NOX proteins (*Thermoanaerobacter tengcogenesis (Tt), Nostoc sp.*) show high sequence and structural similarity with the mammalian member, which is part of sGC. The predicted heme-binding pocket containing histidine and proline as the distal and axial ligands, respectively, is conserved in the bacterial H-NOXs (fig 1-3).

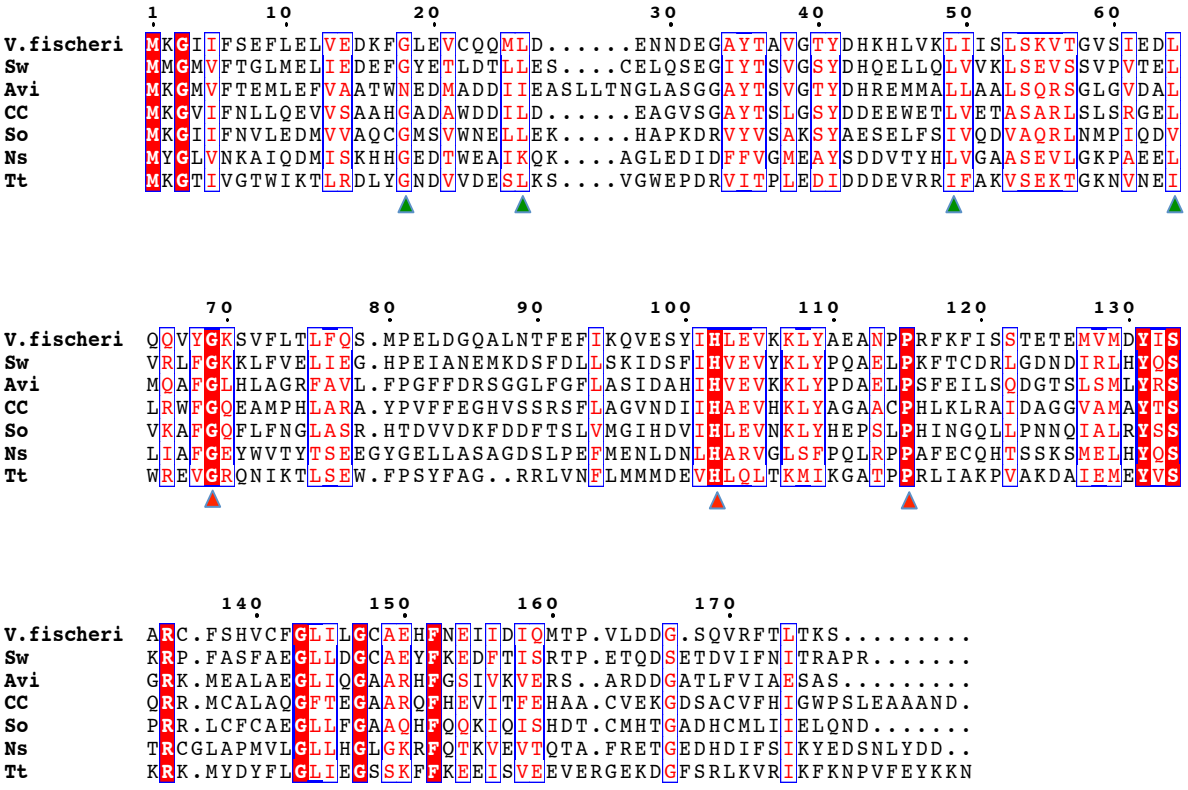

Figure 1-3: Sequence alignment of bacterial H-NOX domain containing proteins to identify conserved residues. The H-NOX proteins used for alignment are: *Vibrio fischeri, Shewanella woodyi, Agrobacterium vitis, Caulobacter cresentus, Shewanella oneidensis, Nostoc species, Thermoanaerobacter tengcogensis.* The green triangles represent residues that are required for certain folds and are part of the heme pocket but are not absolutely conserved. The red triangles represent residues that form the heme pocket and are required for heme binding.

Bacterial H-NOX domains have also been shown to bind various gas ligands - O_2, NO and CO[5]. Certain bacterial H-NOX proteins that bind both O_2 and NO, like *Tt*H-NOX, contain a tyrosine that can provide additional hydrogen binding in the heme pocket for O_2 binding[5]. However, H-NOX binds NO most sensitively and specifically while discriminating against other ligands; this further defines its role as a sensitive and specific NO sensor (fig 1-4, 1-5).

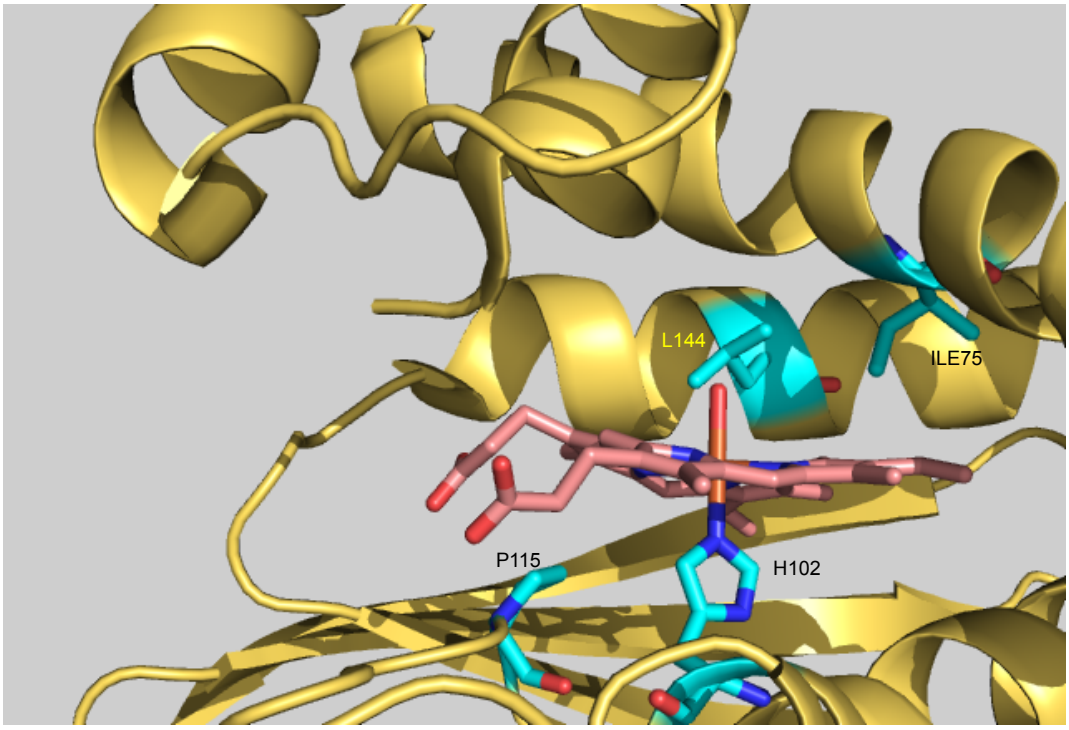

Figure 1-4: Close-up of the O_2-bound heme pocket from *Tt* H-NOX. The ligand binding residues are highlighted: L144, H102 and P115.

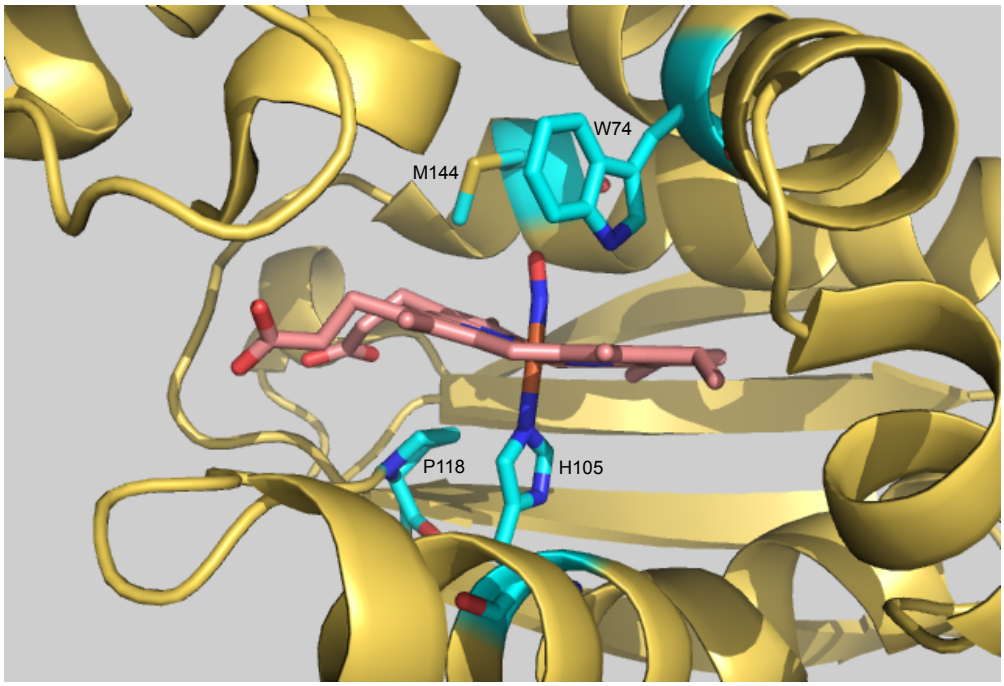

Figure 1-5: Close-up of the NO-bound heme pocket from *Nostoc* H-NOX. The ligand binding residues are highlighted: W74, M144, H105 and P118 (adapted from Ma *et al[7].*).

In bacterial genomes, H-NOX domain containing proteins are often found in the same operon as other enzymes – such as histidine kinases, diguanylate cyclases and phosphodiesterases[8]. These enzymes participate in various signal - regulated pathways such as two-component signaling, biofilm formation and virulence. This co-cistronic arrangement hints towards the possible regulation of such enzymes via NO-sensing, as these enzymes could be associating with NO-bound H-NOX to regulate various pathways (fig 1-6). These include two-component systems, where NO-bound H-NOX regulates the activity of a histidine kinase[9-11]. This further affects the phosphorelay downstream to a response regulator, which may be involved in transcriptional regulation. NO-bound H-NOX can also associate with enzymes called diguanylate cyclases (DGC)/phosphodiesterases (PDE) that are collectively called H-NOX associated cyclic-di-GMP processing enzymes (HaCE). These enzymes are involved in the synthesis/degradation of a small messenger molecule cyclic-di-GMP, which participates in multiple metabolic pathways[12, 13]. NO-bound H-NOX can modulate enzymatic activity to regulate the intracellular concentration of this metabolite, thus directly influencing *in-vivo* signal relay. Recently, NO-bound H-NOX has also been shown to impact bacterial group behavior, which is imperative to quorum sensing and biofilm formation[14-16].

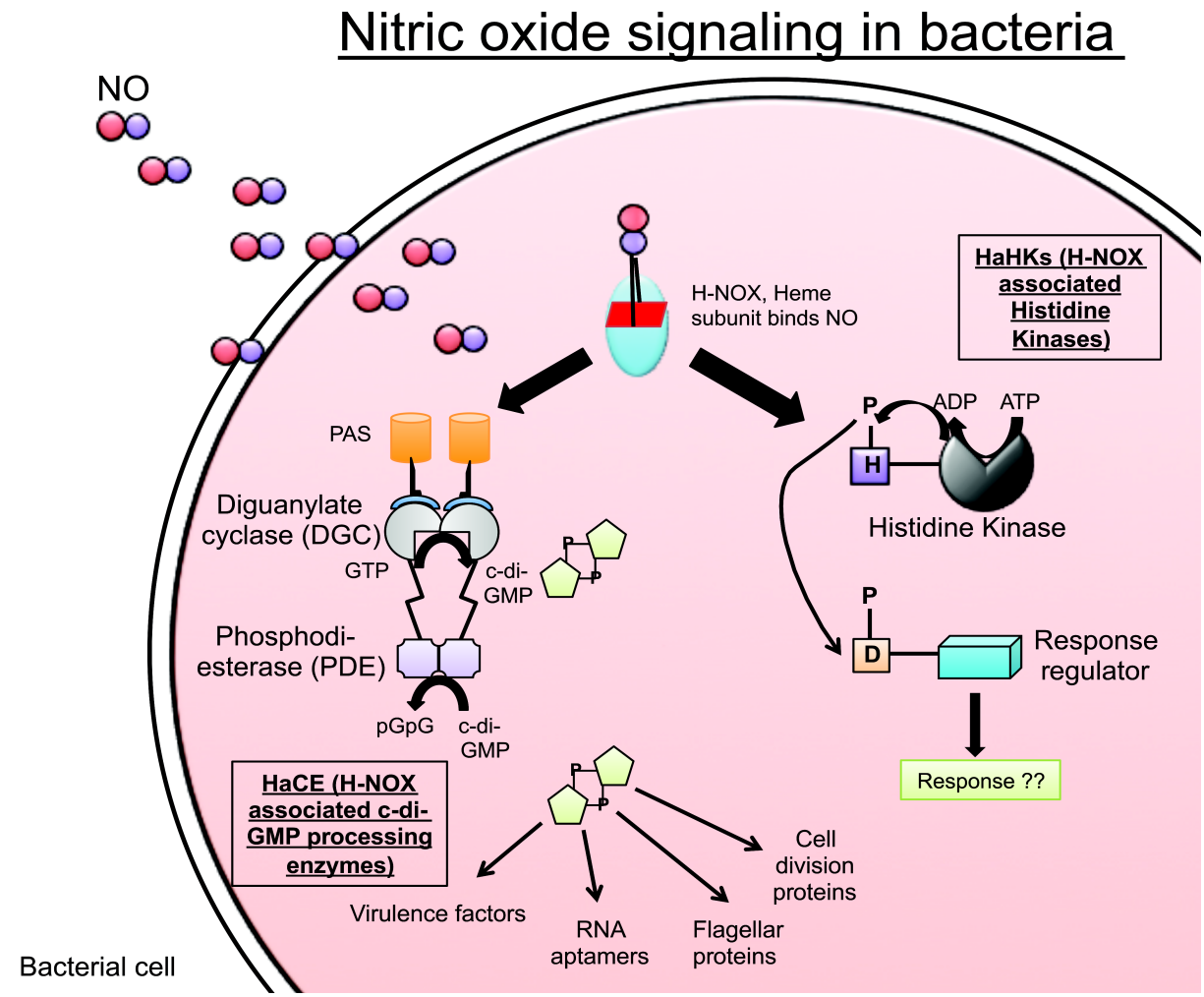

Figure 1-6: NO sensing in bacteria. Exogenous NO diffuses through outer membrane and binds to the bacterial NO sensor, which is a homologue of the N-terminal HNOB heme-bound subunit of sGC. The NO-bound H-NOX can further affect functional proteins.

1.3 Signal regulated group behavior in bacteria

Bacteria display amazing adaptive abilities by probing their environment and reacting accordingly by making subtle or distinct changes to their lifestyle. Some of the traits of these lifestyles are planktonic, free-swimming state, where the cells can glide freely across surfaces in pursuit of nutrients[17, 18]. This is very distinct from the surface-adhered state prevalent in a biofilm, where the cells accumulate together to form a macrocolony engulfed in a layer of matrix

consisting of polysaccharides, extracellular DNA and proteins (fig 1-7). Biofilm formation offers an evolutionary advantage in terms of protection, camouflage and symbiosis[19], and there are definite pathways that regulate these changes. Specific signals help to gather the “quorum” – composed of a group of bacteria, which can then start the attachment process and then mature into a macrocolony.

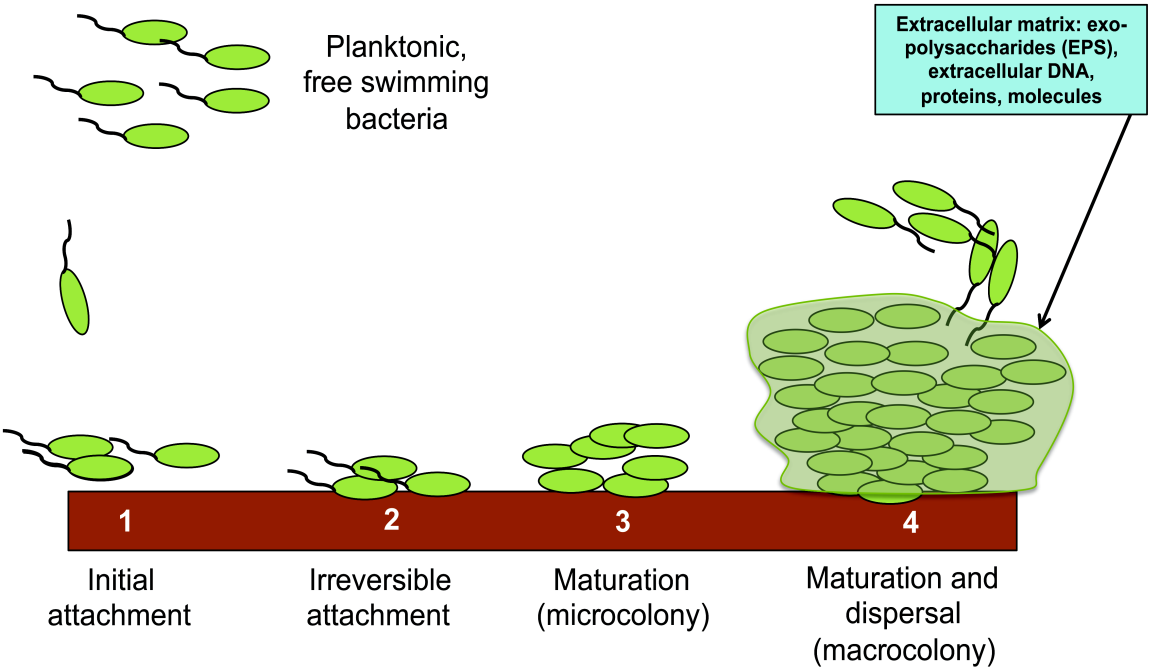

Figure 1-7: A biofilm consists of bacterial colonies engulfed in a polysaccharide matrix attached to a surface. The initial attachment to a surface is followed by irreversible attachment, when the bacteria start losing their flagella. Next, the cells accumulate to form a microcolony, which matures into a macrocolony, surrounded by a polysaccharide matrix. Often, a few cells in the biofilm can regain their flagella to exit the biofilm and recolonize on a different surface.

Several bacteria are responsive to environmental signals that either promote or disperse biofilm by regulating secondary pathways[17]. Recent literature provides evidence for the emergence of NO as a dispersal agent of bacterial biofilms[20-22]. Several studies show that exposure to low nanomolar concentrations of NO causes detachment and release of bacteria from surfaces. This has often been correlated to change in secondary messenger concentration, cyclic-di-GMP (c-di-GMP) within the cell via modulation of the DGC/PDE activity[23-27] (fig 1-8).

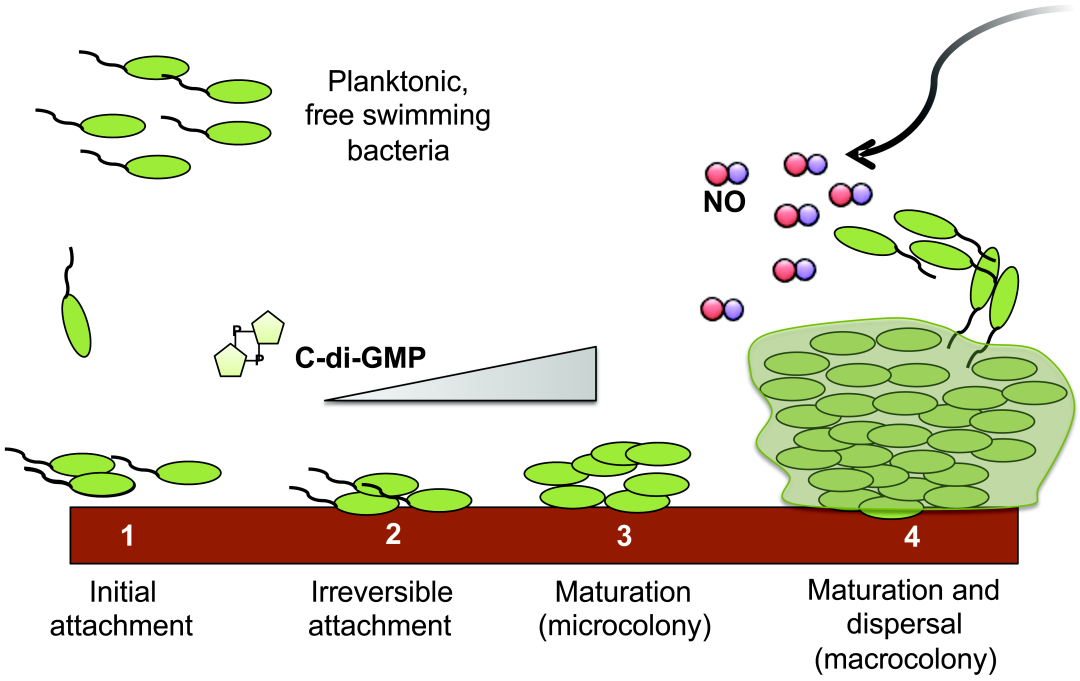

Figure 1-8: Small molecules like exogenous NO and intracellular cyclic-di-GMP play regulatory roles in biofilm formation. Increased levels of cyclic-di-GMP are associated with increased biofilm, whereas NO has been shown to initiate dispersal.

Studies from our lab and other labs examine the role of NO in biofilm dispersal, which includes microbiology studies and identification of proteins that contribute to this pathway. In *Shewanella woodyi (Liu et. al.),* NO was shown to decrease cyclic-di-GMP concentrations by modulating the activity of an H-NOX associated bi-functional enzyme HaCE (H-NOX associated cyclic-di-GMP processing enzymes). Increased PDE activity leading to lower intracellular cyclic-di-GMP levels was correlated with reduced biofilm formation. Also, biofilm formation in Δ*hnox* and Δ*hace* strains were shown to be unaffected by NO, confirming the role of NO/H-NOX/HaCE in this bacteria.

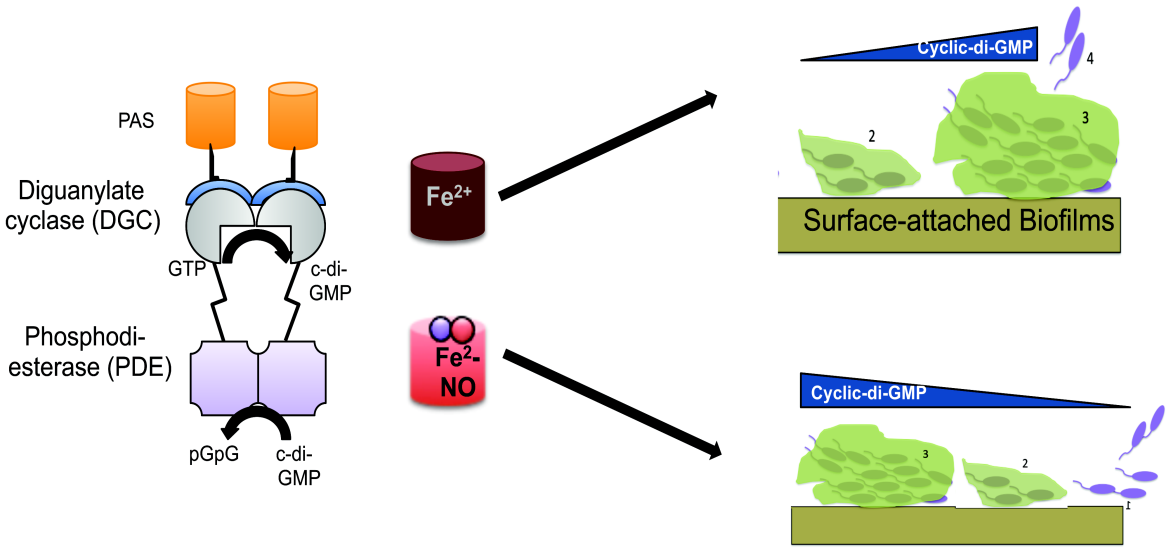

Figure 1-9: In *Shewanella woodyi,* Fe(II)-unligated H-NOX upregulates the diguanylate cyclase activity of *Sw*HaCE, causing an increase in the intracellular cyclic-di-GMP levels and increased biofilm formation. NO-bound H-NOX increases the phosphodiesterase activity of *Sw*HaCE, decreasing cyclic-di-GMP levels in the bacteria, leading to decreased biofilm formation.

1.4 HaCE proteins in bacteria: importance and role in signal transduction

Over recent years cyclic-di-GMP has been implicated in various signal transduction pathways such as virulence, quorum sensing, biofilm formation and flagellar motor movement. Often, a primary environmental stimulus causes a change in the intracellular concentration of cyclic-di-GMP[28]. Many receptor proteins are sensitive to this flux of c-di-GMP and respond by (a) altering gene expression - silence transcription of polysaccharide genes (*pel* and *psl)[24, 29]*, (b) inhibit flagellar motor assembly[30, 31] and (c) activate virulence genes[32-34]. Together, this is part of a multi-layer signaling relay that initiates cellular response (fig 1-10).

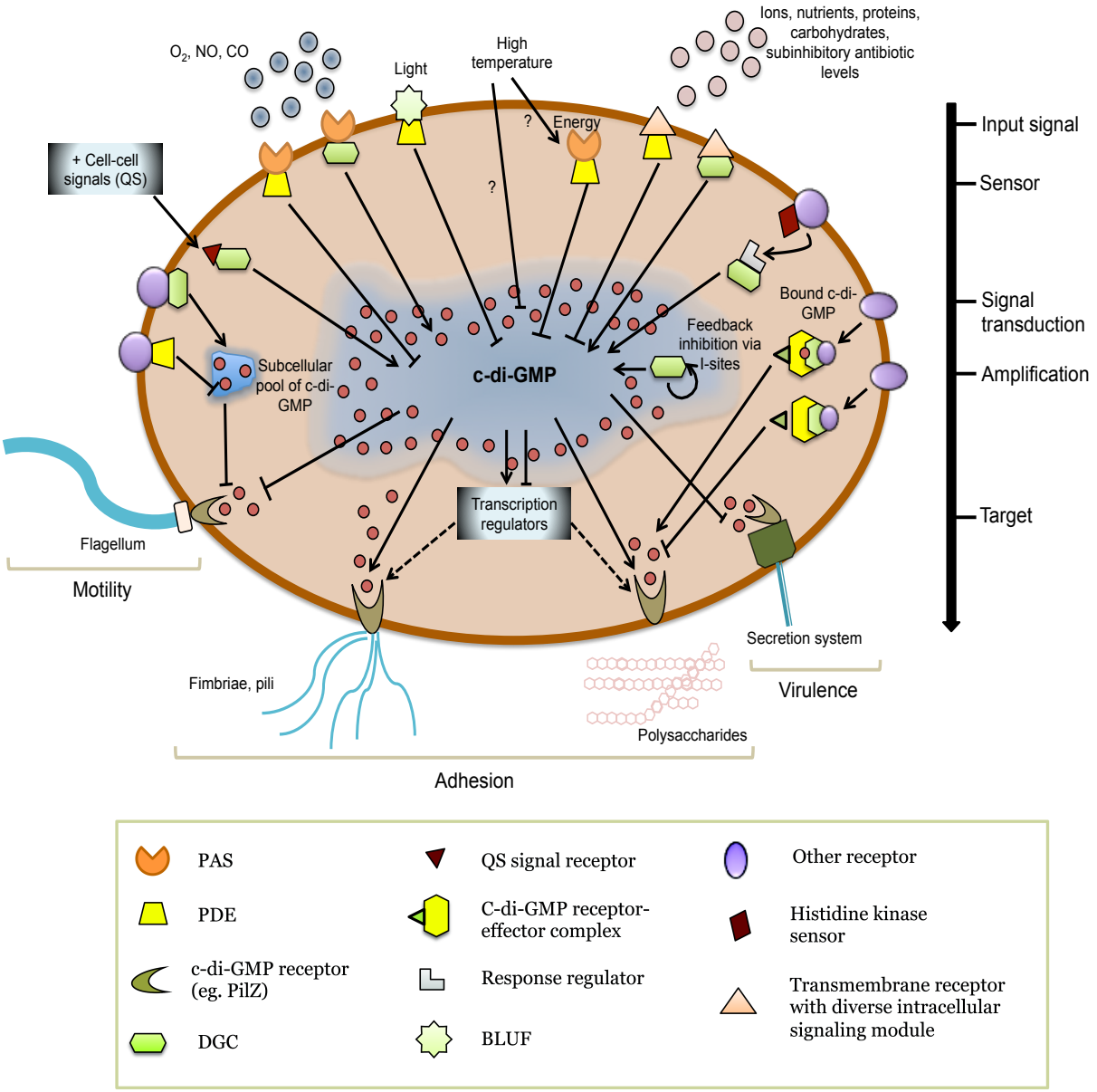

Figure 1-10: Multi-level signaling cascade regulated by cyclic-di-GMP (adapted from review by Hengge, R.[35]).

There are mainly 2 classes of enzymes that control the concentration of c-di-GMP in the cell – diguanylate cyclases (DGCs) and phosphodiesterases (PDEs). DGCs or GGDEF-motif containing domains synthesize one molecule of c-di-GMP from 2 molecules of GTP, and produce 2 molecules of inorganic pyrophosphate (PP_i) as a side product (fig 1-11).

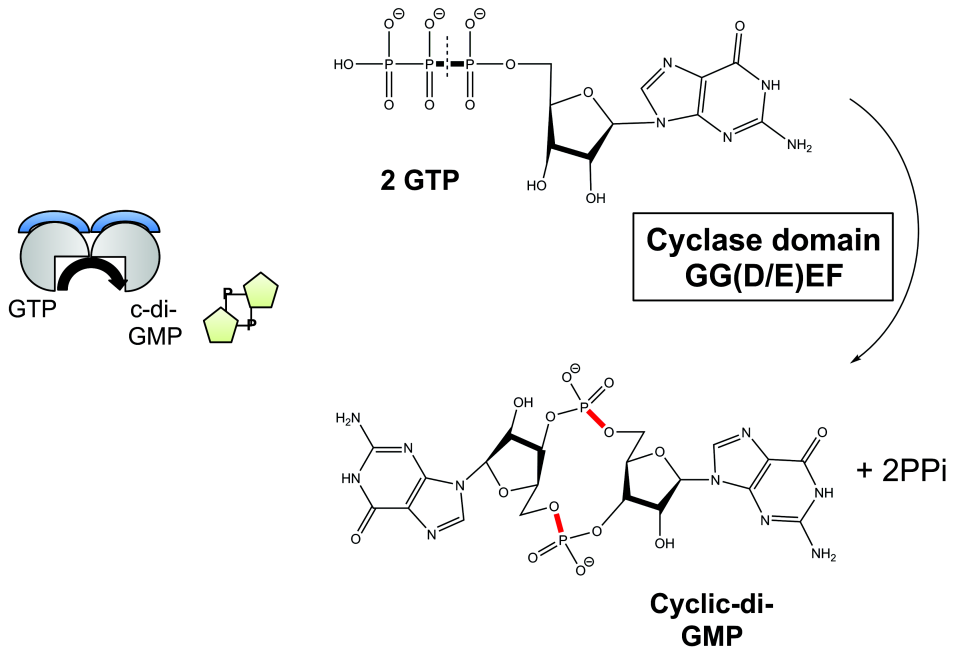

Figure 1-11: Reaction scheme for synthesis of cyclic diguanylate phosphate from 2 molecules of GTP by diguanylate cyclase domains. The bond being made is indicated in red.

PDEs or ExL-motif containing domains hydrolyze c-di-GMP to the linear pGpG (fig1-12).

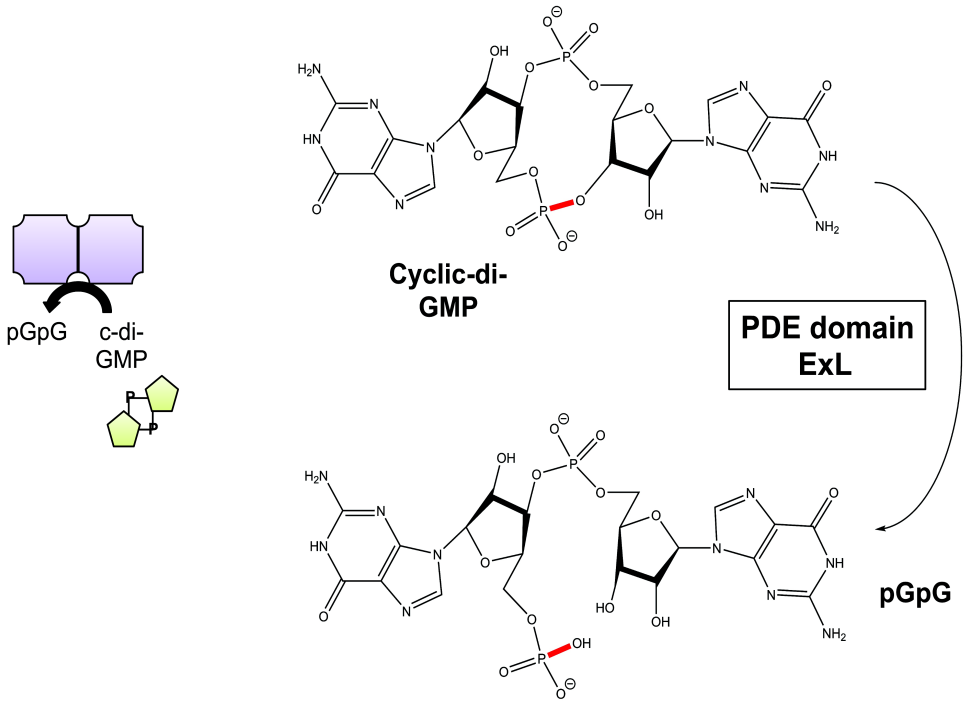

Figure 1-12: Reaction scheme for hydrolysis of cyclic diguanylate phosphate to pGpG by phosphodiesterase domains. The bond being broken is indicated in red.
Other domains, called HD-GYPs, hydrolyze c-di-GMP to pGpG and ultimately to GMP.

Other than these enzymes, some receptors with novel c-di-GMP binding folds have been identified – PilZ, degenerate GGDEF and EAL-containing domains (FimX) and RNA aptamers[36]. These receptors sequester c-di-GMP within the cell, and, together with these enzymes, maintain the spatio-temporal distribution of c-di-GMP within the cell.

It has been recently discovered that bacterial genomes encode multiple copies of GGDEF and EAL domain containing proteins[6]. This genomic distribution hints towards a flux of c-di-GMP concentration rather than a steady state concentration. Bioinformatics analyses show that several of these enzymes contain a regulatory domain – heme-bound PAS, light sensing domain BLUF, oxygen sensing heme-bound domain, NO sensing H-NOX domain and phosphate sensing transmembrane domains[37]. Although most of these regulatory domains have been shown to regulate the activity of the enzymatic domains in a signal-dependent manner, causing phenotypic changes in the cell, the molecular mechanism of signal transduction is still being established.

1.5 Enzymatic regulation of other GGDEF-EAL proteins during signal transduction

Published crystal structures for several characterized GGDEF and EAL domains provide an insight into the mechanism of catalytic activity. The diguanylate cyclase from *P. fluorescens*, WspR, has been well characterized. The N-terminal of WspR has a REC domain that is phosphorylated by a kinase, causing distinct conformation and oligomerization changes in the protein to affect the cyclase activity[38, 39]. In another diguanylate cyclase containing response regulator protein, PleD, it was shown that phosphorylation affects cyclase activity by long-range conformational perturbations[40, 41]. Similar signal induced enzymatic activity studies have also been undertaken for PDE domains. For a BluF domain associated PDE domain, it was shown

that blue light sensed by the BluF domain induced structural changes in the phosphodiesterase domain to affect enzymatic activity[42, 43]. This enzymatic activity was further implicated in phenotypic change in *Acenitobacter baumanii*, where it was shown that blue light regulates biofilm formation. However, the various factors that control the activity of these enzymes are still being identified. Even more intriguing is the presence of multiple proteins encoding GGDEF-ExL di-domain protein. Preliminary studies have indicated that this could be part of a product inhibition regulatory loop to check the activities of individual enzymatic domains. A study of one such bi-functional enzyme showed that higher concentrations of GTP, the substrate for the cyclase domain, enforced allosteric control on the phosphodiesterase activity of the enzyme[44]. These detailed enzymatic analyses indicate a rigorous and stringent mechanism to synchronize the hydrolysis and synthesis of cyclic-di-GMP within the cell, creating subcellular pools for specific functions.

1.6 Signal transfer via heme distortion and ligand binding in H-NOX proteins

Crystal structures of H-NOX in both Fe(II) unligated form, Fe(II)-NO bound form and the Fe(II)-CO bound form indicate substantial shifts in the protein conformation as a function of ligand binding[45]. In the sGC and other bacterial H-NOX domains, it has been established that upon binding NO, the distal histidine ligand disassociates to form a 5-coordinate complex (fig1-13).

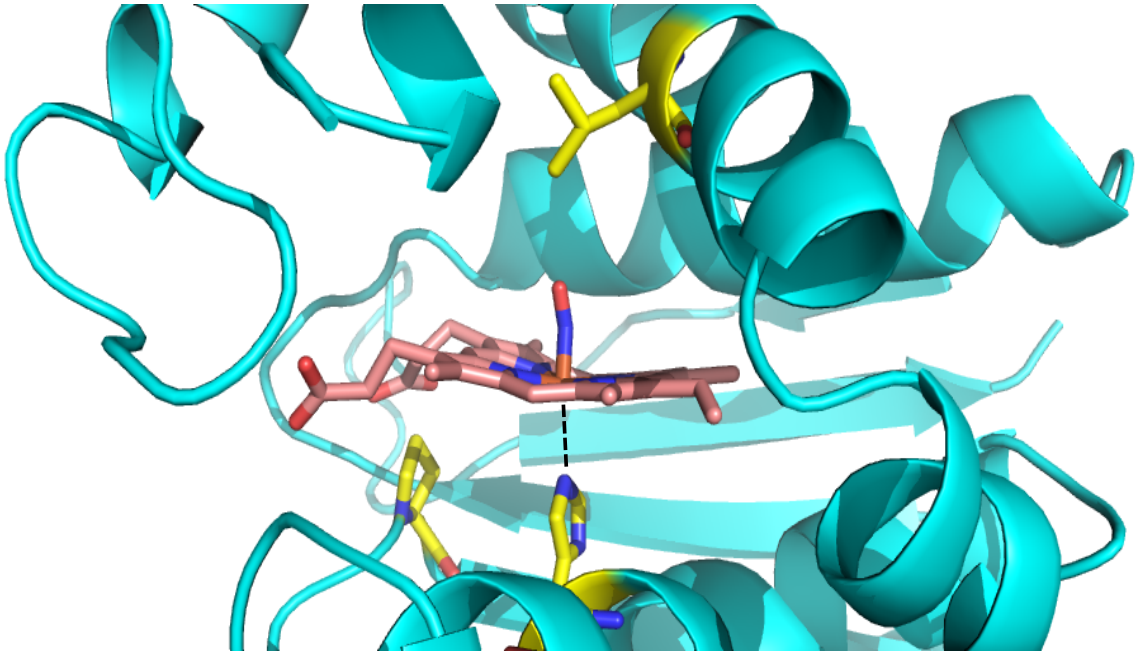

Figure 1-13: NO-bound heme from Ns H-NOX; the disassociated His-heme bind is shown as broken lines.

It has been shown that the disassociation of histidine causes long-range conformational changes to affect the cyclase activity of sGC. In a recent study[4], Underbakke *et al.* have mapped the interactions between individual domains of sGC to determine the path of signal transfer, starting from binding of NO to the sGC H-NOX, leading to the enhanced activation of the cyclase domain. The model described involves direct interactions between the sGC PAS and H-NOX domain upon NO-binding that translate into long distance perturbations. Some of these interaction surfaces include the N-terminal helices (aB-aC) of the H-NOX domain.

Crystal structures of NO-bound H-NOX show the heme to be highly distorted, corresponding to the activated state of sGC. This distortion is accompanied by conformational shifts in the N-terminal helical region of H-NOX. Similar studies have been done in bacterial H-NOX proteins[45], where NO was shown to cause heme bending and rotational shift in N-terminal helices. CO–binding caused similar heme pivoting and bending, but with less shift in N-terminal

helices. The general hypothesis is that signal-binding event (NO) is transduced via these perturbations at the N-terminal helices, which can interact with output domains and modulate their function by protein-protein interactions. This completes the signal relay to affect a cellular function.

1.7 Hypothesis and Overview of projects undertaken in this dissertation.

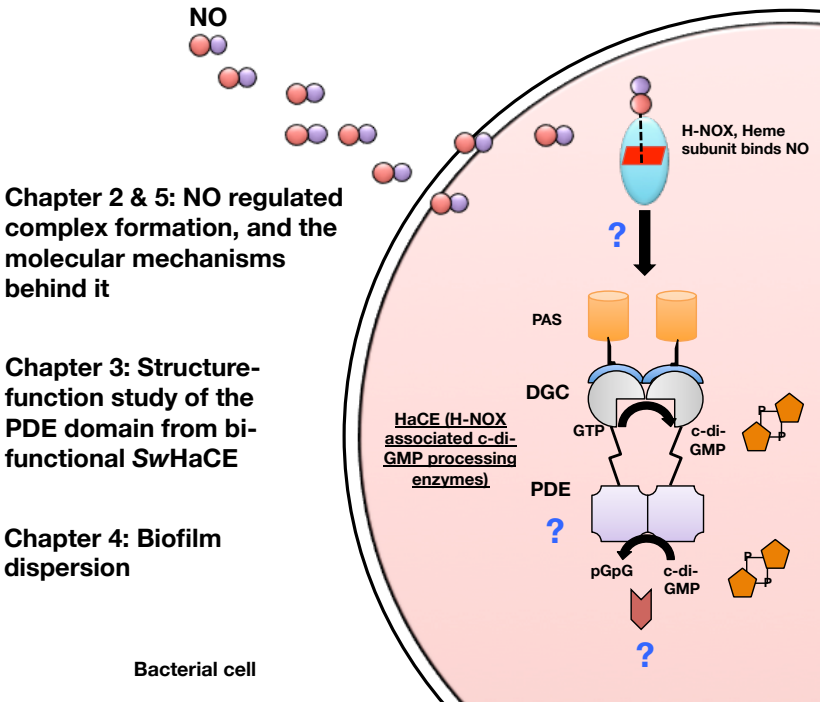

Figure 1-14: Overview of projects and system undertaken in this thesis.

In chapter 2, we have determined the molecular basis of NO-regulated *Sw*H-NOX/*Sw*HaCE protein - protein interaction. Our lab has previously shown that depending on the ligation state, *Sw*H-NOX differentially regulates the diguanylate cyclase and phosphodiesterase activity of the bi-functional enzyme *Sw*HaCE. The NO-dependent regulation of this bi-functional enzyme leads to a decrease in intracellular cyclic-di-GMP concentrations, causing biofilm dispersal. Thus, this

protein complex regulates biofilm dispersal in *Shewanella woodyi* through an NO-dependent mechanism.

In this work, we have elucidated the interaction surface of the *Sw*H-NOX/*Sw*HaCE protein complex, determined the oligomeric state and identify the role of binding surface in the enzymatic regulation of *Sw*HaCE activity.

The *Sw*H-NOX shares significant homology with other characterized bacterial H-NOX and the mammalian sGC H-NOX domain. A homology model generated by structural alignment indicates that the fold is similar to the one observed for other H-NOX protein structures, and the essential heme binding residues (H104, P115) are conserved (fig 1-14).

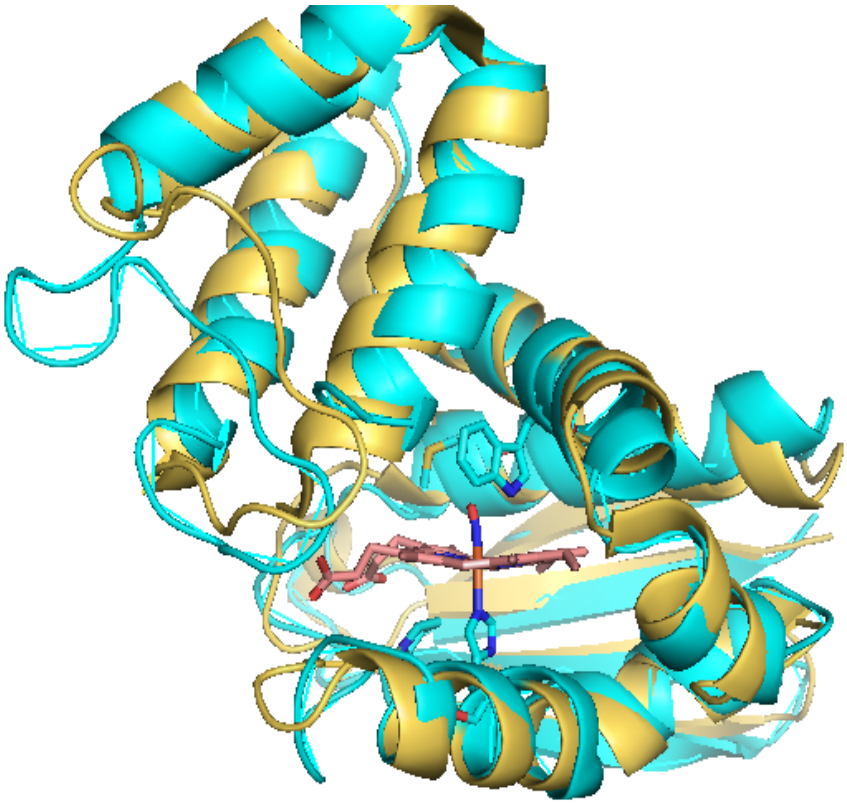

Figure 1-15: Structural alignment of *Sw*H-NOX (cyan) and NO-bound *Ns*H-NOX (mustard yellow), generated using PyMoL. The secondary structural elements (helices and sheets) are also shown. The NO-bound structure of *Ns*H-NOX (PDB ID: 2O0C[7]) was used as template.

We used uniformly labeled (^{15}N, ^{13}C) *Sw*H-NOX Fe(II)-CO to assign about 75% of the backbone resonances in a 2D-HSQC spectra for *Sw*H-NOX. The spectra for ^{15}N, ^{13}C–labeled *Sw*H-NOX Fe(II)-CO by itself was compared to a 1:1.25 molar mix containing ^{15}N, ^{13}C–labeled *Sw*H-NOX Fe(II)-CO and unlabeled *Sw*HaCE. To accomodate for the size of the large protein complex, we used ^{15}N, ^{13}C TROSY-HSQC for higher resolution. Chemical shift perturbation (CSP) studies were used to identify backbone resonances for residues that showed tremendous shift in the presence of *Sw*HaCE, and were found to reside in the N-terminal helices of *Sw*H-NOX (fig 1-15).

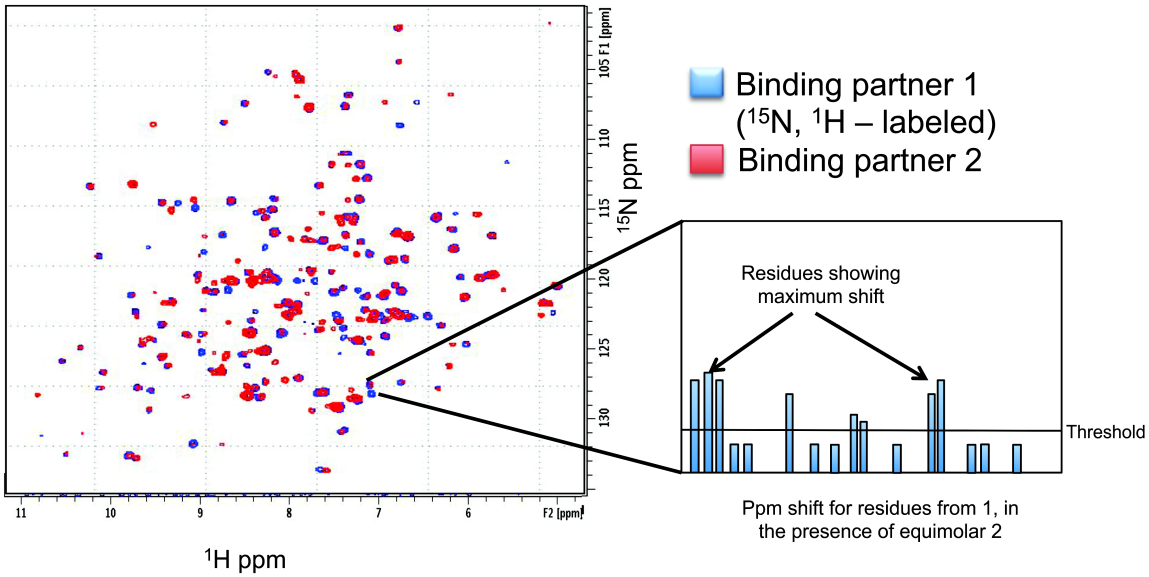

Figure 1-16: Scheme for mapping protein-protein interaction sites using chemical shift perturbation (CSP) studies.

The oligomeric state of this complex, as determined by sedimentation equilibrium, was found to be heterotetrameric. This is the first stoichiometric characterization of a H-NOX/HaCE a_2b_2 complex.

In chapter 3, the functional characterization of catalytic residues and loop 6, an important structural feature of PDE domains, is described for the PDE domain from the bi-functional

enzyme *Sw*HaCE. In this study, we have elucidated the role of the conserved active site residues in the hydrolysis of cyclic-di-GMP. We have also explored the catalytic role of loop 6, a conserved structural loop required for catalysis. These mutants were shown to completely abolish PDE activity, confirming their role in catalysis. We have analyzed point mutations of these residues using oligomerization studies to determine affect on structure. Using enzyme assays, we have shown that *Sw*H-NOX Fe(II) upregulates the cyclase activity of these mutants similar to WT *Sw*HaCE, indicating that mutating the active site residues does not affect H-NOX/HaCE binding.

In chapter 4, we have determined the *in-vivo* effects of NO and *cis*-2-decenoic acid as biofilm dispersal molecules. Individually, NO and DSF are known to disperse biofilms. In this study, we have compared the synergistic vs. additive effects of NO and DSF together as biofilm dispersal agents. We have investigated 3 species – *Shewanella woodyi, Shewanella oneidensis* and *Pseudomonas aeruginosa*, to compare the effects on biofilm dispersal.

In chapter 5, we offer a discussion about preliminary structural studies (SAXS) of the H-NOX/HaCE complex from *Shewanella woodyi.* The SAXS studies have been designed to extract information on the association of NO-bound H-NOX vs. Fe(II)-unligated H-NOX with HaCE. This should also help us determine the individual domain-domain contacts in *Sw*HaCE containing PAS-GGDEF-EAL domains, and how *Sw*H-NOX associates/interacts with the individual domains to affect overall function of the enzyme.

In chapter 6, we summarize the results of experiments described in this dissertation, offering an insight for future studies with respect to such protein complexes, and their detailed biochemical, analytical and structural study.

Appendix includes experiments that contribute to the development of structural models to identify molecular level details of the H-NOX/HaCE interaction. This approach analyzes the H-NOX/HaCE complex from both *Shewanella woodyi* and *Agrobacterium vitis*, which contain bi-functional HaCE enzymes.

CHAPTER 2: STRUCTURAL BASIS OF THE REGULATION OF *Sw*HaCE BY NO-BOUND *Sw*H-NOX

Abstract: Biofilms are surface attached communities of bacteria enclosed in a polysaccharide matrix. Bacteria in a biofilm are extremely resistant to antibiotics. Several recent reports have linked the signaling molecule nitric oxide (NO) with biofilm dispersal. We have reported that an H-NOX (heme-nitric oxide/oxygen binding) protein in the biofilm-dwelling bacterium *Shewanella woodyi* mediates NO-induced biofilm dispersal. In *S. woodyi*, *hnoX* is co-cistronic with a gene coding for a dual-functioning diguanylate cyclase/phosphodiesterase enzyme that we have named HaCE, for H-NOX-associated c-di-GMP processing enzyme. Enzymes such as these are responsible for regulating the intracellular concentrations of cyclic-di-GMP, a secondary signaling molecule essential to biofilm formation in bacteria. We have demonstrated that NO-bound *Sw*H-NOX regulates both enzymatic activities of *Sw*HaCE, resulting in decreased cellular c-di-GMP levels and disruption of biofilm formation. Thus, H-NOX/HaCE represents a potential drug target for regulating biofilm formation. In this work, the *Sw*H-NOX surface residues critical for formation of a protein complex with *Sw*HaCE have been identified using NMR, fluorescent quenching, and co-immunoprecipitation. Enzyme assays confirm this protein-protein interface and its importance for H-NOX/HaCE function.

2.1 Introduction

Biofilm formation is an important phenotype in bacteria, where cells switch from a motile, free-swimming, single cell growth mode to a surface attached, sessile, community of cells encapsulated in a matrix consisting of exo-polysaccharide, protein, and DNA[17, 22]. Bacteria within biofilms are extremely resistant to antibiotics and are thought to be responsible for several drug-resistant infectious diseases. Biofilm development is poorly understood in general, but the intracellular concentration of bis-(3'-5')-cyclic dimeric guanosine monophosphate (cyclic-di-GMP; c-di-GMP) has been shown to be important for the regulation of motility and biofilm formation[46, 47], in addition to many other important signaling processes including cell division, transcriptional regulation, and virulence[32, 33, 35, 48].

2.1.1 Cyclic-di-GMP metabolizing enzymes

In bacteria, two classes of enzymes maintain the intracellular pool of c-di-GMP. C-di-GMP is synthesized from 2 molecules of GTP by GGDEF domain-containing diguanylate cyclases (DGCs)[6, 49, 50]. C-di-GMP is hydrolyzed by ExL domain-containing phosphodiesterases (PDEs)[44, 51, 52] to form the linear metabolite 5'-phosphoguanylyl-(3' → 5')-guanosine (pGpG). Because c-di-GMP signaling and bacterial biofilms are central to many infections diseases, the pathways that contribute to the regulation of intracellular c-di-GMP concentrations are potentially novel and important antibiotic drug targets.

2.1.2 Role of NO as a biofilm dispersal signal

Nitric oxide (NO) is a well-established and important signaling molecule in mammals that regulates a variety of physiological processes including vasodilation and neurotransmission[1]. The enzyme soluble guanylate cyclase (sGC) acts as an NO sensor via its N-terminal heme-nitric oxide/oxygen binding domain[2]. Interestingly, several different groups have recently observed that low concentrations of NO induce biofilm dispersal in a variety of bacterial species[28, 53, 54]. In bacteria, H-NOX domains typically exist as stand-alone proteins that regulate co-cistronic histidine kinase (H-NOX-associated histidine kinase; HahK) or diguanylate cyclase/phosphodiesterase (H-NOX-associated c-di-GMP processing enzyme; HaCE) proteins[5, 10]. In general, biophysical characterization of these H-NOX/enzyme complexes is lacking.

2.1.3 H-NOX proteins regulate bacterial signaling pathways via NO sensing

H-NOX signaling in *Legionella pneumophila and Shewanella woodyi*, both of which encode a diguanylate cyclase/phosphodiesterase protein in the same operon as an H-NOX domain, has been characterized[55]. It is reported that the H-NOX-associated protein Lpg1057 (*Lp*HaCE) from *L. pneumophila* has *in vitro* diguanylate cyclase activity that is inhibited by NO-bound H-NOX[12]. The phosphodiesterase domain was found to be inactive. In *Shewanella woodyi*, H-NOX regulates both the DGC and PDE activities of the bi-functional enzyme *Sw*HaCE (Swoo_2750); previously referred to as *Sw*DGC)[13]. NO-bound *Sw*H-NOX inhibits cyclase activity and up-regulates phosphodiesterase activity, resulting in a dramatic drop in c-di-GMP concentrations. Furthermore, we have shown that nanomolar NO leads to less biofilm and lower intracellular cyclic-di-GMP concentrations in *S. woodyi*. These data are consistent with H-NOX acting as an NO sensor that regulates biofilm formation by modulating the intracellular level of c-di-GMP in bacteria.

Therefore, the H-NOX/HaCE protein-protein interaction is important for regulating the biofilm formation pathway in some bacteria. Here we use a combination of techniques to study how HaCE proteins are regulated by H-NOX. We employ NMR chemical shift perturbation experiments to identify the residues of *Sw*H-NOX that interact with *Sw*HaCE. The role of these residues was confirmed by enzyme activity assays as well as fluorescence binding studies. Sedimentation equilibrium studies were used to assess the stoichiometry of the *Sw*H-NOX/*Sw*HaCE complex. The data were used to generate a model for H-NOX regulation of HaCE activity.

2.2 Materials and Methods

All reagents were obtained in their highest available purity and used as received. All enzymes used were purchased from New England Biolabs.

Protein expression and purification. *Sw*H-NOX and *Sw*HaCE were expressed and purified as described previously[13, 55]. In brief, the plasmid containing the *Sw*H-NOX gene was transformed into *Escherichia coli* Tuner(DE3)pLysS cells for protein expression. The cells were grown in yeast extract media containing a final concentration of 100 mM sodium phosphate. The protein expression was induced with 10 μM IPTG (final concentration) at 18 ºC overnight. The pellet was harvested and stored at -80 ºC until purification. For purification, the pellet was thawed on ice and re-suspended in H-NOX A buffer [50 mM sodium phosphate and 300 mM sodium chloride (NaCl), pH 8.0]. After sonication, the lysate was spun at 18,000 rpm (39,191 g) for an hour. The cleared supernatant was loaded on a Nickel-NTA (GE) column, and the protein was eluted using an imidazole gradient of H-NOX B buffer (50 mM sodium phosphate, 300 mM NaCl, 250 mM imidazole, pH 8.0). The plasmid coding for *Sw*HaCE[13] was transformed into *E. coli* BL21(DE3)plysS cells for protein expression. The cells were grown in 2XYT media

containing 16 g tryptone, 10 g yeast extract, and 5 g NaCl per liter. Protein expression was induced with 100 μM IPTG (final concentration) at 16 ºC overnight. The pellet was re-suspended in lysis buffer containing 50 mM TRIS base, 10 mM magnesium chloride ($MgCl_2$), 25 mM potassium chloride (KCl), 300 mM NaCl, 10% glycerol, and 2 mM βME (β-mercaptoethanol), pH 8.0. Phenylmethylsulfonyl fluoride (PMSF) dissolved in methanol was added to a final concentration of 1 mM to the re-suspended pellet prior to lysis to inhibit protease activity. After sonication, the lysate was spun at 18,500 rpm (41,399 g) for an hour. The cleared supernatant was loaded on a Nickel-NTA column (GE), and the protein was eluted using an imidazole gradient in the lysis buffer. After elution off the Ni-column, the protein was loaded on Superdex-200 (GE) equilibrated in the lysis buffer without glycerol and PMSF to obtain protein which was >95% pure.

For 2D and 3D NMR experiments, *E. coli* strain Tuner(DE3)pLysS transformed with the *Sw*H-NOX plasmid were grown in M9 minimal media supplemented with $N^{15}H_4Cl$ and C^{13}-labeled glucose (Cambridge Isotope Laboratories, Inc.) as the sole source of ^{13}C and ^{15}N. Protein expression was induced by adding 10 μM IPTG (final concentration) at 25 ºC and allowing cultures to grow overnight. Then the protein was purified by Nickel-NTA affinity chromatography followed by gel filtration using Superdex 200. The yield of the isotope labeled protein was ~10 mg/mL. For all protein-based assays described below, the protein concentrations were determined using the Bradford Protein Assay (Thermo Scientific Pierce)[56]. The standard curve for the assay was prepared using BSA (Thermo Scientific Pierce).

Site-directed mutagenesis. The Stratagene quikchange protocol was used to carry out several *Sw*H-NOX point mutations. The following complementary primers were used to make the E16K, F17A, and E20K *Sw*H-NOX mutants: E16K: 5'-GGAG TTG ATT GAA GAT AAA TTC GGA TAT GAA ACC-3'; F17A: 5'-GAG TTG ATT GAA GAT GAG GCT GGA TAT GAA ACC-3'; and E20K:

5'-GAG TTC GGA TAT AAA ACC TTA GAT ACT TTA CTT G-3' (the underline indicates the mutated codon). Phusion polymerase was purchased from New England Biolabs. The mutagenesis products were transformed into *E. coli* Dh5α cells for propagation. The mutations were confirmed using DNA sequencing results obtained from the DNA sequencing facility at Stony Brook University. The expression and purification of *Sw*H-NOX surface mutants was carried out using same protocols as described above for the wild-type *Sw*H-NOX protein.

NMR and data analysis. The *Sw*H-NOX Fe(II)-CO complex was used in the NMR studies in order to avoid paramagnetic effects resulting from the unpaired electron in the Fe(II)-NO and Fe(II)-unligated *Sw*H-NOX complexes. The Fe(II)-CO complex was prepared in an anaerobic glove bag as previously described[9]. The *Sw*H-NOX concentration was 400 mM, dissolved in 50 mM sodium phosphate, 50 mM NaCl, and 10 mM sodium dithionite at pH 7.6. Triple resonance NMR experiments for the backbone assignments of *Sw*H-NOX (HNCO, HNCACB, CBCACONH, and HNCA) were performed at 25°C on a Bruker 900 MHz spectrometer equipped with a cryo probe at the New York Structural Biology Center, New York, NY. Data were processed using the NMRPipe software package[57] and followed by the analysis using the program Sparky[58]. 75% of the backbone resonances were assigned.

Transverse relaxation optimized spectroscopy (TROSY) edited ^{15}N-^{1}HSQC experiments were performed on the same spectrometer at 25°C for the following samples: 1) the ^{15}N-labed Fe(II)-CO *Sw*H-NOX complex and 2) the ^{15}N-labed Fe(II)-CO *Sw*H-NOX complex and the non-isotopic labeled binding partner *Sw*HaCE, at a ratio of 1:1.25. The buffer used was the same as in the 3D NMR experiments. Then the weighted average chemical shift difference (Δ in p.p.m.) was calculated using the equation:

$$\Delta\delta=([(\Delta H)^2+(\Delta N/5)^2]/2)^{1/2} \quad (1)$$

Tryptophan quenching. Intrinsic fluorescence experiments were carried out on a PTI spectrofluorometer. *Sw*HaCE (1 μM) was placed in a cuvette, and the *Sw*H-NOX Fe(II)-NO complex (WT and mutants E16K, F17A, and E20K, separately) was titrated serially into the protein with constant stirring at 25 °C. *Sw*HaCE was diluted to 10% of the starting volume (2000 μl) . Titration was continued until saturation was achieved. The data was fit to a first order binding equation in Origin:

$Temp=(P+x+Kd)^2-4*P*x;y=A1*(P+x+Kd-temp^{1/2})/P/2$ (2)

Sedimentation velocity and sedimentation equilibrium. Experiments were carried out at 4 °C on Beckman Optima XL-Analytical ultracentrifuge using an An-60 Ti rotor. For sedimentation velocity experiments, *Sw*HaCE was incubated with the *Sw*H-NOX Fe(II)-NO complex (WT and mutant E16K, separately), and the protein complex was centrifuged at 50,000 rpm (201240 g-force) for 24 hours with 60 scans at 280 nm. The protein concentration was adjusted so that the absorbance was 0.8 at 280 nm. The data was analyzed using SEDFIT[59]. The buffer used was 50 mM TRIS-Cl, 250 mM NaCl, 25 mM KCl, 10 mM $MgCl_2$, and 2 mM βME (β-mercaptoethanol), pH 8.0.

For the equilibrium experiments with *Sw*HaCE alone, *Sw*HaCE was analyzed at 3 rotor speeds (9000 rpm, 14000 rpm, and 18000 rpm; g-force of 6500, 15,800 and 26,100 respectively), which were calculated using the molecular weight of *Sw*HaCE (74.5 kDa). Two scans were collected at the end of each speed. Protein absorbance was followed at 280 nm and 260 nm. The data was analyzed using HeteroAnalysis software (University of Connecticut Analytical Ultracentrifugation Facility) to determine molecular weight for *Sw*HaCE alone in solution. The data were fit globally across samples and speeds to yield apparent molar mass.

For the equilibrium experiments with the *Sw*H-NOX/*Sw*HaCE complex, *Sw*HaCE was incubated with the *Sw*H-NOX Fe(II)-NO complex (WT and mutant E16K, separately) in a 1:1, 1:2, and 1:5 molar ratio, and analyzed at 3 rotor speeds (9000 rpm, 14000 rpm, and 18000 rpm; g-force of 6500, 15,800 and 26,100 respectively) with 2 scans at the end of each speed. The scans were collected at an absorbance of 400 nm to follow the heme absorbance of the *Sw*H-NOX Fe(II)-NO complex. The protein concentration was adjusted so that the absorbance was 0.5 at 400 nm. For the equilibrium experiments with *Sw*H-NOX alone, *Sw*H-NOX was analyzed at 3 rotor speeds (17000 rpm, 27000 rpm and 34000 rpm; g-force of 23,300, 58,700 and 93,000 respectively), which were calculated using the molecular weight of *Sw*H-NOX (22.5 kDa).

Enzyme activity measurements using the Malachite Green Assay. The SensoLyte® MG phosphate assay kit was purchased from AnaSpec. For the enzyme assays, *Sw*HaCE by itself (1 μM), or in the presence of the *Sw*H-NOX Fe(II)-unligated complex (WT, E16K, F17A, or E20K in a 1:20 concentration ratio), was incubated on ice for 10 min to allow the proteins to form a complex. The protein mixtures (20 μL) were then added to 180 μL a prepared solution containing 200 μM GTP (substrate), 5 mM $MgCl_2$, 1x buffer (50 mM Tris base, 10 mM $MgCl_2$, pH 7.5). The reaction was incubated for 10 min at 25 °C followed by boiling at 100 °C to quench the reaction. After cooling, the mixture was spun at 14000 rpm (16,873 g) for 5 min to remove any precipitate. 70 μL of the supernatant was mixed with 10 μL of 3U/ml IPP (inorganic pyrophosphatase, NEB) in a 96-well plate and incubated at 25 °C for 10 min to hydrolyze inorganic pyrophosphate (PPi) produced during the reaction. Following this, 20 μL of Malachite Green reagent was added, mixed, and the plate was read at 610 nm using a Perkin Elmer Viktor X5 microplate reader. The absorbance readings were corrected for protein only and GTP only background. This experiment measured the initial velocity for the diguanylate cyclase activity for *Sw*HaCE and *Sw*HaCE in complex with *Sw*H-NOX. This experiment was repeated in at least three fully independent experiments.

NO dissociation kinetics. NO dissociation kinetics of *Sw*H-NOX mutants E16K, F17A and E20K were carried out as previously described[60].

2.3 Results

Despite the importance of biofilms in infectious diseases, the mechanisms that regulate biofilm formation and dispersal are poorly understood. In this study, we have characterized the H-NOX/HaCE protein complex from *Shewanella woodyi* in order to increase understanding of how NO causes biofilm dispersal in this bacterium.

Chemical shift perturbation assays reveal the binding interface for SwHaCE. We collected HNCO, HNCACB, CBCACONH, and HNCA spectra in order to assign the backbone resonances for *Sw*H-NOX. Using standard methods, 75% of the *Sw*H-NOX residues (~140 residues) could be assigned, and these assignments were used to probe the binding of *Sw*HaCE (Fig. 2-1).

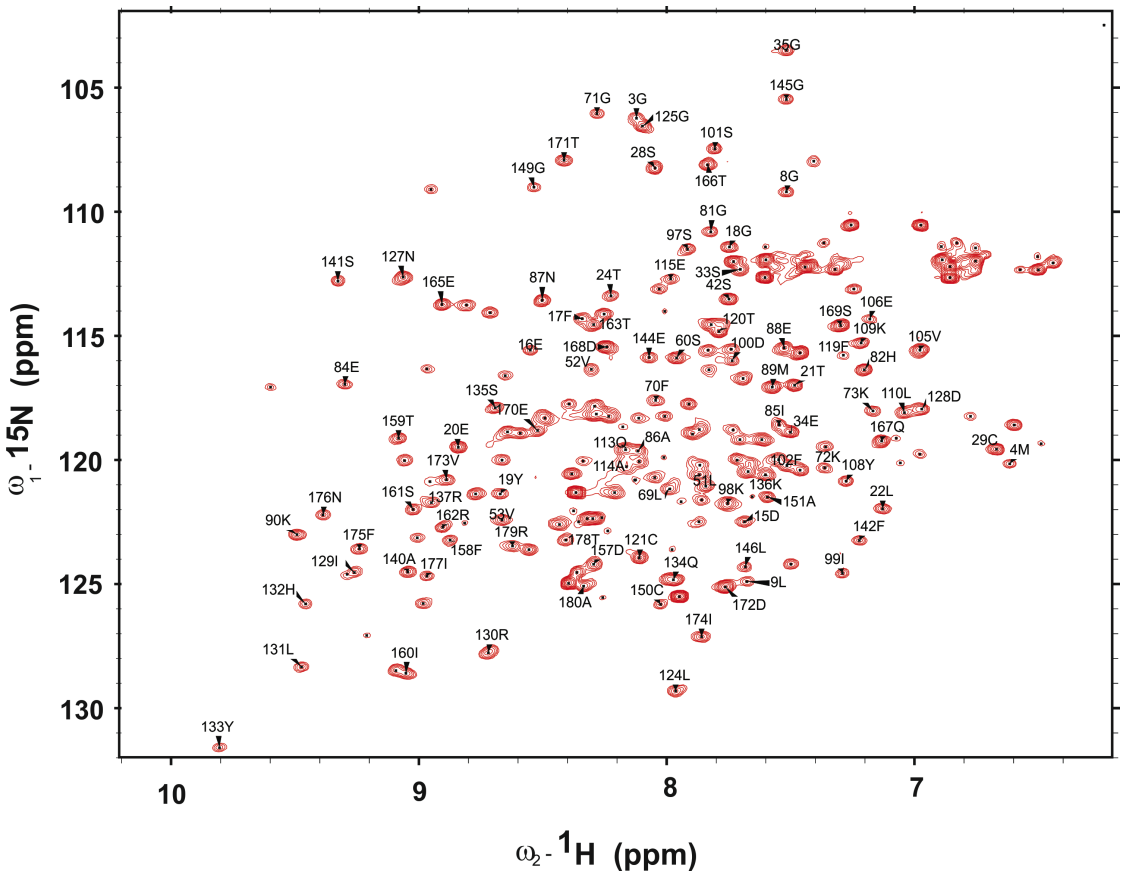

Figure 2-1: Backbone assignment for *Sw*H-NOX [as the Fe(II)-CO complex]. About 75% of the peaks were assigned using extensive 3D experiments. The x-axis represents the chemical shift in 1H, the y-axis represents the chemical shift in 15N.

HSQC NMR spectra collected for the N^{15} labeled *Sw*H-NOX Fe(II)-CO complex were compared to the spectra of the 1:1.25 complex of the N^{15} labeled *Sw*H-NOX Fe(II)-CO complex in the presence of *Sw*HaCE. In the presence of *Sw*HaCE, there was significant loss of signal in the *Sw*H-NOX HSQC spectrum due to peak broadening, presumably because the total size of the *Sw*H-NOX/*Sw*HaCE complex is expected to be at least 100 kDa (MW *Sw*HaCE = 74.5 kDa, MW *Sw*H-NOX = 22.5 kDa). Hence, TROSY spectra were collected for *Sw*H-NOX alone (Fig. 2-2, red) and in complex with *Sw*HaCE (Fig. 2-2, blue). No line broadening effects were observed, and the TROSY spectrum for the complex showed only one set of peaks, indicating fast exchange on the NMR time-scale.

The chemical shifts of some residues shifted significantly for the protein/protein complex (Fig. 2-2, blue), compared to the spectrum of *Sw*H-NOX alone (Fig. 2-2, red).

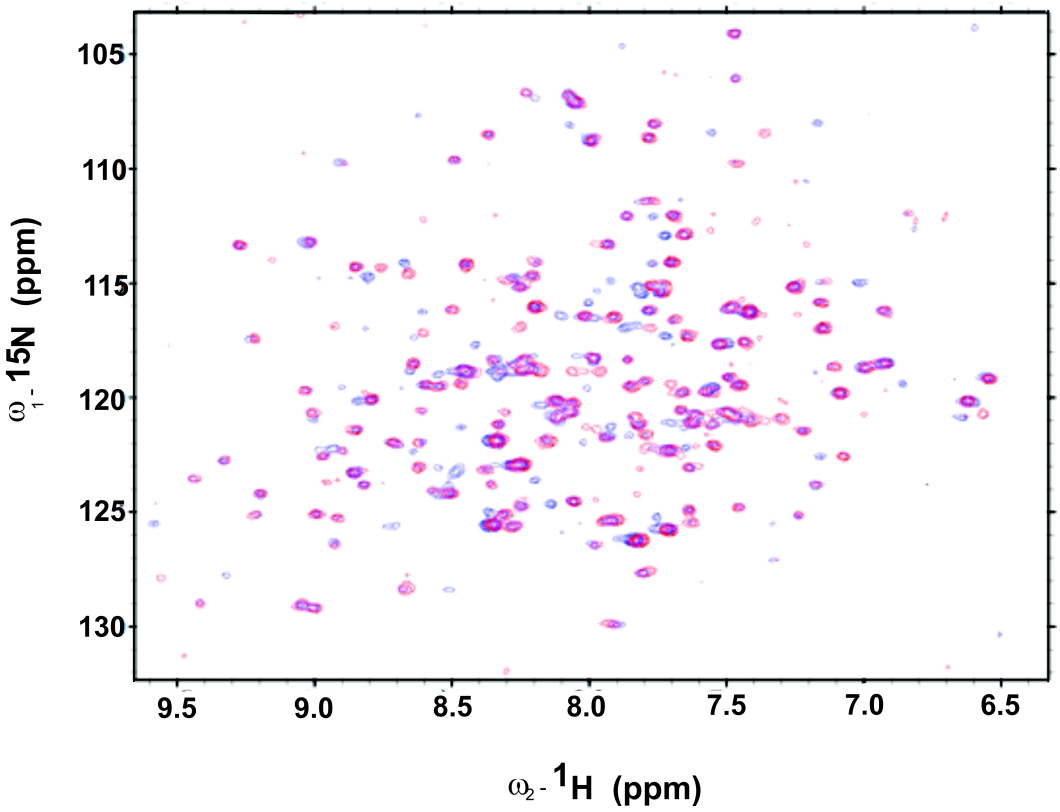

Figure 2-2: Chemical shift mapping for *Sw*HaCE and *Sw*H-NOX complex formation. The ^{15}N-^{1}H HSQC spectrum in red was collected for a sample containing uniformly ^{15}N-labeled 50 μM *Sw*H-NOX [as the Fe(II)-CO complex]. The spectrum in blue was collected for a ratio (1:1.25) of labeled ^{15}N-labeled *Sw*H-NOX [as the Fe(II)-CO complex] and unlabeled *Sw*HaCE . An overlay of these spectra indicate that peaks for some residues are shifted, indicating a change in their chemical environment in the presence of *Sw*HaCE.

To correlate the changes in chemical shift with structure, a homology model of *Sw*H-NOX was generated (Fig. 2-3a). The change in chemical shift for each assigned residue of *Sw*H-NOX (with and without *Sw*HaCE) was plotted (Fig. 2-3b). Assuming a ratio of 0.02 to be a significant change, there are 11 *Sw*H-NOX residues that shift upon exposure to *Sw*HaCE, including a set of 4-5 residues in the N-terminal helices of *Sw*H-NOX that show the maximum shift. These residues form a cluster in the N-terminal αB–αC helices on the surface of *Sw*H-NOX, suggesting this contributes to the binding site for *Sw*HaCE.

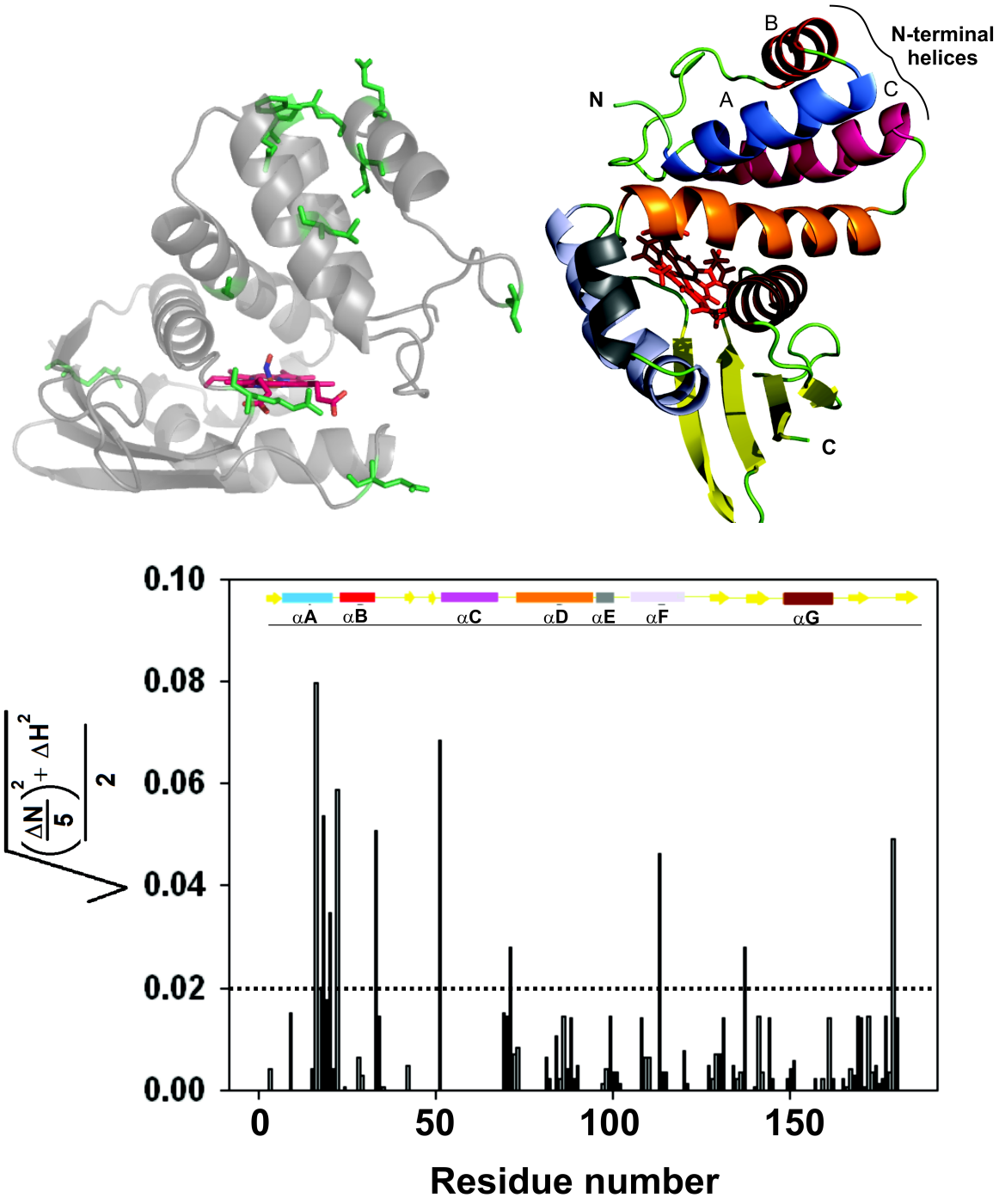

Figure 2-3: **A.** Ribbon structure of *Sw*H-NOX protein from *Shewanella woodyi* generated in PyMOL using the solution state NMR structure of *Shewanella oneidensis [9]* (So2144, PDB ID code: 2KII_A). The heme is shown in red in stick format. The 7 different helices are depicted by different color scheme – *helix αA (blue), αB (red), αC (hot pink), αD (orange), αE (gray), αF (purple) and αG (chocolate brown)*. **B.** Chemical shift changes for *Sw*H-NOX upon adding *Sw*HaCE. The ppm shifts (*Sw*H-NOX ppm to *Sw*H-NOX/*Sw*HaCE ppm), calculated as √[(ΔN/5)2 + (ΔH)2]/2, are plotted against the primary sequence residue number. The cut-off ppm shift was kept 0.02, and shifts above 0.02 (dashed line) were considered significant. The secondary

structure of *Sw*H-NOX is shown in cartoon (α-helices, β-strands). The color code corresponds to the ribbon diagram in **Figure** 2-3a.

To test this hypothesis, *Sw*H-NOX residues E16, F17 and E20 in this cluster were chosen for further investigation (highlighted in Fig. 2-4). We constructed three *Sw*H-NOX point mutants: E16K and E20K, reasoning that charge reversal mutants would be expected to significantly perturb binding if these residues play a key role, and F17A. This phenylalanine, which is a bulky residue, could participate in hydrophobic interactions during binding. To reduce the bulk of this residue, a F17A mutant was constructed.

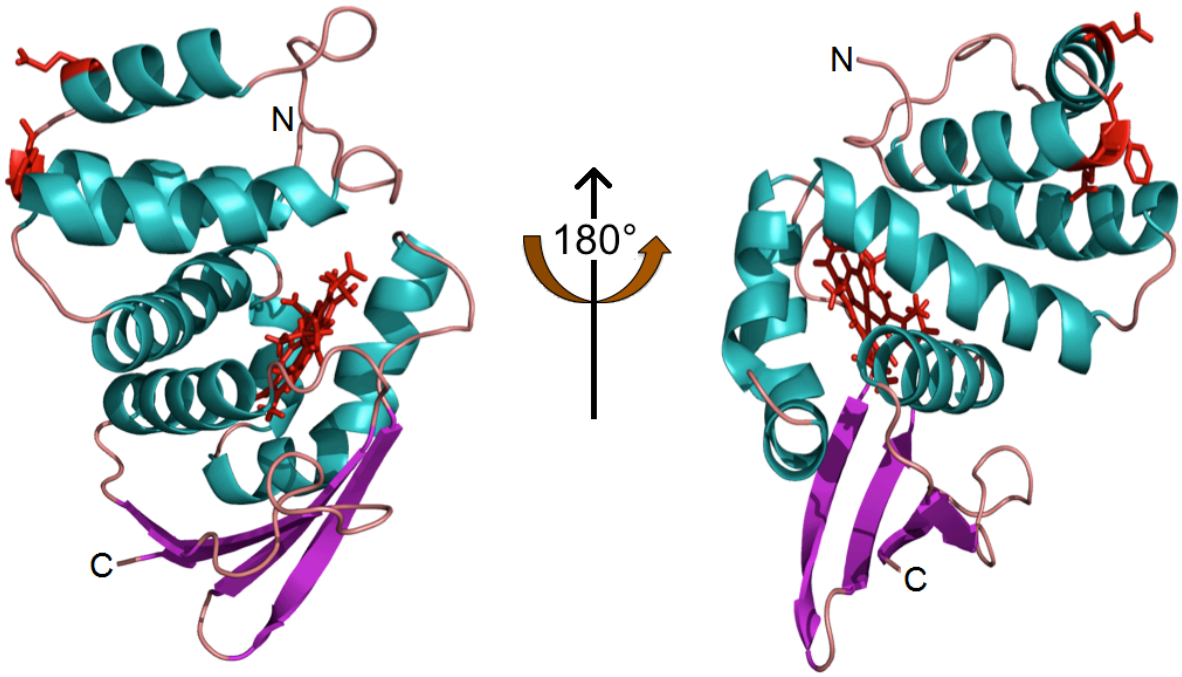

Figure 2-4: *Sw*H-NOX surface residues identified from chemical shift mapping. The *Sw*H-NOX residues with the maximum perturbation (E16, F17, and E20) upon incubation with *Sw*HaCE are highlighted in red. These residues likely represent the binding patch for *Sw*HaCE.

Characterization of ligand binding (CO and NO binding to ferrous *Sw*H-NOX and CN^- binding to ferric *Sw*H-NOX), as well as NO dissociation kinetics were carried out for the WT and the

surface mutants of *Sw*H-NOX. The Soret values and k_{off}(NO) calculated for H-NOX surface mutants were similar to WT H-NOX (Appendix table A1), confirming that mutating these surface residues does not affect the overall structure and heme properties of the *Sw*H-NOX protein.

Fluorescence quenching assays indicate binding to *Sw*HaCE is disrupted for surface mutants E16K, F17A and E20K, as compared to WT *Sw*H-NOX. SwHaCE has 7 Trps while *Sw*H-NOX has none, thus we reasoned that binding of *Sw*H-NOX to *Sw*HaCE might perturb the Trp fluorescence intensity of *Sw*HaCE. Therefore, the fluorescence of 1 μM *Sw*HaCE was followed at 370 nm in a time-based manner to assess *Sw*H-NOX/*Sw*HaCE binding. The *Sw*H-NOX Fe(II)-NO complex (WT or mutant, separately; ~1-10 μM) was added to this *Sw*HaCE solution with constant stirring to achieve saturation. We observed a quenching of the fluorescence signal as a function of increasing *Sw*H-NOX Fe(II)-NO complex in solution (Fig. 2-5).

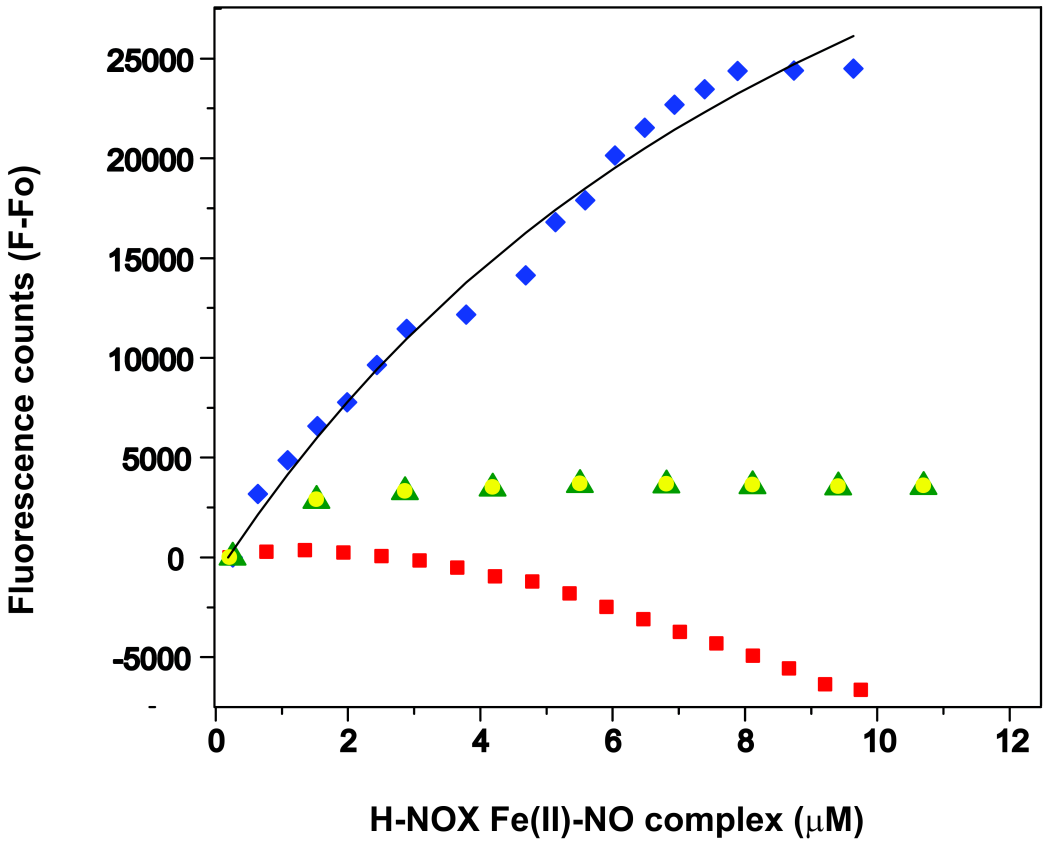

Figure 2-5: Tryptophan fluorescence quenching experiments to determine *Sw*H-NOX/*Sw*HaCE binding. The Fe(II)-NO complex of *Sw*H-NOX [WT -◆- (blue diamond), E16K -■- (red square), F17A –Δ- (green triangle) and E20K -○- (yellow circle)] was titrated into a *Sw*HaCE solution (1 μM) to determine the amount of *Sw*HaCE Trp quenching. The difference was plotted as a function of *Sw*H-NOX Fe(II)-NO concentration (μM) in solution. WT *Sw*H-NOX caused significant quenching. In general, the *Sw*H-NOX mutants do not quench *Sw*HaCE fluorescence, indicating a loss of binding. From these data, the apparent equilibrium dissociation constant for the *Sw*H-NOX/*Sw*HaCE complex was determined to be ~2.5 μM (the gray line shows the fit used to determine $K_{D,\ app}$). Each titration was done in triplicate.

The data were corrected for dilution and inner-filter effects and plotted against *Sw*H-NOX Fe(II)-NO concentration. The apparent dissociation constant ($K_{D,\ app}$) for the complex was determined to be 2.5 - 3 μM from 3 independent runs. This likely overestimates the true K_D, as the concentrations used were high and not under pseudo-first order conditions, in order to account for sensitivity of the detector. Nonetheless, the effect of *Sw*H-NOX surface mutations on binding to *Sw*HaCE could be easily determined in this assay.

For the titrations with the Fe(II)-NO complex of the E16K mutant of *Sw*H-NOX, the fluorescence signal for *Sw*HaCE did not decrease over time, and actually showed a slight increase (Fig. 2-5, **-■-**). This indicates that the E16K mutation abolished binding of *Sw*H-NOX to *Sw*HaCE. The slight increase in the fluorescence signal towards the end of the titration could be due to conformational changes resulting from interactions of the mutant E16K *Sw*H-NOX with other regions of *Sw*HaCE at high H-NOX concentration. For the F17A and E20K *Sw*H-NOX mutants, we observed significantly less quenching of the *Sw*HaCE signal than WT, suggesting a reduced binding affinity for each of these mutants to *Sw*HaCE (Fig. 2-5, **–Δ-** F17A, -○- E20K). These results confirm that the surface residues E16, F17, and E20 in the N-terminal αB–αC helices of *Sw*H-NOX each contribute to *Sw*HaCE binding, and likely, together form a binding surface for interaction with *Sw*HaCE.

Sedimentation equilibrium indicates that *Sw*HaCE forms a dimer in solution and the *Sw*H-NOX/*Sw*HaCE complex is a heterotetramer. Based on the NMR and fluorescence titration experiments described above, we concluded that *Sw*H-NOX and *Sw*HaCE form a protein/protein complex. We used sedimentation equilibrium measurements to determine the stoichiometry of this complex. Sedimentation equilibrium experiments are extensively used to determine the molecular weight of proteins and protein complexes in solution[61]. Based on previously characterized diguanylate cyclases, it is expected that active diguanylate cyclases exist as dimers in solution[38-40]. Since *Sw*HaCE is an active cyclase enzyme[13], we wanted to determine if *Sw*HaCE also forms oligomers (dimers) in solution, and we wanted to determine if the oligomerization state changes upon forming a complex with *Sw*H-NOX.

Sedimentation equilibrium experiments were carried out for *Sw*HaCE alone, *Sw*H-NOX [as the Fe(II)-NO complex] alone, and a mixture of *Sw*HaCE and *Sw*H-NOX [as the Fe(II)-NO complex] at a ratio of 1:1.5. These data are summarized in Table 2-1. For *Sw*HaCE, the HeteroAnalysis

indicates a molecular weight of 144.3 kDa, which is close to the theoretical molecular weight expected for a dimer, 149 kDa (Fig. 2-6a; Table 2-1). For WT *Sw*H-NOX, our analysis indicated a molecular weight of 23 kDa, which is close to the theoretical molecular weight of 22.5 kDa (appendix fig A3-a; Table 2-1). Thus, WT *Sw*H-NOX alone exists as a monomer and *Sw*HaCE alone exists as a dimer. The molecular weight for the *Sw*H-NOX/*Sw*HaCE complex, which was followed at 400 nm (to follow heme absorbance), was calculated to be 197.2 kDa (Fig. 2-6b; Table 2-1), which is close to the theoretical molecular weight of 193 kDa for a heterotetrameric complex of four molecules comprised of two *Sw*HaCE monomers and two *Sw*H-NOX monomers.

TABLE 2-1: Summary of sedimentation equilibrium results and controls.

Protein/Protein complex	**Calculated MW (Theoretical MW) (kDa)[c]**
HaCE by itself[a, 1]	144.3 (149.0-dimer; 74.5-monomer)
HaCE + WT H-NOX Fe(II)-NO[a, 2]	197.2 (193.0)
HaCE + E16K H-NOX Fe(II)-NO[a, 2]	76.0 (-)
WT H-NOX Fe(II)-NO[a, 2]	75.0 (-)
WT H-NOX Fe(II)-NO[b, 2]	23.3 (22.5)
E16K H-NOX Fe(II)-NO[b, 2]	23.8 (22.5)

[a]The sedimentation equilibrium run was carried out at 3 rotor speeds calculated for the molecular weight of *Sw*HaCE (74.5 kDa); 9000 (6520 g-force), 14,000 (15,800 g-force), 18,000 rpm (26,100 g-force). [b]The sedimentation equilibrium run was carried out at 3 rotor speeds calculated for the molecular weight of *Sw*H-NOX (22.5 kDa); 17,000 (23,300 g-force), 27,000 (58,700 g-force), 34,000 (93,100 g-force) rpm. [c]HeteroAnalysis and Sednterp were used to calculate the molecular weight. [1]The scans for the sedimentation equilibrium runs were collected at 280 nm. [2]The scans for the sedimentation equilibrium runs were collected at 400 nm.

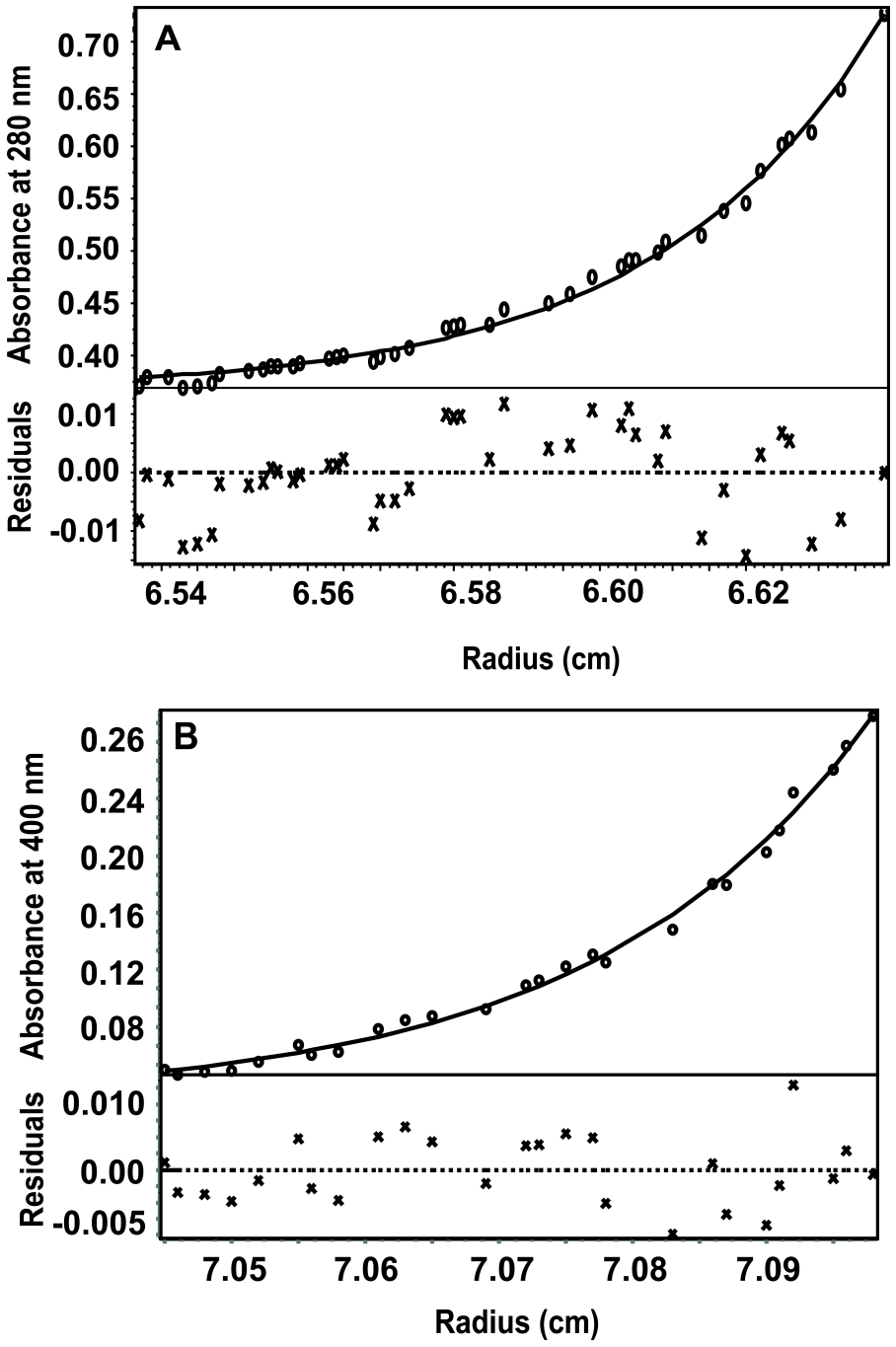

Figure 2-6: **A.** Sedimentation equilibrium experiments for *Sw*HaCE in solution. Using rotor speeds of 9000, 14,000, and 18,000 rpm (g-force of 6500, 15,800 and 26,100 respectively), and following protein at 280 nm, the calculated molecular weight of *Sw*HaCE is 144.3 kDa, indicating a dimer in solution at equilibrium. **B.** Sedimentation equilibrium experiment for *Sw*HaCE in solution with the *Sw*H-NOX Fe(II)-NO complex. Using rotor speeds of 9000, 14,000 and 18,000 rpm (g-force of 6500, 15,800 and 26,100 respectively), and following protein complexes at 400 nm, the calculated molecular weight for the complex is 197.2 kDa at equilibrium. This matches the molecular weight expected for a heterotetramer of 2 *Sw*H-NOXs and 2 *Sw*HaCEs. Each experiment was done triplicate.

The molecular weights computed from the AUC experiments are within 3% of the theoretical value, which is within the experimental error of the instrument. Therefore, we conclude that *Sw*HaCE and *Sw*H-NOX form a 2:2 heterotetrameric protein complex in solution. This is the first H-NOX/HaCE protein complex whose stoichiometry has been determined.

The E16K *Sw*H-NOX mutant [as the Fe(II)-NO complex] was analyzed both by itself and as a complex with *Sw*HaCE. The mutant was determined to be a monomer by itself (calculated molecular weight 23 kDa; appendix fig. A3-b; Table 2-1), similar to WT *Sw*H-NOX. The E16K/*Sw*HaCE protein mixture, followed at the heme absorbance, did not form a complex, as suggested by the calculated molecular weight of 76.5 kDa (appendix fig. A3-c; Table 2-1), which is consistent with un-complexed *Sw*H-NOX alone. In support of this, when *Sw*H-NOX was run alone at speeds appropriate to analyze a *Sw*H-NOX/*Sw*HaCE complex, we obtained a calculated molecular weight of 75 kDa (appendix fig. A3-d; Table 2-1). This result again suggests loss in *Sw*H-NOX/*Sw*HaCE binding due to this *Sw*H-NOX surface mutation.

Enzyme assays confirm the SwH-NOX/SwHaCE binding interface. Next we tested the effect of *Sw*H-NOX and *Sw*H-NOX surface mutants on regulation of *Sw*HaCE activity. We have previously reported that the diguanylate cyclase activity for *Sw*HaCE increases in the presence of the WT *Sw*H-NOX Fe(II)-unligated complex[13]. In these studies we used a new reaction end-point assay for cyclase activity, based on detection of phosphate in solution by the dye Malachite Green.

In a diguanylate cyclase catalyzed reaction, 2 molecules of GTP are condensed to generate PPi (inorganic pyrophosphate) as a by-product along with cyclic-di-GMP[62] (2 GTP → Cyclic-di-GMP + 2 PPi). In the presence of the enzyme Inorganic Pyrophosphatase (IPP), PPi is hydrolyzed to Pi (inorganic phosphate) in solution[63] (2 PPi → 2 Pi). Malachite Green is a

commercially available reagent, which is used to determine the concentration of free Pi in solution[64]. This end-point assay can be used to quantify diguanylate cyclase activity by measuring the amount of PPi generated during the reaction, which can in turn be quantified by measuring the amount of Pi generated. Since this is an end-point assay, the *Sw*HaCE enzyme was boiled before adding IPP to the solution to determine the amount of PPi generated, to ensure that IPP does not interfere with the activity of the enzyme. To confirm that IPP is not the rate-limiting enzyme in this reaction, the concentration of IPP was doubled to confirm that the same amount of Pi was generated (appendix table A2). Since we are detecting the amount of PPi produced in the reaction, the turnover of cyclic-di-GMP into pGpG by the phosphodiesterase domain of *Sw*HaCE does not affect the measurement. As control, the amount of Pi generated was determined at various concentrations of *Sw*HaCE (appendix fig. A4-b). A linear correlation was observed between enzyme concentration and amount of Pi produced, confirming that only *Sw*HaCE is the rate-limiting enzyme in the reaction.

This assay was used to determine the concentration of Pi generated during the reaction of *Sw*HaCE with GTP in the presence of the WT, E16K, F17A, and E20K *Sw*H-NOX Fe(II)-unligated complexes. The specific activity values are reported in Table 2-2 as concentration of Pi (μM/min/mg).

TABLE 2-2: Regulation of *Sw*HaCE diguanylate cyclase activity by *Sw*H-NOX.

Reaction[a]	Pi (μM/min/mg)[b]	P-test
HaCE	41.011 ± 2.66	0.000025
HaCE + H-NOX Fe(II)	81.671 ± 4.64	
HaCE + E16K H-NOX Fe(II)	57.092 ± 5.35	0.00145
HaCE + F17A H-NOX Fe(II)	28.858 ± 9.28	0.00307
HaCE + E20K H-NOX Fe(II)	52.962 ± 7.90	0.00559

[a]All reactions contained 200 μM GTP, 50 mM Tris (pH 7.5) and 5 mM $MgCl_2$.[b]Refer to supporting information for the PPi standard curve.

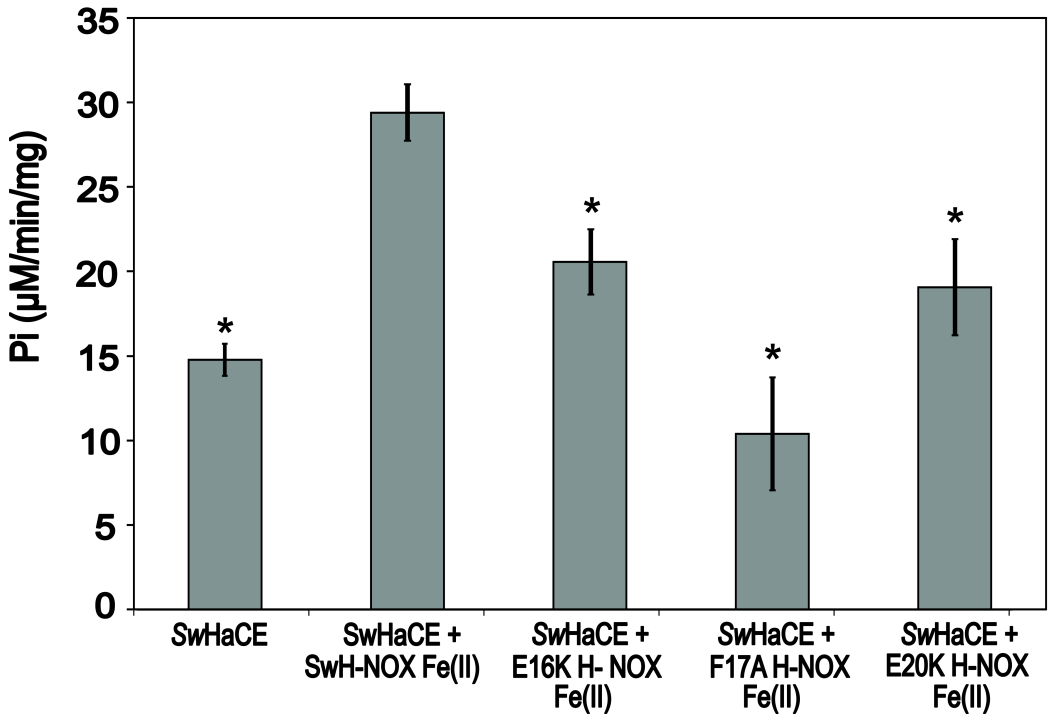

Figure 2-7: Regulation of *Sw*HaCE diguanylate cyclase activity by *Sw*H-NOX. Addition of 20 μM of the Fe(II)-unligated complex of *Sw*H-NOX to *Sw*HaCE causes a significant increase in the specific activity of *Sw*HaCE. Addition of any of the Fe(II)-unligated *Sw*H-NOX surface mutants (E16K, F17A, E20K; all at 20 μM), however had less, or no effect on *Sw*HaCE activity, indicating decreased binding to *Sw*HaCE. All assays contained 1 μM *Sw*HaCE and 200 μM GTP as substrate. Error bars represent three independent trials on different days. A student's P-test was done to determine significance. The star (*) indicates p≤0.006. Each data set was compared to the activity of *Sw*HaCE + WT *Sw*H-NOX Fe(II).

It was observed that the WT *Sw*H-NOX Fe(II)-unligated complex (20 μM) increased the initial velocity of the cyclase activity of *Sw*HaCE (1 μM) by 2.5-fold in the presence of 200 μM GTP, as expected from our previous work[13] (Fig. 2-7; Table 2-2).

In general, addition of the *Sw*H-NOX mutants led to a loss of this enhanced effect, indicating a loss in *Sw*H-NOX binding and regulation of *Sw*HaCE cyclase activity. For the E16K and E20K *Sw*H-NOX mutants, the observed initial velocity was lower than that of *Sw*HaCE with WT *Sw*H-NOX, but slightly higher than the enzyme by itself, indicating some residual binding and regulation by *Sw*H-NOX, but significantly less than observed with WT *Sw*H-NOX. For F17A *Sw*H-NOX, we observed the same initial velocity as *Sw*HaCE without *Sw*H-NOX. These data, like all of the experiments described above, also indicate that *Sw*H-NOX/*Sw*HaCE binding has been disrupted by the surface mutations and support our conclusion that *Sw*H-NOX binds to *Sw*HaCE, at least in part, using the N-terminal helical region of H-NOX.

2.4 Discussion

The spatio-temporal regulation of intracellular cyclic-di-GMP is central to many important cellular processes like virulence, biofilm formation, quorum sensing, motility and cell division[65, 66]. Diguanylate cyclase and phosphodiesterase enzymes, which maintain the intracellular pool of cyclic-di-GMP, are usually found associated with regulatory domains/proteins that modulate their activity. However, very few of these enzymes have been characterized with their regulatory partner protein.

NO has been shown to play an important role in bacterial signaling, and recent studies have indicated that low concentrations of NO disperse biofilms in bacteria through regulation of c-di-GMP concentrations[67]. We have previously reported that NO disperses biofilm in the marine, bioluminescent, biofilm-dwelling bacterium *S. woodyi* through H-NOX by regulating the production of c-di-GMP by HaCE[13]. It was shown that *Sw*H-NOX and NO differentially modulate the enzymatic activities of both the diguanylate cyclase and phosphodiesterase domains of *Sw*HaCE. These results necessitate a model in which H-NOX and HaCE are associated independent of the ligation state of H-NOX.

This study investigates the structural and biophysical details of the association between *Sw*H-NOX and *Sw*HaCE. We have used NMR chemical shift perturbation analysis along with peak assignments for *Sw*H-NOX to identify the critical surface H-NOX residues that are involved in binding to *Sw*HaCE. The tremendous change in the chemical environment of a patch of N-terminal residues, including residues E16, F17, and E20, indicates a binding region for *Sw*HaCE on *Sw*H-NOX (Fig. 2-3a,b). We also identified other residues (~6-7) with a significant chemical shift perturbation upon binding to *Sw*HaCE that are spread out on other parts of *Sw*H-NOX.

These chemical shift perturbations may indicate additional binding surface area, or, alternatively, a conformational rearrangement of *Sw*H-NOX that is triggered upon binding to *Sw*HaCE.

To determine the role of identified *Sw*H-NOX N-terminal amino acids (E16, F17, E20) in binding *Sw*HaCE, we made mutants of each and investigated the effect of mutation in several binding and enzymatic assays. Fluorescent binding assays indicate significant loss of binding (Fig. 2-5) and enzyme regulation (Fig. 2-7) for individual mutants of these surface residues (E16, F17, E20). Hence, we can conclude that these residues mediate interaction of *Sw*H-NOX with *Sw*HaCE. Sedimentation equilibrium experiments reveal the WT *Sw*H-NOX/*Sw*HaCE protein complex to be a heterotetramer (Fig. 2-6b) whereas *Sw*H-NOX alone and all the surface mutants in the presence of *Sw*HaCE were determined to be monomeric in solution.

Based on the results, we have developed a model for the *Sw*H-NOX/*Sw*HaCE protein complex. Because *Sw*H-NOX and *Sw*HaCE are co-cistronic[13], we hypothesize that they are expressed together in the cell, and always associate to form this heterotetrameric complex. This association likely occurs via dimerization of *Sw*HaCE, followed by binding of 2 molecules of *Sw*H-NOX to the *Sw*HaCE dimer, as illustrated in figure 2-8.

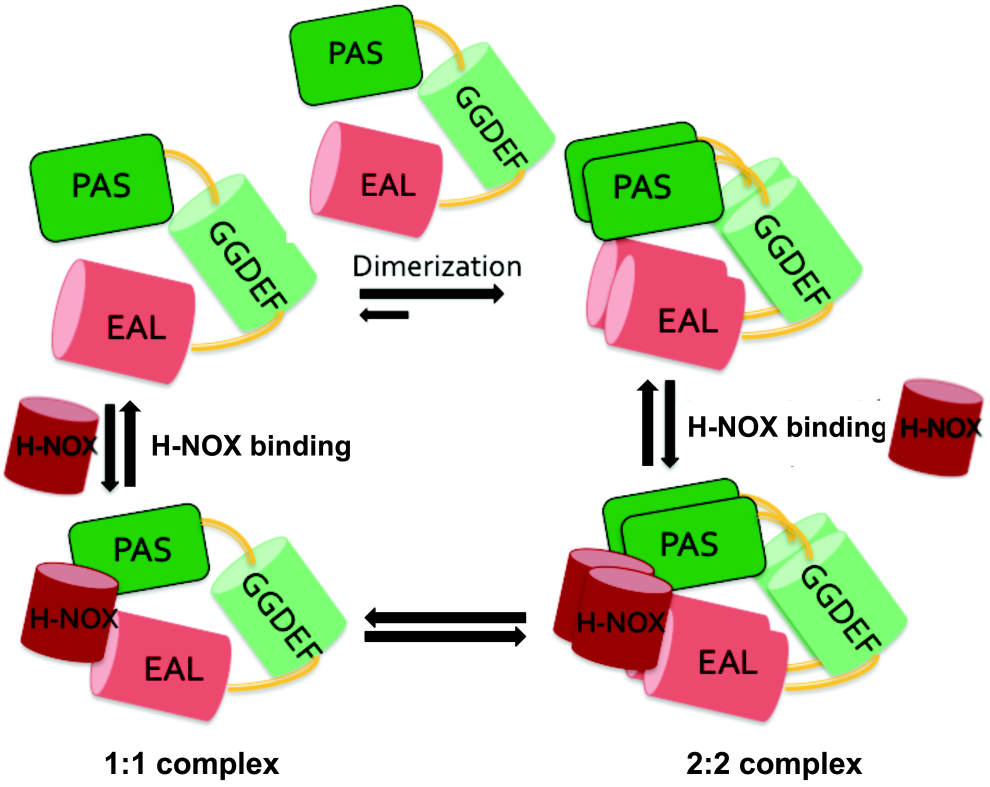

Figure 2-8: Possible mechanism of complex formation between *Sw*HaCE and *Sw*H-NOX. Monomeric *Sw*HaCE is likely in equilibrium with dimeric *Sw*HaCE, with the equilibrium lying towards the dimer. Monomeric or dimeric *Sw*HaCE may associate with 1 or 2 molecules of *Sw*H-NOX, respectively. The most abundant species at equilibrium is the heterotetrameric complex (2:2), containing 2 molecules each of *Sw*HaCE and *Sw*H-NOX.

Upon expression, presumably, *Sw*H-NOX is in the Fe(II)-unligated state, and hence, the cyclase activity of *Sw*HaCE is enhanced to generate more c-di-GMP. Upon binding the signal (NO), there must be a change in the conformation of the heterotetrameric protein complex, leading to a change in the activity of *Sw*HaCE that results in less c-di-GMP produced, ultimately causing biofilm dispersal. If monomeric *Sw*HaCE also binds *Sw*H-NOX, there may be a complex equilibrium involving dimerization of *Sw*HaCE, monomeric association of *Sw*H-NOX/*Sw*HaCE, and 2 monomers of *Sw*H-NOX binding to the *Sw*HaCE dimer to form the final heterotetrameric species. However, sedimentation equilibrium cannot be used to determine the ratio of these species in solution.

Furthermore, the data presented here indicate that the N-terminal αA-αC helices mediate binding to *Sw*HaCE. This result is supported by several previous studies that also point to the role of the N-terminal helices in transmitting the signal of NO-binding to H-NOX partner proteins. In crystal structures of the H-NOX domain from *Nostoc punctiforme*[7], the N-terminal helices have been shown to have maximum displacement upon binding of the signaling ligands NO/CO, suggesting that movement in the αA-C helices constitutes part of the signal transfer mechanism. Furthermore, a recent study from the Marletta lab describes the important higher order interactions in sGC, elucidating the mechanism of NO-regulated stimulation of activity[4]. They found that in the N-terminal region of sGC, H-NOX participates in the signal transfer mechanism by binding to the PAS domain. Mutational studies confirm that NO binding triggers these local interactions, leading to global conformational changes, ultimately increasing activity.

Further evidence that the N-terminal helices of H-NOX are important for interaction with partner proteins and signal propagation comes from studies on the structure of the heme cofactor of H-NOX. The heme unit in H-NOX is highly distorted from planarity[68], but structural studies have indicated that mutation of a conserved proline residue in the proximal heme pocket causes substantial heme flattening[69]. The conformational change caused by heme flattening propagates to the surface of H-NOX, causing a shift in the position of the N-terminal helices. We have shown in *Sw*H-NOX that the heme-flattened mutant affects *Sw*HaCE activity exactly the same as binding of NO to WT *Sw*H-NOX[70], indicating heme-flattening causes a similar structural change to the *Sw*H-NOX/*Sw*HaCE complex as binding NO. These data suggest that transmission of the NO signal involves the N-terminal helices, which is highly supportive of our results reported here, indicating the N-terminal helices are involved in binding HaCE, which is required for translation of NO binding to the enzymatic active sites.

Taken together, there is strong evidence that ligand-binding events in bacterial H-NOX domains cause conformational changes that are relayed to the N-terminal helices, which serve as a binding site for interaction with partner enzymes such as HaCEs or HahKs (H-NOX-associated histidine kinases), ultimately resulting in functional changes within the cell.

In conclusion, NO and c-di-GMP are becoming increasingly important as signaling molecules that direct bacteria on how to make the choice between motile and sessile lifestyles. This study is the first of its kind that provides a structural understanding of how a bacterial NO-sensing protein, H-NOX, can regulate its associated enzyme activity (HaCE, HahK), to control the downstream functions such as biofilm-formation. Such studies add to understanding of how small-molecule signaling regulates downstream functions and of how enzymes that regulate cyclic-di-GMP concentration in the cell are functionally regulated by a signal-sensing protein.

CHAPTER 3: STRUCTURE-FUNCTION ANALYSIS OF THE PDE ENZYME FROM THE NO-REGULATED BI-FUNCTIONAL ENZYME *Sw*HaCE FROM *Shewanella woodyi*

Abstract: Cyclic-di-GMP has been established as a ubiquitous signaling molecule in bacteria playing multiple roles in cellular pathways like virulence, biofilm formation and quorum sensing. Bacteria contain multiple genes encoding cyclic-di-GMP metabolizing enzymes – diguanylate cyclase (DGC) and phosphodiesterase (PDE). Stand-alone PDE domains have been characterized to identify key functional residues, including 14 conserved polar residues, 5 glutamate residues, and an unstructured loop, that participate in catalysis. However, characterization of PDE domains that are part of bi-functional GGDEF-ExL di-domain proteins is still sparse. This study confirms the role of conserved glutamate residues in the bi-functional enzyme HaCE from *Shewanella woodyi*. *Sw*HaCE exhibits dual activities that are regulated by NO-bound *Sw*H-NOX (chapter 2). Also determined is the catalytic role of loop 6 and its contribution to enzyme structure. Mutational studies combined with biophysical studies and enzymatic analysis offer an insight into the catalytic mechanism of ExL domains.

3.1 Introduction

The bacterial signaling molecule cyclic-di-GMP was first found to regulate polysaccharide synthesis in *Acetobacter xylinum*[71]. Since then, many studies have been undertaken that identify a bigger role for this molecule ranging from virulence to cell-cell signaling, biofilm formation and quorum sensing[46-48]. This secondary messenger plays a regulatory role at the transcriptional level, where it regulates gene transcription[72]; as well as post-translational level by binding to proteins that participate in various cellular machinery[66].

In chapter 2, we elucidated the interactions of H-NOX/HaCE from *Shewanella woodyi,* and this protein complex has been shown to regulate biofilm formation in an NO-dependent manner. *Sw*HaCE has been previously shown to exhibit dual activities – both the diguanylate cyclase and phosphodiesterase activities were found to be active *in-vitro.* In this chapter, we investigate the catalytic residues from the phosphodiesterase (PDE) domain of this bi-functional *Sw*HaCE protein.

3.1.1 Ubiquitous presence of DGC/PDE enzymes in bacterial genomes

Two classes of enzymes - diguanylate cyclase (DGC, synthetase), and phosphodiesterase (PDE, hydrolase), encoding conserved enzymatic domains maintain the turnover of intracellular c-di-GMP. Bioinformatics and genetic studies have shown that a bacterial genome often encodes multiple copies of these enzymes (*E.coli* – 19 DGCs and PDEs, *Pseudomonas aeruginosa*[65]). These enzymatic domains are often encoded in an operon along with a sensor/adapter protein[73]. These genetic arrangements hint at functional regulation of the activity of these enzymes by various stimuli. Certain characterized DGC and PDE enzymes are turned on/off by certain signals[28], thereby creating a flux of c-di-GMP concentration within the cell. Other stand-alone enzymes, which are generally on, contribute to the general pool of c-di-

GMP. Thus, understanding the mechanisms that regulate the spatio-temporal distribution of this secondary messenger is important to understand the role of c-di-GMP in signaling relays.

3.1.2 Diguanylate cyclase (DGC) enzymes

Crystal structures for GGDEF-motif containing DGC domains show the mechanism of catalysis. Diguanylate cyclase domains have a fold similar to adenylate cyclases. Though information about the mechanism of catalysis is still limited, especially about the regulation of activity, WspR and PleD offer insights into the mechanistic aspects of DGC domains. PleD, a diguanylate cyclase from *Caulobacter crescentus*, contains a phospho–receiver domain (CheY) and a GGDEF domain[40, 41]. Phosphotransfer to the CheY domain causes the GGDEF domain to switch to an active conformation. Crystal structures for some of these domains indicate 2 sites where cyclic-di-GMP can bind: the A–site or active site (GGDEF) and an allosteric site or I-site (RxxD) on the catalytic loop. The structure of the inactive conformation of PleD shows c-di-GMP bound to the I-site (Fig 3-1).

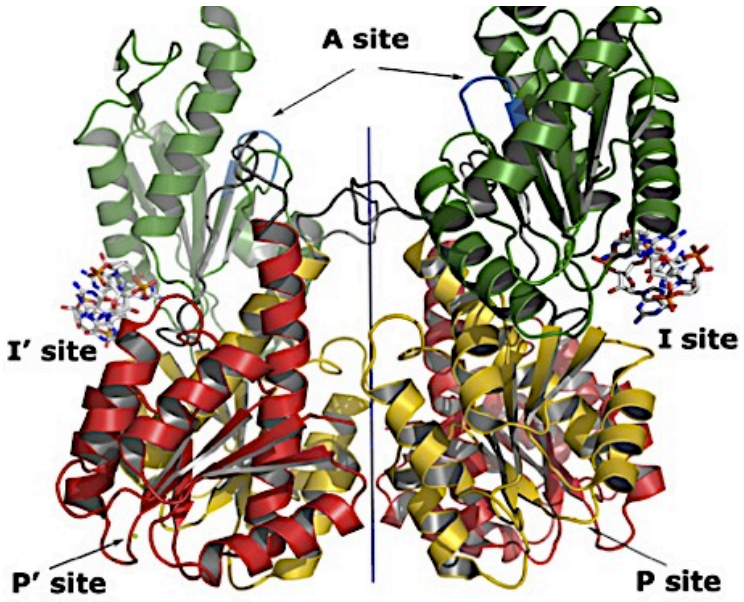

Figure 3-1: Crystal structure of the diguanylate cyclase domain from PleD (PDB ID: 2V0N). The active site (A site) and the inhibitory site (I site) are highlighted. The stick format of cyclic-di-GMP is shown bound to the I-site.

The allosteric site is also called the inhibitory site (I-site), since enzymes that purify with cyclic-di-GMP bound to this site are locked in a particular conformation and rendered inactive. This involves product inhibition by c-di-GMP to regulate its synthesis in the cell, where c-di-GMP acts as a non-competitive inhibitor of the cyclase activity (Fig 3-2). Hydrolysis of the bound cyclic-di-GMP results in an active conformation. The allosteric site has since been identified as a conserved inhibitory site (I-site) on some GGDEF domains[74].

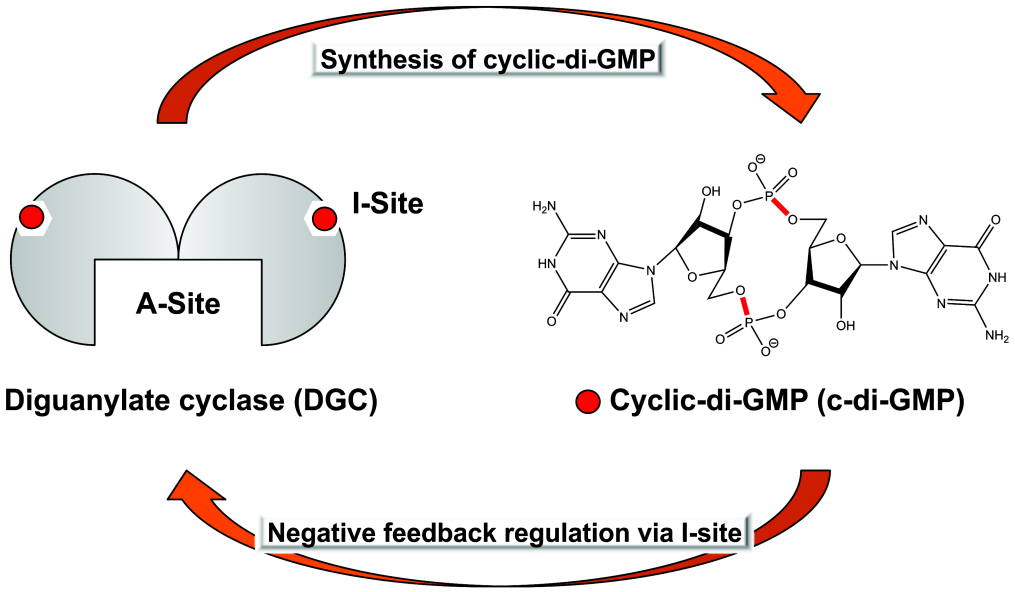

Figure 3-2: Scheme for allosteric control of cyclic-di-GMP synthesis and regulation via I-site of the GGDEF domains.

WspR is an ortholog of PleD from *P. aeruginosa,* and has been shown to be a conserved response regulator participating in various chemotactic processes[38, 39]. Similar to PleD, the DGC activity of WspR is regulated by phosphorylation. WspR has a long helical stalk that connects the c-terminal of the REC domain and the GGDEF domain. The stalk is important for regulating oligomerization, activation and autoinhibition of WspR. WspR forms an inactive tetrameric complex with c-di-GMP bound to the I-site. It was shown that the c-di-GMP bound at

the I-site can cause the dimeric enzyme to assume inactive conformations via formation of the tetramer, which is in equilibrium with the inactive dimer. Enzyme concentration is one of the key factors that is understood to regulate the equilibrium of these oligomeric forms and control the cyclase activity.

3.1.4 Phosphodiesterase (PDE) enzyme

The EAL–motif containing PDE domain was first identified as a DUF gene (domain of unknown function[44]). Since then, crystal structures and biochemical studies of a number of stand-alone PDE domains have elaborated upon the structure and function of these domains. Active cyclic-di-GMP specific phosphodiesterases bind and hydrolyze cyclic (5' → 3')–diguanosine monophosphate (c-di-GMP) to the linear dimeric GMP metabolite 5' pGpG. This catalysis occurs via an attack on the 3' cyclic phosphate–oxygen bond. These are also called class I enzymes. Some inactive PDE enzymes do not contain the conserved amino acids required for catalysis. They are called class II ExL enzymes.

Crystal structure of the inactive PDE enzyme YkuI (*Bacillus subtilis*) reveals a β/α-fold similar to a TIM-barrel fold (Fig 3-3). Based on this structure, the mechanism for another PDE enzyme, RocR (*P. aeruginosa)* was proposed[75], and observed to be analogous to other $(\alpha/\beta)_8$. As compared to YkuI, RocR contains conserved residues including the 'ExL' motif and a functional loop called the 'loop 6', identified by the motif - DDFGTGxS. In YkuI, some of these residues, as well as the loop were found to be degenerate, causing the enzyme to be inactive.

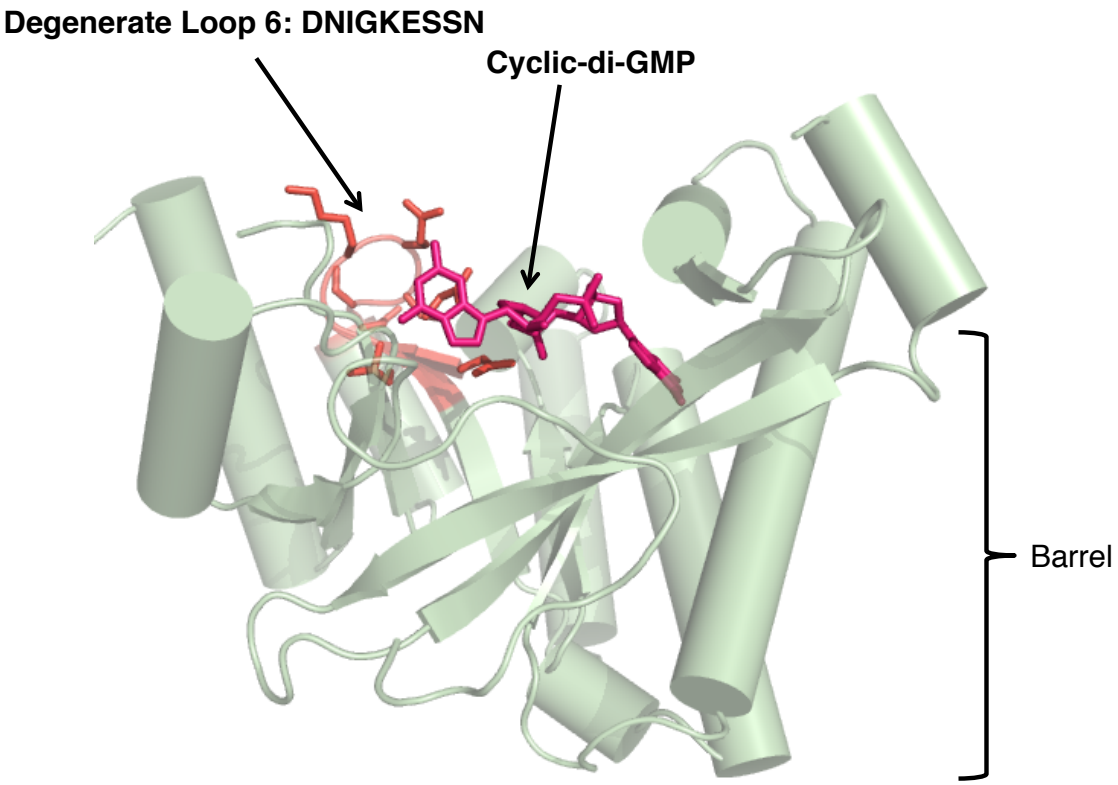

Figure 3-3: Crystal structure of the PDE domain from YkuI (*Bacillus subtilis,* PDB ID: 2W27) showing the barrel. The position of the catalytic loop 6 (in red) in the active site is indicated. Also shown is the bound substrate (c-di-GMP, pink) in the TIM-barrel shaped catalytic pocket.

The proposed mechanism scheme for catalysis by phosphodiesterase domains involves a general active site base (usually a Glu/E), which activates a water molecule and coordinates a metal ion (fig 3-4). The activated water molecule then attacks the P–O bond of cyclic-di-GMP and forms a linear molecule. This linear molecule can take up a proton to form the linear product – pGpG, which is the released. Though the involvement of one or two metal ions is still ambiguous, the affect of different metal ions on the phosphodiesterase activity has been analyzed, with evidence that Mg^{2+} and Mn^{2+} enhance activity, whereas Ca^{2+} and Zn^{2+} inhibit activity[51, 75].

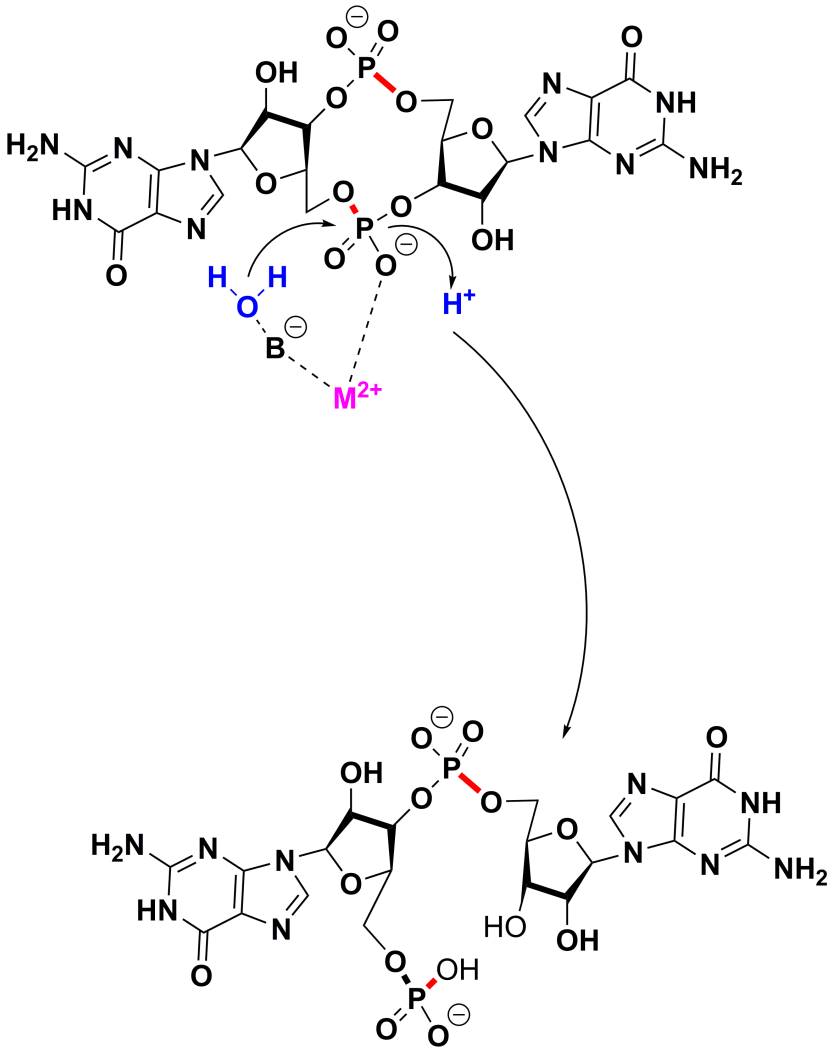

Figure 3-4: Proposed mechanism for catalysis of cyclic-di-GMP hydrolysis by ExL domains, involving a divalent metal cation (Mg^{2+}), a general base (Glu, E) and water. The bond being broken is depicted in red.

Crystal structures of PDE domains also show oligomerization induced multimeric structures. This includes dimerization along an interface involving loop 6, leading to formation of tetramers[43, 76], and is believed to be part of the conformational changes that regulate PDE activity.

The presence of catalytically active and inactive PDE domains in bacterial genomes suggests multiple roles for these domains in c-di-GMP signaling pathways in substrate (c-di-GMP) turnover and as substrate (c-di-GMP) receptor[31]. These domains are often associated with a REC-domain, PAS, BLUF or an N-terminal GGDEF (cyclase) domain, suggesting a design for dual-functioning enzymes. Along with the signature ExL motif, there are 14 other residues identified and conserved for catalysis (including substrate and metal binding), as observed from various bioinformatics and structural studies. Also conserved is a functional loop, as observed from the structure of RocR (fig 3-5). This motif, called the loop 6, is identified by DFG(T/A)GYxS motif, and connects a β-sheet and a α-helix.

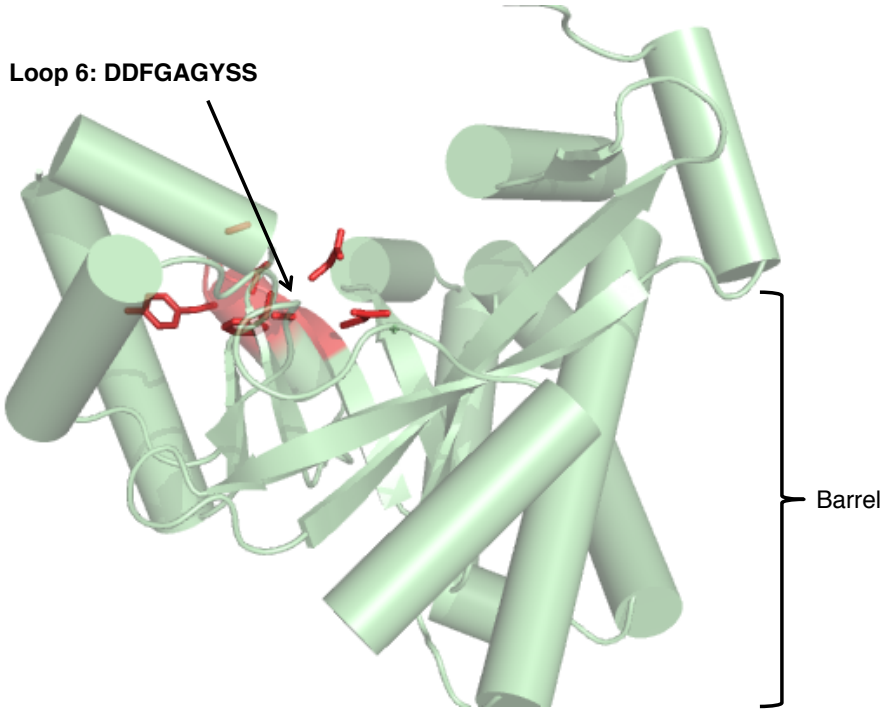

Figure 3-5: Crystal structure of the PDE domain from RocR (*Bacillus subtilis,* PDB ID: 3SY8-2) showing the barrel. The loop 6 is highlighted in red.

Located at the C-terminal end of the barrel, this loop was shown to act as a lid responsible for substrate sequestration, solvent exclusion and product release. Inactive ExL phosphodiesterase

domains containing the conserved charged residues have a degenerate loop 6 missing conserved residues; this supports the role of loop 6 in phosphodiesterase activity.

3.1.5 Di-domain enzymes in bacterial genomes

Di-domain enzymes containing GGDEF-ExL have been found in many bacterial genomes. Some of them are bi-functional, whereas others contain degenerate enzymes domains with no demonstrable *in-vitro* activity. Interestingly, these inactive domains can function as receptors of cyclic-di-GMP, thus contributing to the regulation of intracellular levels.

3.1.6 Bi-functional HaCE enzymes from Shewanella woodyi

A primary structure alignment of the bi-functional enzymes from *Shewanella woodyi/Agrobacterium vitis* with other characterized PDE domain containing enzymes shows several conserved residues that could be important for acid/base catalysis. Among these residues are seven conserved glutamic acids that could serve as a general base in the catalytic cycle. Of these residues five are located within the putative phosphodiesterase active site, as identified in our homology model generated using crystal structures available for other PDE enzymes (fig 3-6).

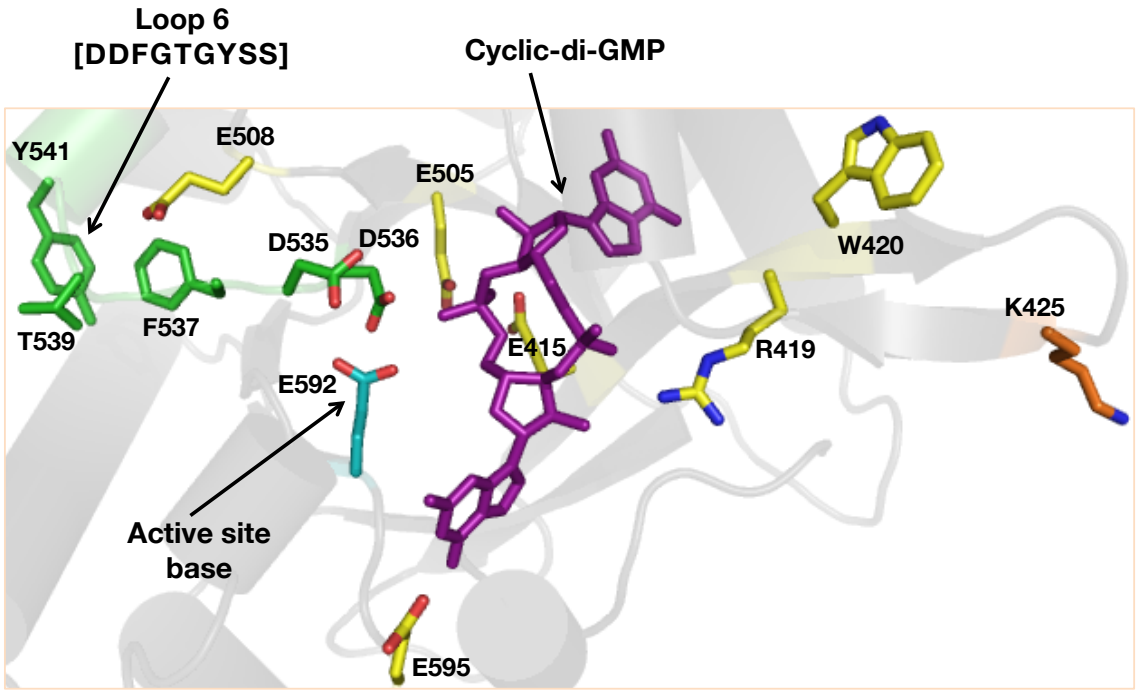

Figure 3-6: Putative catalytic pocket for the *Sw*HaCE PDE domain. The position and identity of conserved residues implicated in catalysis is shown, along with bound substrate (c-di-GMP).

We have altered these five residues in the bi-functional enzyme HaCE from *S. woodyi* to determine if they are essential for phosphodiesterase activity. We observed abrogation of enzymatic activity when the glutamic acid in the signature ExL motif was altered (E415) as well as the proposed active site base (E592). A third glutamic acid, E595, present in the conserved EGxE motif with the proposed active site base is also important for phosphodiesterase activity (HPLC studies show abrogation of activity). It should be noted that alteration of these residues does not affect diguanylate cyclase activity, indicating that these residues are only important for phosphodiesterase activity. We also tested additional conserved residues that are in the phosphodiesterase active site, based on our structural model, to gain better insight into the oligomerization of this domain, and how it contributes to the catalytic mechanism of the phosphodiesterase domain of this bi-functional enzyme.

3.2 MATERIALS AND METHODS

All reagents were obtained in their highest available purity and used as received. All enzymes used were purchased from New England Biolabs.

Protein expression and purification. WT *Sw*HaCE was expressed and purified as described previously. The plasmid coding for *Sw*HaCE was transformed into *E. coli* BL21(DE3)plysS cells for protein expression. The cells were grown in 2XYT media containing 16 g tryptone, 10 g yeast extract, and 5 g NaCl per liter. Protein expression was induced with 100 μM IPTG (final concentration) at 16 ºC overnight. The pellet was re-suspended in lysis buffer containing 50 mM TRIS base, 10 mM magnesium chloride ($MgCl_2$), 25 mM potassium chloride (KCl), 300 mM NaCl, 10% glycerol, and 2 mM βME (β-mercaptoethanol), pH 8.0. Phenylmethylsulfonyl fluoride (PMSF) dissolved in methanol was added to a final concentration of 1 mM to the re-suspended pellet prior to lysis to inhibit protease activity. After sonication, the lysate was spun at 18,500 rpm (41,399 g) for an hour. The cleared supernatant was loaded on a Nickel-NTA column (GE), and the protein was eluted using an imidazole gradient in the lysis buffer. After elution off the Ni-column, the protein was loaded on Superdex-200 (GE) equilibrated in the lysis buffer without glycerol and PMSF to obtain protein which was >95% pure. The yield of the isotope labeled protein was ~0.8–1.0 mg/mL. For all protein-based assays described below, the protein concentrations were determined using the Bradford Protein Assay (Thermo Scientific Pierce). The standard curve for the assay was prepared using BSA (Thermo Scientific Pierce).

Site-directed mutagenesis. The Stratagene quikchange protocol was used to carry out several *Sw*HaCE point mutations. The complementary primers used to make the corresponding mutants are listed in the appendix (the underline indicates the mutated codon).

Phusion polymerase was purchased from New England Biolabs. The mutagenesis products were transformed into *E. coli* Dh5α cells for propagation. The mutations were confirmed using DNA sequencing results obtained from the DNA sequencing facility at Stony Brook University. The expression and purification of *Sw*HaCE mutants was carried out using same protocols as described above for the wild-type *Sw*HaCE protein.

Enzyme activity measurement assays. Two assay systems were used to analyze diguanylate cyclase and phosphodiesterase activity *in-vitro.* The first one use Malachite Green to detect the formation of inorganic phosphate via the following reaction scheme (equations 3-6). The shift in absorbance maxima from 446 nm (yellow) to 640 nm (green) indicates presence of of Pi.

GTP + GTP → cyclic-di-GMP + 2 PPi (inorganic pyrophosphate) (3)

2 PPi + IPP (Inorganic pyrophosphatase) → 4 Pi (inorganic phosphate) (4)

$Pi + (NH_4)MoO_4 + H^+ \rightarrow H_3PMo_{12}O_{40}$ (5)

$H_3PMo_{12}O_{40}$ (yellow) + $HMG^{2+} + H^+ \rightarrow (MG^+)(H_2PMo_{12}O_{40})$ (green) (6)

The SensoLyte® MG phosphate assay kit was purchased from AnaSpec. Synthetic GTP was purchased from Promega, synthetic c-di-GMP and pGpG were purchased from Biolog. For the enzyme assays, *Sw*HaCE by itself (final concentration of 1 μM) was added to a prepared solution containing 0.2 mM GTP (substrate), 5 mM $MgCl_2$, 1x buffer (50 mM Tris base, 10 mM $MgCl_2$, pH 7.5) in a final volume of 200 *μ*L. The reaction was incubated for 10 min at 25 °C followed by boiling at 100 °C to quench the reaction. After cooling, the mixture was spun at 14000 rpm (16,873 g) for 5 min to remove any precipitate. 70 μL of the supernatant was mixed with 10 μL of 3U/ml IPP (inorganic pyrophosphatase, NEB) in a 96-well plate and incubated at 25 °C for 10 min to hydrolyze inorganic pyrophosphate (PPi) produced during the reaction. Following this, 20 μL of Malachite Green reagent was added, mixed, and the plate was read at

610 nm using a Perkin Elmer Viktor X5 microplate reader. The absorbance readings were corrected for protein only and GTP only background. This experiment measured the initial velocity for the diguanylate cyclase activity for WT *Sw*HaCE and *Sw*HaCE PDE enzyme mutants. This experiment was repeated in at least three fully independent experiments. For quantifying the effect of *Sw*H-NOX Fe(II) on the cyclase activity of *Sw*HaCE mutants, *Sw*HaCE by itself (1 μM), or in the presence of the WT *Sw*H-NOX Fe(II)-unligated complex in a 1:20 concentration ratio, was incubated on ice for 10 min to allow the proteins to form a complex. The protein mixtures (20 μL) were then added to 180 μL a prepared solution containing 200 μM GTP (substrate), 5 mM $MgCl_2$, 1x buffer (50 mM Tris base, 10 mM $MgCl_2$, pH 7.5) in a final volume of 200 μL. the rest of the procedures was same as WT *Sw*HaCE.

The second assay involved separating nucleotides on a reverse-phase HPLC column and detecting them using a 254 nm detector. For this the proteins were incubated with 0.2 mM GTP as the substrate along with the buffer- 5 mM $MgCl_2$, 1x buffer (50 mM Tris base, 10 mM $MgCl_2$, pH 7.5) in a final volume of 200 μL. after removing a 0 time point, the reactions were allowed to incubate overnight. The next day, the reaction was quenched by boiling at 100 °C. After cooling, the mixture was spun at 14000 rpm (16,873 g) for 5 min to remove any precipitate. Then, a 1 mL syringe and 0.2 μm filter was used to remove any insoluble particles. 25 μL of the filtered supernatant was injected on a C18 reverse phase column (Waters) with an attached C18 guard column, and the nucleotides were separated using a methanol-phosphate-TBAOH gradient (buffer A: 100 mM potassium diphosphate, TBAOH, pH 7.0; buffer B: 10 mM potassium diphosphate, TBAOH, 30% methanol, pH 5.5). Nucleotide eluents were collected and analyzed by comparison to standard nucleotides and also by mass spectrometry.

Sedimentation equilibrium. Experiments were carried out at 4 °C on Beckman Optima XL-Analytical ultracentrifuge using an An-60 Ti rotor. For the sedimentation equilibrium experiments

with wild-type *Sw*HaCE and *Sw*HaCE PDE mutants alone, the enzymes were analyzed at 3 rotor speeds (9000 rpm, 14000 rpm, and 18000 rpm; g-force of 6520, 15777 and 26081 respectively), which were calculated using the molecular weight of *Sw*HaCE (74.5 kDa). Two scans were collected at the end of each speed. Protein absorbance was followed at 280 nm and 260 nm. The data was analyzed using HeteroAnalysis software (University of Connecticut Analytical Ultracentrifugation Facility) to determine molecular weight for *Sw*HaCE/*Sw*HaCE PDE mutants alone in solution. The data were fit globally across samples and speeds to yield apparent molar mass.

For the equilibrium experiments with the complex of *Sw*H-NOX/*Sw*HaCE PDE mutants, the enzymes were incubated with the WT *Sw*H-NOX Fe(II)-NO complex in a 1:1, 1:2, and 1:5 molar ratio, and analyzed at 3 rotor speeds (9000 rpm, 14000 rpm, and 18000 rpm; g-force of 6520, 15777 and 26081 respectively) with 2 scans at the end of each speed. The scans were collected at an absorbance of 400 nm to follow the heme absorbance of the *Sw*H-NOX Fe(II)-NO complex. The protein concentration was adjusted so that the absorbance was 0.5 at 400 nm. For the equilibrium experiments with *Sw*H-NOX alone, *Sw*H-NOX was analyzed at 3 rotor speeds (17000 rpm, 27000 rpm and 34000 rpm; g-force of 23263, 58682 and 93053 respectively), which were calculated using the molecular weight of *Sw*H-NOX (22.5 kDa).

3.3 RESULTS

Sequence analysis shows conservation of residues catalytic residues and loop6 residues in the bi-functional enzyme, SwHaCE. Sequence alignment of class I ExL domains (active PDE enzymes) and *Sw*HaCE reveals conserved residues required for catalysis and have predicted function in other characterized PDE domains (Fig 3-7).

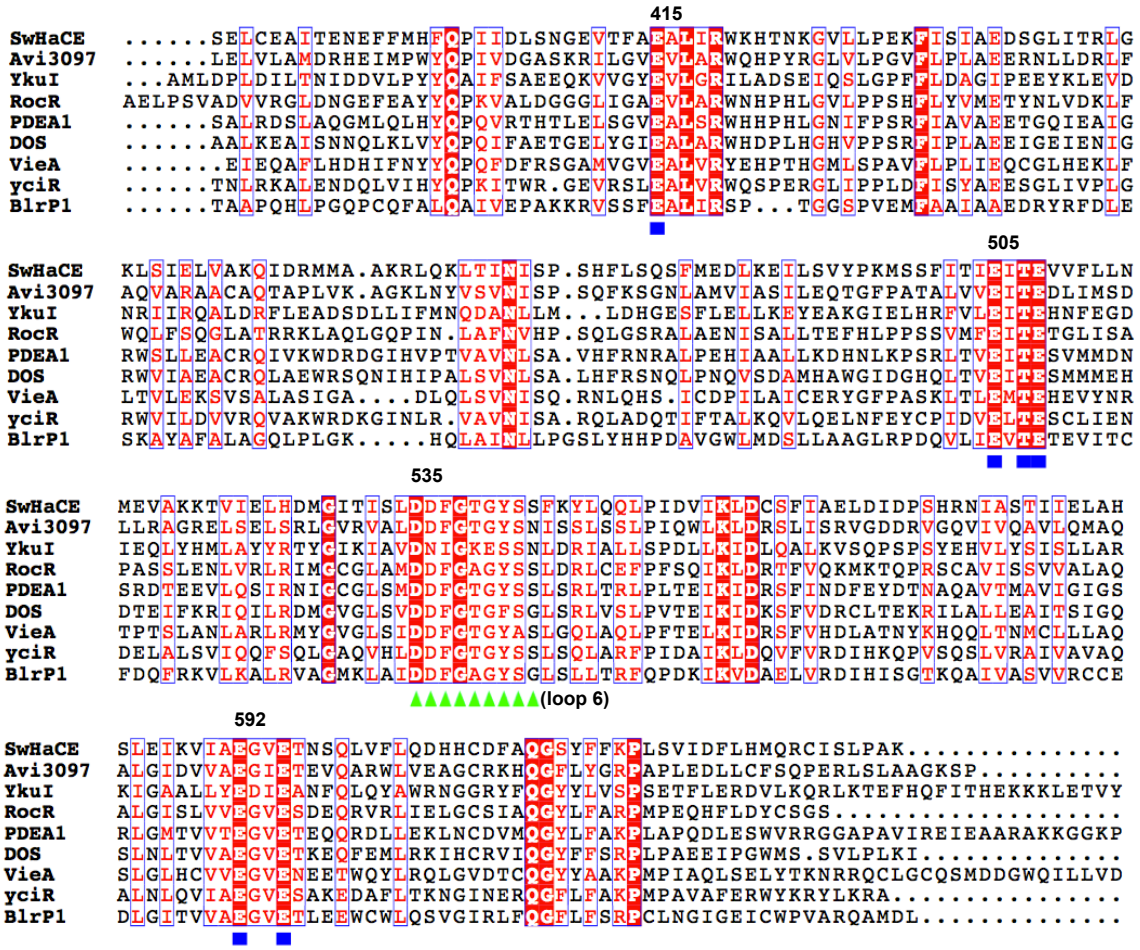

Figure 3-7: Sequence alignment for *Sw*HaCE EAL domain and other characterized EAL domains. The conserved residues are highlighted in red; the charged (Glu/E) residues are indicated by a blue box; green triangles indicate loop 6 for these enzymes.

A homology model of the PDE domain from *Sw*HaCE generated from other EAL domain crystal structures indicates conservation of the barrel shaped catalytic pocket (Fig 3-8). This conserved

active site in *Sw*HaCE contains the conserved loop 6 (as seen from sequence alignment), which is responsible for substrate sequestration, solvent exclusion and product release.

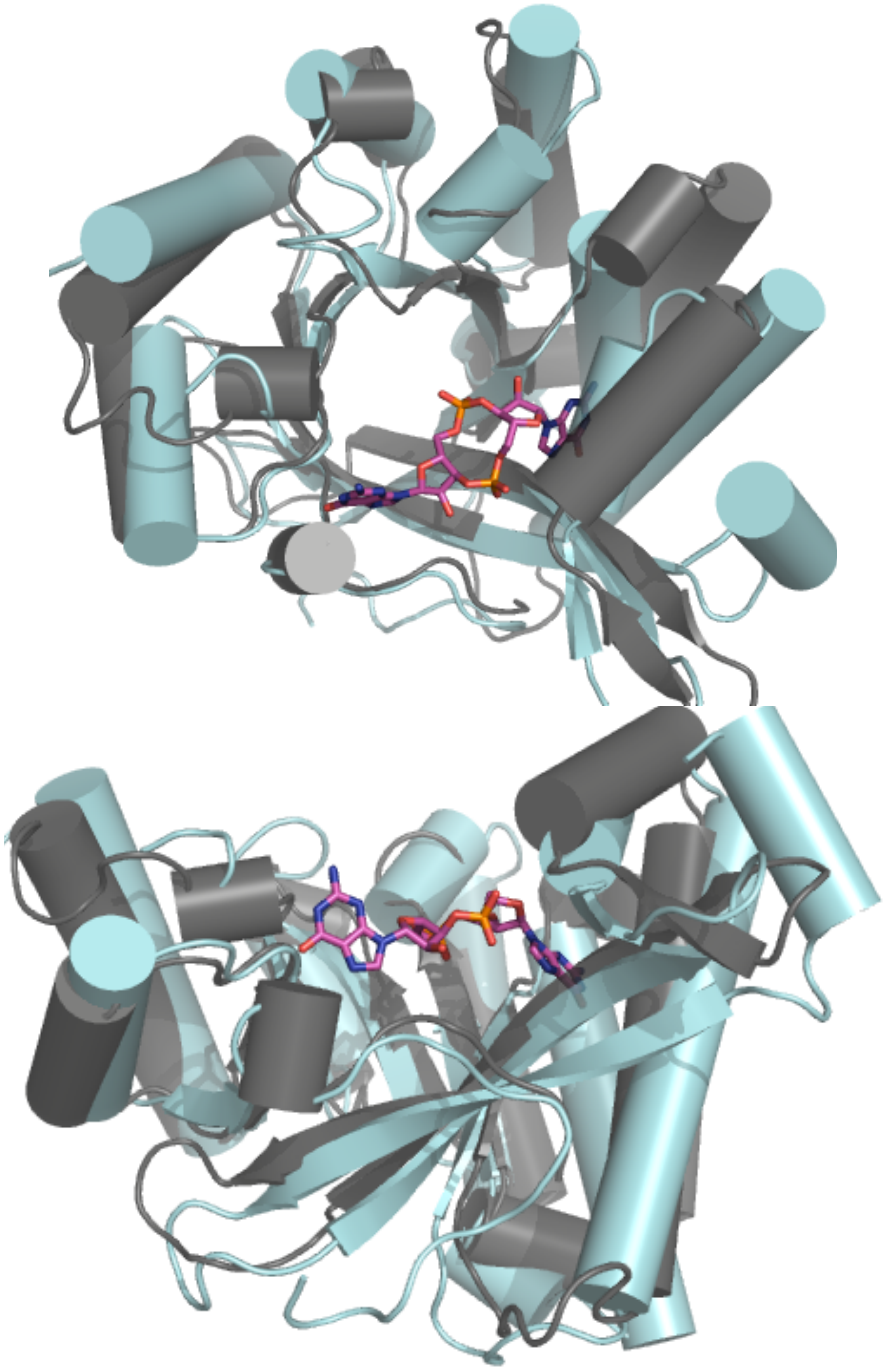

Figure 3-8: Structural alignment of *Sw*HaCE EAL domain (gray) with YkuI (*Bacillus subtilis,* PDB ID: 2W27, cyan); the top-and side- view of the domains is shown as bound to cyclic-di-GMP.

This includes 8 acidic residues (E415, D535, D536, E505, E501/9, E592, E595, D427), 2 basic residues (R419, K425, N, Q) and 4 neutral residues (F537, G538, Y541, S542) (Fig 3-6). Some of these residues were found in the conserved structural loop, loop 6. These 14 residues were further targeted for mutational studies to determine their role in acid/base catalysis.

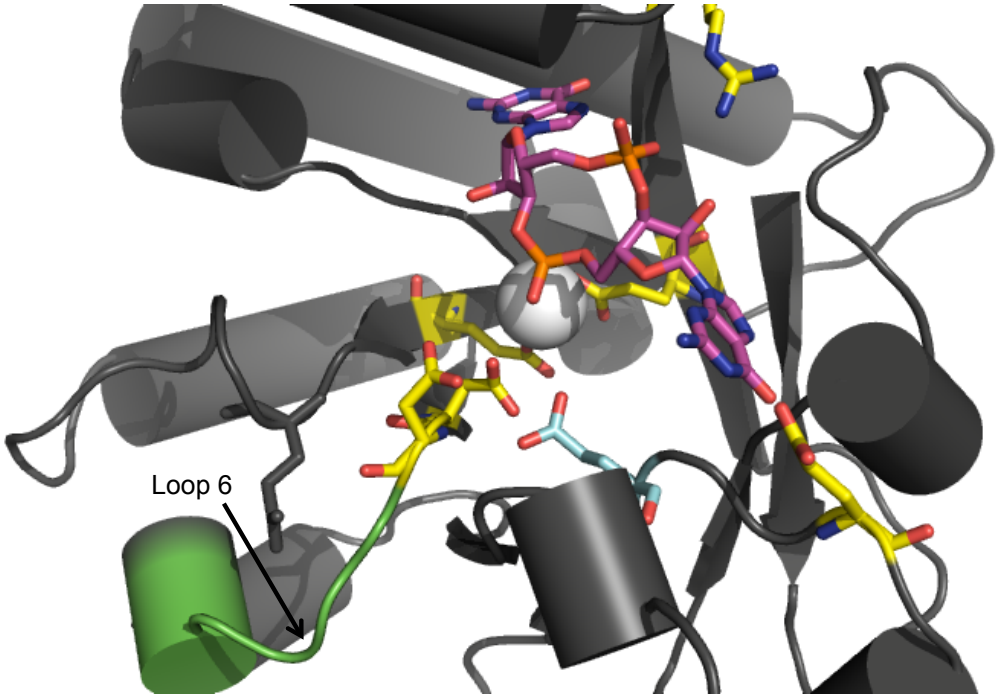

Figure 3-9: The proposed catalytic pocket of *Sw*HaCE EAL domain; the figure shows all the residues in the pocket required for catalysis. The important residues are highlighted in stick format - loop 6 (green), charged residues (yellow), the general base (blue) and substrate (pink).

A homology model generated using the crystal structure of RocR (PDB ID: 3SY8) was used to predict the putative active site for the PDE domain of *Sw*HaCE (Fig 3-9, 3-10). A closer look into the mapped active site illustrates the putative positions of various residues with respect to the bound substrate, cyclic-di-GMP. Mutants were designed to either achieve charge reversal or affect hydrophobicity, and determine the effect on catalytic activity.

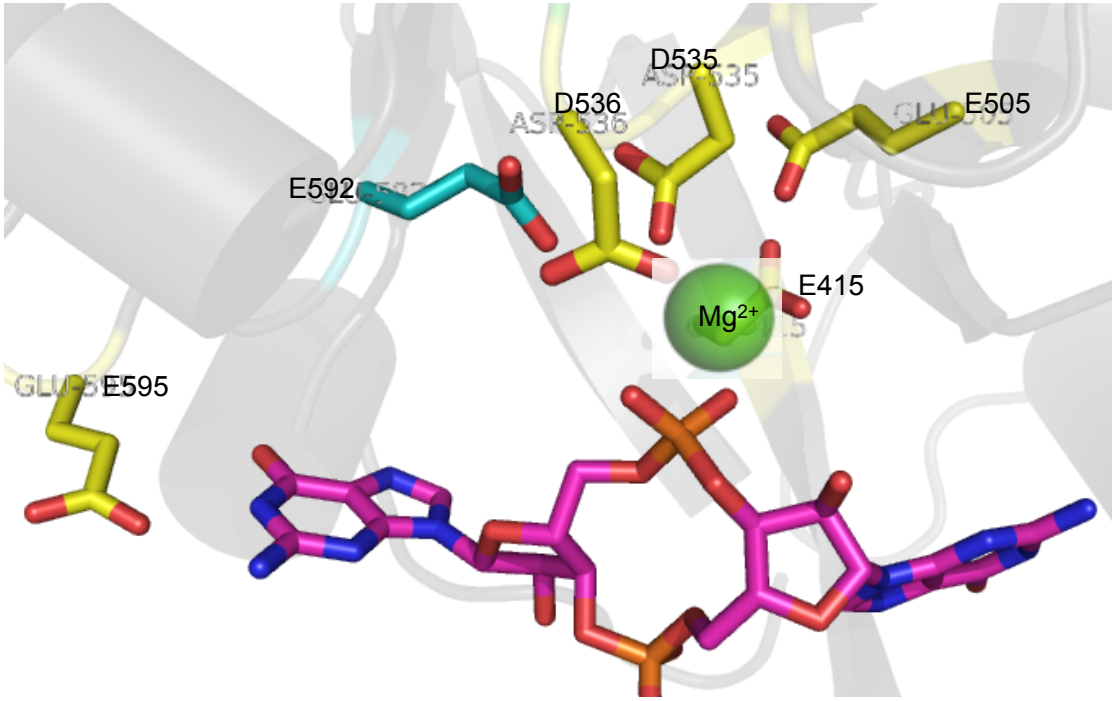

Figure 3-10: Close-up view of the proposed catalytic pocket of the EAL domain from *Sw*HaCE, with the substrate (cyclic-di-GMP, pink) bound. The main residues are highlighted in stick format, with the proposed general base (E592) in blue. The metal ion, Mg^{2+}, is shown in green.

Effect of catalytic and loop 6 mutants on activity.

In order to determine the role of each residue in the turnover of cyclic-di-GMP, we made point mutants to introduce charge reversal or decrease hydrophobicity. Table 3-1 highlights the residues chosen for mutation, the mutation made, and the proposed role of the residue in catalysis.

Table 3-1: List of residues in the PDE domain of *Sw*HaCE chosen for mutation to determine contribution to catalysis.

Mutation	Proposed Role in the PDE activity of *Sw*HaCE
E415A	Mg^{2+} binding
R419A	Mg^{2+} binding
W420A	Not determined
E505A/K	Cyclic-di-GMP coordination
D535A/K	Mg^{2+} binding
D536A	Mg^{2+} binding
F537A	Cyclic-di-GMP coordination
S542A	Mg^{2+} binding
S543A	Mg^{2+} binding
K556A	Not determined
E592Q	General base catalyst
E595A	Mg^{2+} binding

To determine the effect on cyclase and PDE activity, we followed the formation of pGpG by HPLC. Using GTP and cyclic-di-GMP as the substrates, the reactions with enzymes (wild-type and mutant *Sw*HaCE) were analyzed for the formation of cyclic-di-GMP and pGpG. With the wild-type enzyme, we saw formation of cyclic-di-GMP in the initial time-points, and complete

turnover to pGpG in the overnight reactions. However, for the mutant enzymes, we observed the accumulation of cyclic-di-GMP in the overnight reactions (Fig 3-11), but did not detect the appearance of any pGpG, proving abrogation of PDE activity due to various point mutants that we made in the EAL domain (table 3-2).

Table 3-2: Analysis of diguanylate cyclase and phosphodiesterase catalytic activity for wild-type *Sw*HaCE and mutants in the PDE domain of *Sw*HaCE. ✓ - indicates active enzyme, × - indicates inactive enzyme.

Enzyme	DGC activity	PDE activity
Wild type *Sw*HaCE	✓	✓
E415A	✓	×
R419A	✓	×
W420A	✓	×
E505A/K	✓/✓	×/×
D535A/K	✓/✓	×/×
D536A	✓	×
F537A	✓	×
S542A	✓	×
S543A	✓	×
K556A	Not tested	Not tested
E592Q	✓	×
E595A	✓	×

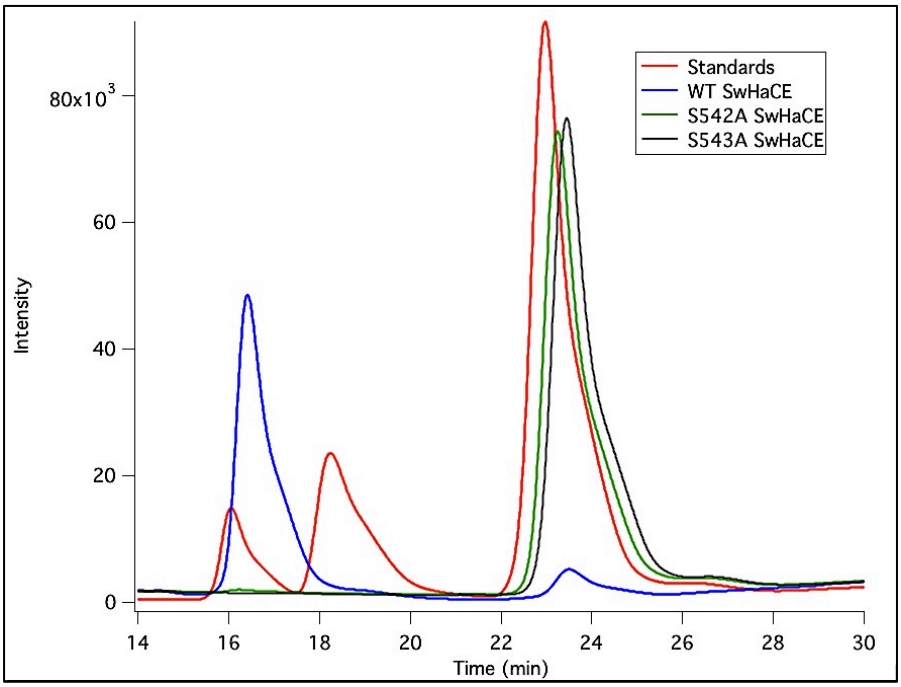

Figure 3-11: HPLC trace for EAL mutants with various mutations in active-site residues. The comparable trace for wild-type *Sw*HaCE is shown in blue. The retention time for standards is as follows: GTP - 18.4 min, cyclic-di-GMP – 23.7 min, and pGpG – 16.4 min.

SwH-NOX Fe(II) binds and increases the cyclase activity of WT and mutant SwHaCE enzymes. We have previously reported that in the presence of *Sw*H-NOX Fe(II), the diguanylate cyclase activity of *Sw*HaCE increases. We wanted to see if *Sw*H-NOX Fe(II) has the same effect on the PDE and loop 6 mutants, which would indicate that these mutations do not lie at the Fe(II) H-NOX/HaCE interaction. The enzymatic reaction of mutants only, or mutants in the presence of H-NOX Fe(II), using GTP as the substrate, was compared to WT HaCE reactions. These reactions were done under initial velocity conditions and do not represent kcat/Km changes. The change in initial velocity for WT HaCE cyclase activity upon adding H-NOX Fe(II) was comparable to the change in cyclase activity of the HaCE PDE mutants, showing around 33% increase in initial velocity (Fig 3-12). This confirms that the HaCE PDE and loop 6 residues do

not participate in the formation of the H-NOX/HaCE protein complex, and only control the PDE activity of HaCE.

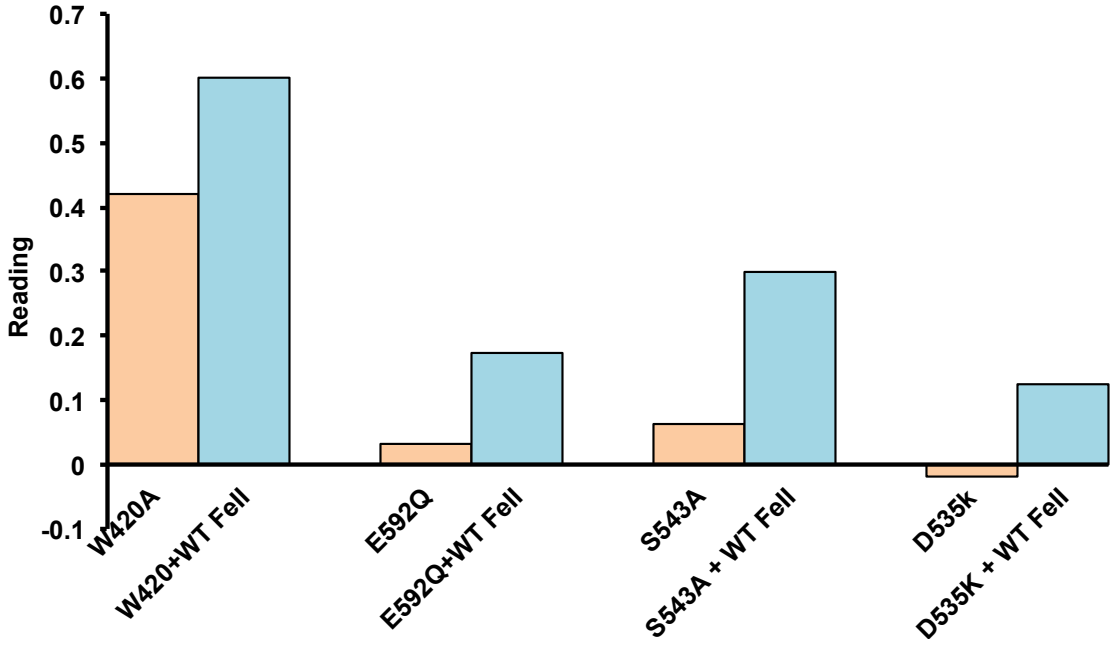

Figure 3-12: Effect of Fe(II) *Sw*H-NOX on the cyclase activity of *Sw*HaCE PDE mutants.

Mutations in loop6 and active site residues affect the oligomerization state of SwHaCE. Published crystal structures for PDE domains indicate that a homodimer/homotetramer formation is required for active PDE domains[77]. However, there is other evidence available supporting the activity of monomeric PDE domains. The unstructured loop, loop 6, which is located at the C-terminal of the active site pocket, is essential for activity. Structural studies also indicate that specific residues in loop 6 are part of the dimerization interface of EAL domain homodimers. We have previously determined that WT *Sw*HaCE is a dimer in solution. To confirm if loop 6 in *Sw*HaCE also mediates oligomerization, we analyzed the PDE and loop 6 mutants of HaCE by sedimentation equilibrium analysis. Since wild-type *Sw*H-NOX/*Sw*HaCE form a heterotetramer in solution, we also analyzed a mix of NO-bound *Sw*H-NOX and mutants to follow oligomerization of the formed protein complex.

Some of the analyzed mutants were observed to be monomeric in solution (table 3-3), which is different from the expected dimeric state of the wild-type enzyme. We observed both 1:1 and 1:2 stoichiometry for the NO-bound *Sw*H-NOX/mutant *Sw*HaCE enzyme mix. We hypothesize that the introduced mutations cause this change and ambiguity in oligomeric state due to disruption of the EAL-EAL protein dimerization interface.

Table 3-3: Sedimentation equilibrium analysis for *Sw*HaCE PDE mutants.

Protein sample[a]	**Calculated Mw/(Theoretical Mw) kDa**	**Oligomeric state**
Wild type *Sw*HaCE	144.0/ 74.5	Dimer
D535K	98.3/ 74.5	Monomer
S543A	82.5/ 74.5	Monomer
S542A + NO-bound *Sw*H-NOX	86.5	1:1
S543A + NO-bound *Sw*H-NOX	142.0	1:2

[a]Whenever applicable, all samples contain a 1:1 molar mix of the binding partners.

Analysis of divalent metal cations required for PDE activity.

Functional analyses of other phosphodiesterase enzymes report the divalent metal cation dependency of PDE activity. For the wild-type *Sw*HaCE activity, we did an activity analysis to determine the effect of different metal cations. Hydrolysis of cyclic-di-GMP and formation of pGpG was followed in the absence of any metal ion, with subsequent addition of different divalent metal cations individually - Mg^{2+}, Mn^{2+}, Ca^{2+}, Zn^{2+}, Co^{2+} and Ni^{2+} (Fig 3-13).

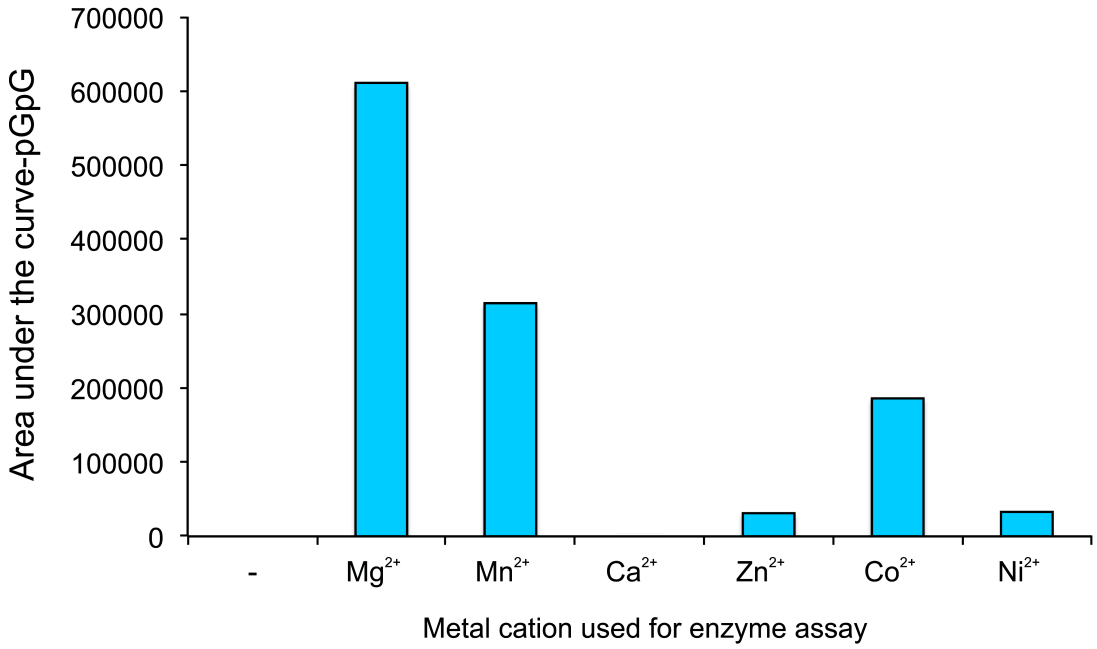

Figure 3-13: PDE activity of *Sw*HaCE wild-type enzyme in the presence of different metal cations.

In the presence of Mg^{2+} and Mn^{2+}, *Sw*HaCE demonstrated the highest PDE activity. In the presence of Co^{2+}, the activity was slightly lower. The PDE activity was lowest for Zn^{2+} and Ni^{2+}, whereas Ca^{2+} completely inhibited PDE activity. This is similar to the trend observed in previous studies, where Ca^{2+} is a known to be an inhibitor of PDE activity.

3.4 Discussion

DGC and PDE enzymes maintain the intracellular pool of cyclic-di-GMP via synthesis and hydrolysis. ExL motif containing PDE domains have been characterized in stand – alone proteins to determine the functional and structural aspects of this unique enzyme domain, whose catalytic pocket is similar to TIM barrel proteins. In this study, we have elucidated the catalytic role of the residues found in the PDE domain of a bi-functional enzyme *Sw*HaCE. This is the first biophysical and enzymatic characterization of an NO/H-NOX regulated PDE domain from a bi–functional enzyme. These in-vitro assays further interpret the domain organization and inter relationship of GGDEF and EAL domains in bacteria, which are often encoded in the same protein and catalyze functionally reversed reactions. This dynamic switch in the same protein, where the activity of one enzymatic domain is dramatically upregulated over the other in the presence of a signal (NO), hints at the cryptic regulation of cyclic-di-GMP levels within the cell.

Sequence alignment of *Sw*HaCE with class I ExL enzymes shows conservation of residues predicted to participate in the catalysis of cyclic-di-GMP. This includes charged residues that coordinate a divalent metal cation (Mg^{2+}, Mn^{2+}), bind the substrate cyclic-di-GMP and catalyze the cleavage of the phosphodiester (P–O) bond. Along with these conserved residues, we also investigated the role of the structural loop (loop 6), with respect to substrate turnover. The loop 6, which was identified by the motif DDFGTGYSS, was found to be conserved (fig 3-5). From these conserved polar residues, the ones predicted to be most pertinent to catalytic activity were chosen for mutational study (figure 3-8, table 3-1). The mutations were designed to switch charge (E → K), completely abolish charge (E → A) to disrupt ionic interactions and salt bridges, and disrupt hydrophobic interactions (F → A). A hydrophobic residue, W420, was found to be conserved in active EAL domains, and was mutated to an alanine (W → A) to test its role in

enzymatic activity. As seen in the structural model of *Sw*HaCE, this residue is positioned outside the catalytic pocket. This residue has never been shown to participate in enzymatic catalysis. We show here that mutating this tryptophan abolishes activity, indicating that this residue might be playing a structural role in catalysis by monitoring substrate entry into the pocket.

All the mutations we made in the active site as well as loop 6 residues completely abolished activity, confirming their participation in cyclic-di-GMP hydrolysis. An important difference in the bi-functional enzyme *Sw*HaCE compared to the mutations in other characterized EAL domains like RocR, was that while some of the mutations led to a slower enzyme in RocR but did not completely abolish activity, we observed complete abrogation of activity for the *Sw*HaCE mutants. This indicates that in bi-functional enzymes, the catalytic pocket containing the active site residues could be arranged in a different fold, or the secondary structure of the catalytic pocket could be different. These subtle differences could be a consequence of the N-terminal active GGDEF domain, making this observation important for bi-functional enzymes. This also stresses the need to analyze PDE enzymes from bi-functional, as this can offer more insight into their function.

Sedimentation equilibrium experiments done to elucidate the structural effect of the catalytic and loop 6 mutations showed change in oligomerization state of the mutants as compared to WT *Sw*HaCE (table 3-3). As compared to RocR, we observed a monomeric state for some of the mutants, whereas the corresponding RocR mutants were found to aggregate in inclusion bodies. This result also hints towards a possibly distinct structural orientation of bi-functional enzymes as compared to stand-alone PDE domains.

Lastly, we wanted to know if these catalytic and loop 6 residues in *Sw*HaCE mediate/affect its interaction with *Sw*H-NOX. We have previously shown that *Sw*H-NOX/*Sw*HaCE interact to form a heterotetrameric complex in solution. We have also shown that *Sw*H-NOX Fe(II) complex increases the cyclase activity of WT *Sw*HaCE by forming a protein complex. Hence, we analyzed the cyclase activity of *Sw*HaCE mutants in the presence of *Sw*H-NOX Fe(II) to determine if there is a change in cyclase activity due to protein – protein interactions. Enzymatic assays show that *Sw*H-NOX Fe(II) does indeed increase the cyclase activity of active site and loop 6 mutants similar to WT *Sw*HaCE.

These studies show that the residues chosen for the study play important role in the regulation of the phosphodiesterase catalytic activity from the bi-functional enzyme *Sw*HaCE. The role of these predicted residues in the proposed active site, as determined by homology models, has been confirmed using structure-function studies. Overall, structure-function studies of these enzymatic domains increase our understanding about the functional regulation of such enzymes, and the general control of the intracellular pool of cyclic-di-GMP.

CHAPTER 4: EXPLORING THE SYNERGISTIC ROLE OF NITRIC OXIDE AND *CIS*-2-DECENOIC ACID AS BIOFILM DISPERSAL AGENTS

Abstract: Bacterial lifestyle involves formation of the surface – attached, matrix enveloped biofilm state, from where a few cells disperse to colonize a new surface. This dispersal is often regulated by small molecules, which can be environmental factors (nitric oxide, NO; nutrient availability), intercellular and intracellular cues. The role of nitric oxide as a biofilm dispersal agent is well established. Also, secreted unsaturated fatty acids isolated from several bacteria have been shown to dictate interspecies signaling. One such organic compound, identified as *cis*-2-decenoic acid, has been isolated from *P. aeruginosa,* and shown to induce dispersion of biofilm microcolonies. This fatty acid is also shown to disperse biofilm in other bacteria. Reports indicate a possible adduct formation of fatty acid compounds and nitrating agents (NO, NO_2^-, NO_3^-, $ONOO^-$). There also have been reports that such adducts can act as signaling molecules to activate pathways. We have investigated the role of NO and DSF as required for biofilm formation and development. The biofilm growth studies in *Shewanella woodyi, Shewanella oneidensis* and *Pseudomonas aeruginosa* indicate a synergistic effect of NO and DSF in regulating biofilm dispersal in all of these species.

4.1 Introduction

Biofilms consist of bacterial communities living in close association under a protective camouflage, composed of an extracellular matrix[78]. Biofilms have been implicated in many infectious diseases, including hospital - acquired infections, oral and medical implant related health conditions[79]. The various stages of biofilm consist of initial attachment of cells to a viable surface, irreversible attachment, formation of a microcolony, and formation of a macrocolony, coupled with dispersion[80] (fig 4-1).

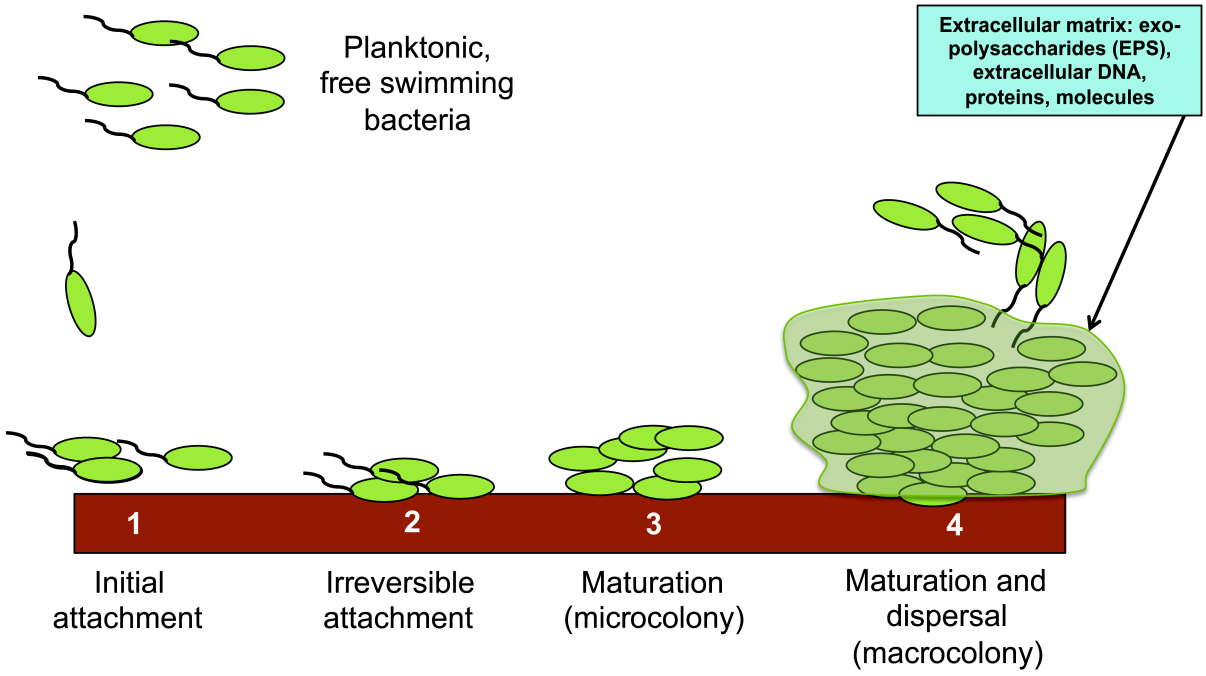

Figure 4-1: A biofilm consists of bacterial colonies engulfed in a polysaccharide matrix attached to a surface. The initial attachment to a surface is followed by irreversible attachment, when the bacteria start losing their flagella. Next, the cells accumulate to form a microcolony, which matures into a macrocolony, surrounded by a polysaccharide matrix. Often, a few cells in the biofilm can regain their flagella to exit the biofilm and recolonize on a different surface.

4.1.1 Small molecule regulated biofilm dispersal

Dispersal of cells from the biofilm is important for re-propagation of the colony[67]. These cells are responsible for repopulation of the biofilm at a different location. A number of environmental, intercellular and intracellular factors have been implicated in dispersal of bacterial biofilms[22, 81]. The environmental signals include nitric oxide (NO), which is a primary gaseous signaling molecule, and availability of nutrients. Various small molecules that participate in inter- and intra-cellular signaling have been isolated from bacteria (fig 4-2). These include fatty acids, acyl homoserine lactones (QS, quorum-sensing molecules), *Pseudomonas* quinolone, furanosylborate, glycopeptidolipids, phenazines, peptide signals, and cyclic-di-GMP (intracellular bacterial secondary messenger molecule)[81]. Most of these synthesized molecules are autoinducer QS molecules that regulate bacterial cell-cell communication. Together, these molecules have been implicated in cell-cell communication, interspecies signaling, and biofilm dispersal[82, 83].

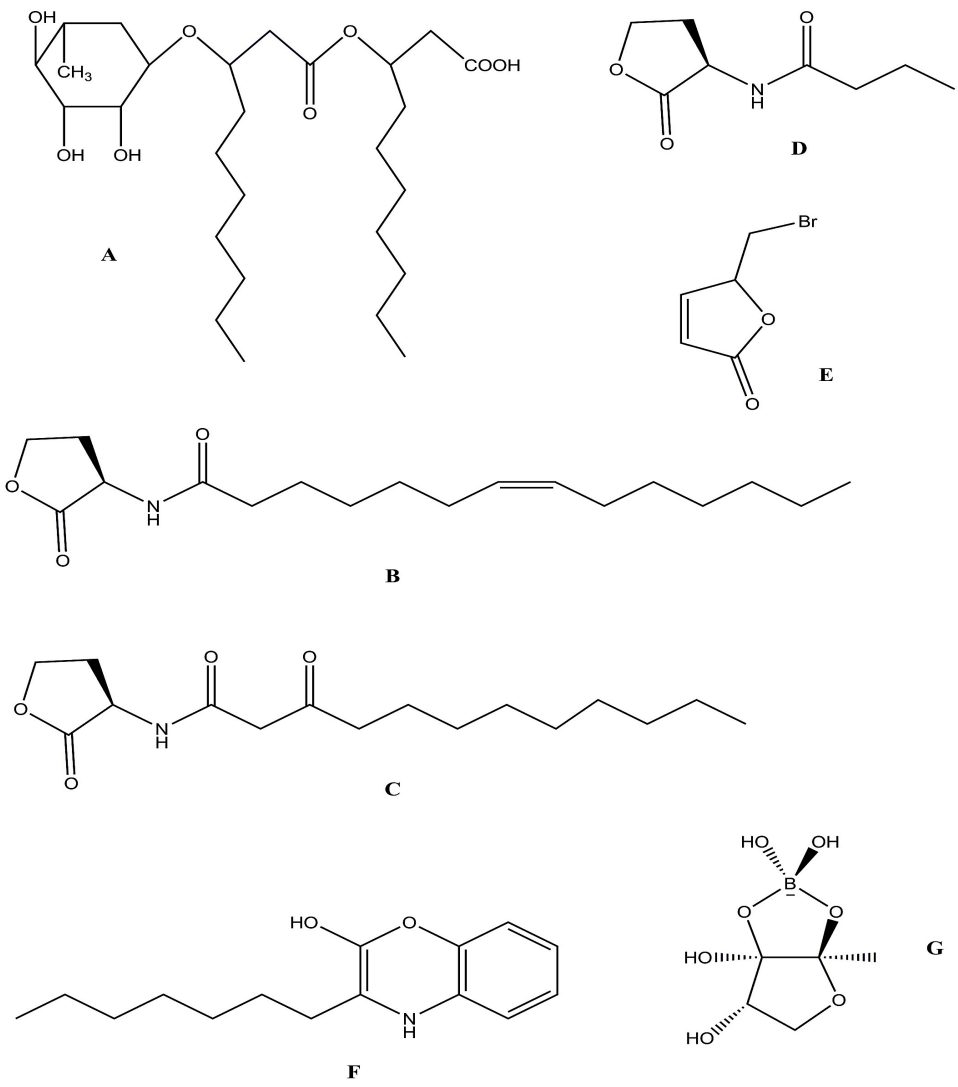

Figure 4-2: Chemical signals implicated in biofilm dispersal. (A) - Rhamnolipid, (B), (C) and (D) – acyl homoserine lactones (AHLs), (E) – furanone, synthetic inhibitor of PAO1 biofilms, (F) *Pseudomonas* quinolone signal, (G) – Furanosylborate (*V. cholera).*

Published reports have shown that low doses of NO can disperse biofilm in different species (*Pseudomonas aeruginosa, Shewanella woodyi, Staphyloccocus aureus, Staphyloccocus epidermidis, Candida albicans)[20, 84].* In most species, dispersion involves a significant change in the intracellular concentration of the bacterial secondary messenger molecule cyclic-di-GMP[13, 53]. NO was shown to affect and decrease the cyclic-di-GMP concentrations, inducing detachment.

Recent reports on fatty acid signaling indicate their definite role in detachment of cells[85]. Some unsaturated fatty acids from the DSF-family[86], such as *cis*-2-decenoic acid or DSF (Diffusible signal factor) isolated from *P.aeruginosa*, and *cis*-2-dodecenoic acid or BDSF (*Burkholderia* Diffusible signal factor), fig 4-3, isolated from *Burkholderia* have been shown to regulate intra- and interspecies biofilm dispersal[87-89].

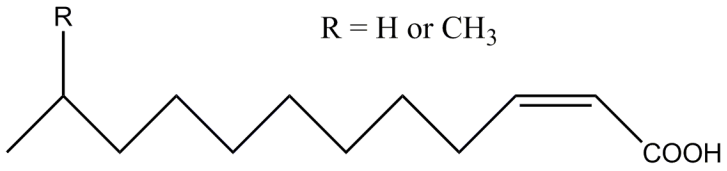

Figure 4-3: Fatty acid signal, *cis*-2-decenoic acid, also known as diffusible signal factor (DSF).

A recent study in *Burkholderia cenocepacia* identified a receptor protein RpfR for BDSF[90], containing Per/Ant/Sim (PAS), GGDEF and EAL domains. It was shown that BDSF negatively regulates the intracellular concentration of cyclic-di-GMP by stimulating the activity of the phosphodiesterase domain.

4.1.2 Nitrated fatty acid adducts

NO is a small, diffusible, rapidly reacting molecule containing an unpaired electron. Various nitrogen containing chemical signals have been shown to regulate bacterial lifestyle[91]. Studies indicate that certain nitrated molecules (NO, NO_2^-, NO_3^-, $ONOO^-$) add to the double bond in the unsaturated fatty acids, forming a transient adduct[92]. These adducts can participate in signaling processes[93, 94], although further investigation remains to be done to detect more of these adducts, and determine their role in signaling pathways.

This report discusses pilot studies quantifying the synergistic role of *cis*-2-decenoic acid and NO. We have quantified biofilms in both and non-pathogenic bacteria in the presence of NO by itself, *cis*-2-decenoic acid by itself, and NO + *cis*-2-decenoic acid. We also determined the effect of these molecules on growth rate to conform effect on biofilm formation as result of effect on pathway and not slower growth rate. This study provides an insight into the synergistic effect of *cis*-2-decenoic acid and NO on biofilm formation.

4.2 Materials and Methods

Bacterial strains and growth conditions. Steady-state biofilms for *S. woodyi and S. oneidensis* were grown as described previously[11, 13]. The following strains were used for biofilm growth: *S.woodyi (Sw)* strain MS32 (wild-type and Δ*hnox* mutant), *P. aeruginosa* strain PAO1 and *S.oneidensis (So)* strain MR-1. *Sw*MS32 was grown in Marine Media Broth (MM, 28 g/L, BD Difco) at 25 °C with agitation at 250 rpm. PAO1 was grown in Luria Broth (LB, 20 g/L, EMD chemicals) at 37 °C with agitation at 250 rpm. *So*MR-1 was Marine Media Broth (MM, 28 g/L, BD Difco) at 28 °C with agitation at 250 rpm. To determine growth rate, the optical density at 600 nm (OD_{600}) was measured every hour for 24 hours. Whenever required, the medium was supplemented with *Sw* and *So* colonies were selected on MM (14 g/L)/Bacto Agar (BA, 10g/L, BD Difco) plates. PAO1 colonies were selected on LB (20 g/L)/Bacto Agar (BA, 10g/L, BD Difco) plates.

Crsytal violet quantification of biofilms. For all the 3 strains, steady-state biofilm formation (at the air-liquid interface) was examined in 96-well polyvinyl chloride (PVC) plates, as described previously[95]. Briefly, a 100 μL subculture (overnight dilution of an overnight culture) in MM was incubated at 25 or 28 °C for 24 hours, for *S. woodyi or S. oneidensis,* respectively. For PAO1, a 100 μL subculture (overnight dilution of an overnight culture) in LB was incubated at 37

°C for 4 hours. The planktonic cells and media were then removed, and the biofilm was washed rigorously thrice with water followed by staining with 200 μL of 0.1% crystal violet (CV, dissolved in water). After staining for 5 minutes, the CV solution was removed, and the wells were washed with water thrice. Then, 100 μL of DMSO was added to the wells to dissolve the CV adsorbed by the cells in the biofilm. The CV in DMSO solution was transferred to a clear 96-well polystyrene plate, and the absorbance at OD_{570} was read using a Perkin-Elmer Victor X5 fluorescence plate reader. The data is reported as CV_{570}/OD_{600}, as the absorbance at 570 nm (CV_{570}) is divided by the absorbance at 600 nm (OD_{600}, for the planktonic and biofilm cells). For biofilms grown in the presence of nitric oxide, diethylenetriamine (DETA) NONOate was used as NO donors. NONOates (DETA/NO, Cayman chemicals, $t_{1/2}$ = 20 and 56 h at 37 and 22-25 °C) are compounds that are stable as solids and at basic pH, but dissociate spontaneously in a pH-dependent manner. The 100-fold diluted overnight cultures were diluted into fresh MM or LB medium supplemented with 200 μM DETA NONOate. The protocol for biofilm set-up was same as described above.

For biofilms grown in the presence of *cis*-2-decenoic acid and *cis*-2-decenoic acid/NO, 2 μL of the fatty acid compound (*cis*-2-decenoic acid, Sigma Aldrich) was dissolved in 100 μL of 100% ethanol to achieve a concentration of 10 μM. Then, the 100-fold overnight cultures were diluted into fresh MM or LB medium supplemented with 10 nM *cis*-2-decenoic acid or 10 nM *cis*-2-decenoic acid/200 μM DETA NONOate. The protocol for biofilm set-up was same as described above. The experiment was repeated in triplicate for generating error bars.

Confocal microscopy (CSLM) imaging for PAO1 and S. woodyi biofilms in the presence of NO and DSF. Microscopy images were collected on a Ziess LSM 510 metanlo two-photon Laser Scanning Confocal Microscope system. 15 mL of a 1:1000 dilution of an overnight culture of

*S.woodyi (*wild-type and Δ*hnox* mutant) or *S.oneidensis* in MM, and PAO1 in LB was added to a sterile 50 mL conical tube containing a glass slide. Biofilms were grown under steady-state conditions for 24 hours at 25 or 28 °C. For PAO1, the biofilms were grown for 4 hours at 37 °C. the medium was supplemented with DETA NONOate or *cis*-2-decenoic acid for growing biofilms with NO or *cis*-2-decenoic acid or NO/*cis*-2-decenoic acid.. Following the growth period, the slide was washed thrice with water, and the adhered biofilm cells were stained with the LIVE/DEAD *Bac*Light kit (Invitrogen), according to the manufacturer's protocol, for 15 minutes in the dark. For PAO1, the cells were fixed with 70% ethanol before adding the stain. The biofilm formed at the air-liquid interface was then analyzed and imaged. The biofilm thickness was (X–Z dimension) was measured at three different locations in each experiment to average the determined mean biofilm thickness.

Growth curves for cultures in the presence of NO and cis-2-decenoic acid*.* To determine the effect of NO and *cis*-2-decenoic acid on the growth rate of the bacterial strains, the cultures were grown in MM or LB supplemented with 10 nM *cis*-2-decenoic acid or 10 nM *cis*-2-decenoic acid/200 μM DETA NONOate. *Sw*MS32 was grown in Marine Media Broth (MM, 28 g/L, BD Difco) at 25 °C with agitation at 250 rpm. PAO1 was grown in Luria Broth (LB, 20 g/L, EMD chemicals) at 37 °C with agitation at 250 rpm. *So*MR-1 was Marine Media Broth (MM, 28 g/L, BD Difco) at 28 °C with agitation at 250 rpm. To determine growth rate, the optical density at 600 nm (OD_{600}) was measured every hour for 24 hours.

Pellicle formation for Shewanella oneidensis in the presence of NO and cis-2-decenoic acid*.* Pellicle biofilms for *S. oneidensis* were grown as described previously[96]. Briefly, overnight cultures containing *So*MR-1 strain in MM were inoculated into 15 mL fresh MM medium (1:100

dilution) in 50 mL conical tubes. After this, the cultures were left standing at 28 °C for 24 hours. To determine the effect of *cis*-2-decenoic acid, the fresh medium was supplemented with 10 nM *cis*-2-decenoic acid. After 24 hours, the medium was carefully discarded so as to not disturb the floating mass of pellicle biofilm formed on the air-liquid interface. Then, fresh medium was added to the tube, and the pellicles were vortexed to dissolve the cells. 5 μL of the dissolved pellicle was diluted in 500 μL of fresh buffer, and the OD at 600nm was read. This was repeated in triplicate for all cultures. To normalize the OD, different dilutions of the dissolved pellicle (1:10,000, 1:100,000 and 1:10,00,000) were plated on LB plates to determine the C.F.U units (colony forming units). The number of colonies on each plate was counted to determine the C.F.U., and dividing by the C.F.U. number normalized the OD for each culture.

4.3 Results

Small molecule signaling has been shown to play regulatory role biofilm dispersal. Two such well studied agents, NO and *cis*-2-decenoic acid, are shown here to induce a synergistic effect in biofilm dispersal.

Increasing concentrations of cis-2-decenoic acid *decreases the amount of biofilm formation.* It has been shown previously that *cis*-2-decenoic acid, molecule synthesized by *P. aeruginosa,* induces dispersal in various species[82, 88]. We used increasing concentrations of *cis*-2-decenoic acid in the growth medium to determine the effect on *S. woodyi* and *S. oneidensis* biofilms. Starting at 6 nM, we already observed around 50% decrease in steady-state biofilm formation in the presence of 12 nM *cis*-2-decenoic acid (fig 4-4). This confirmed the effect

observed earlier for flow biofilms in PAO1, where biofilm formation decreased in the presence of 2-5 nM *cis*-2-decenoic acid.

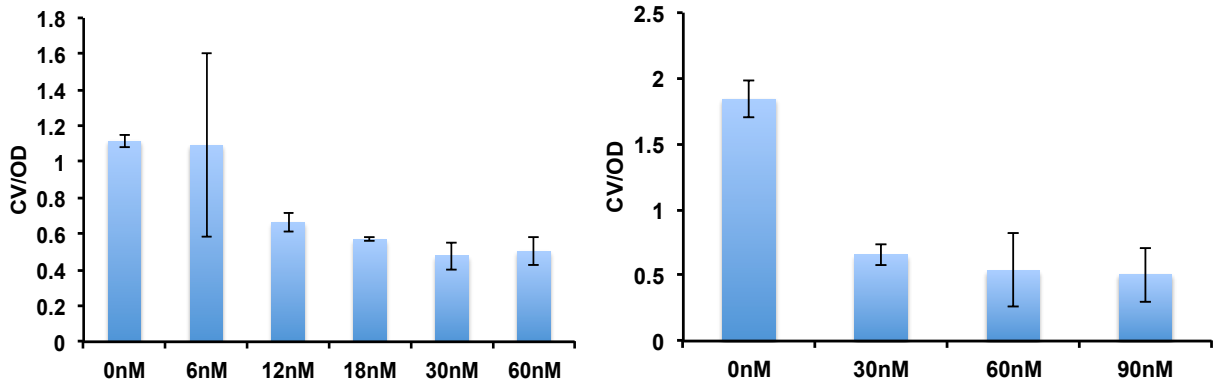

Figure 4-4: Crystal violet quantification of *S. oneidensis* in the presence of increasing concentrations of DSF.

We also did growth curves for *S. woodyi* and *S. oneidensis* in the presence of *cis*-2-decenoic acid, to rule out the decrease in biofilm formation due to impaired growth of the bacteria. The growth curve in the absence and presence of *cis*-2-decenoic acid was similar (fig 4-5), indicating that the effect on biofilm formation is not due to impaired growth.

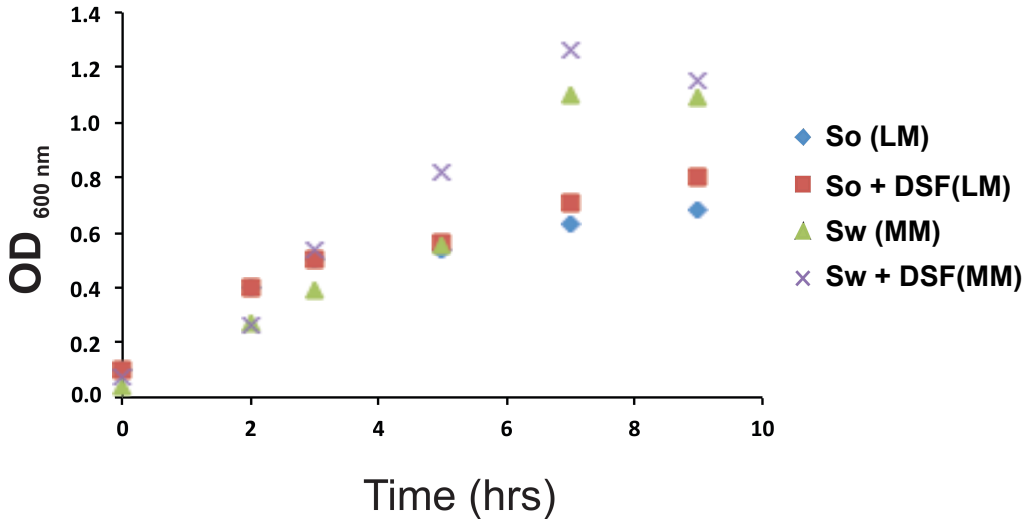

Figure 4-5: Growth curves for *S. oneidensis* and *S. woodyi* in LM and MM media, with and without 10 nM DSF.

To determine the co–effect of NO and *cis*-2-decenoic acid on biofilm formation, we grew steady-state biofilms for cultures supplemented with the NO-donor DETA NONOate, and *cis*-2-decenoic acid (fig 4-6).

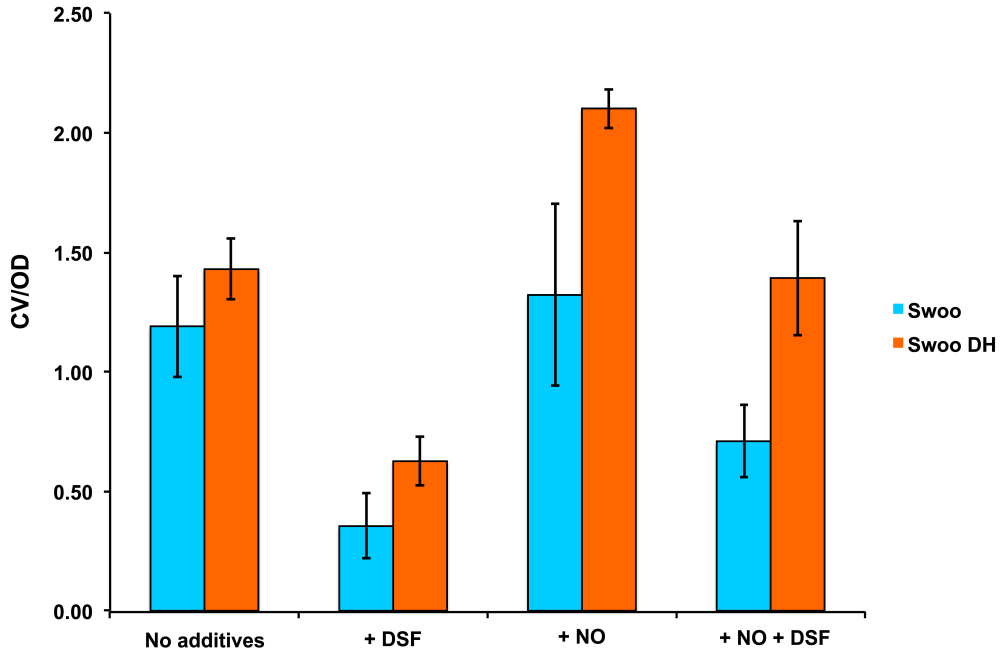

Figure 4-6: Crystal violet quantification for *Shewanella woodyi* biofilms *(*wild-type, Swoo and Δ*hnox* mutant, Swoo DH) in the presence of NO and 30 nM *cis*-2-decenoic acid.
S. woodyi showed biofilm formation in the presence of *cis*-2-decenoic acid and NO + *cis*-2-decenoic acid, as compared to NO only.

A few bacteria show pellicle formation during steady-state biofilm growth[97, 98]. Pellicles form in standing cultures as a floating mass of cells, which are essentially biofilms formed at the air-liquid interface, and not attached on a solid surface. These are quite fragile, and upon being shaken, can disintegrate. *S. oneidensis* is one such bacteria which has been shown to form pellicle biofilms[96, 99].

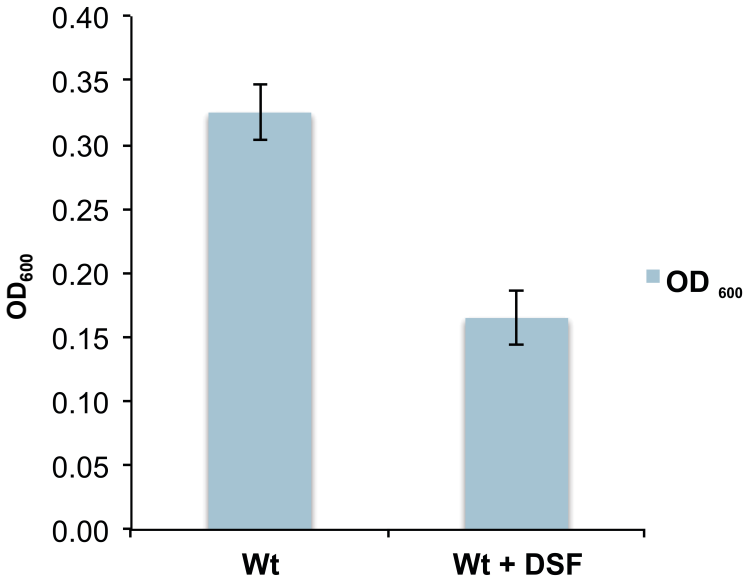

Figure 4-7: Pellicle formation in *Shewanella oneidensis* in the absence and presence of 10 nM *cis*-2-decenoic acid.

We wanted to confirm of *cis*-2-decenoic acid also affects and reduces pellicle biofilm formation in *S. oneidensis,* similar to the effect on steady-state biofilms. Incubation of the standing cultures for wild-type *S. oneidensis* pellicle biofilms with 10 nM *cis*-2-decenoic acid, as compared to no *cis*-2-decenoic acid, showed more than 50% decrease for the pellicles containing *cis*-2-decenoic acid (fig 4-7). This shows that *cis*-2-decenoic acid can affect different biofilm pathways (air-liquid, liquid-solid) in the same bacteria, establishing its role as a universal dispersal agent.

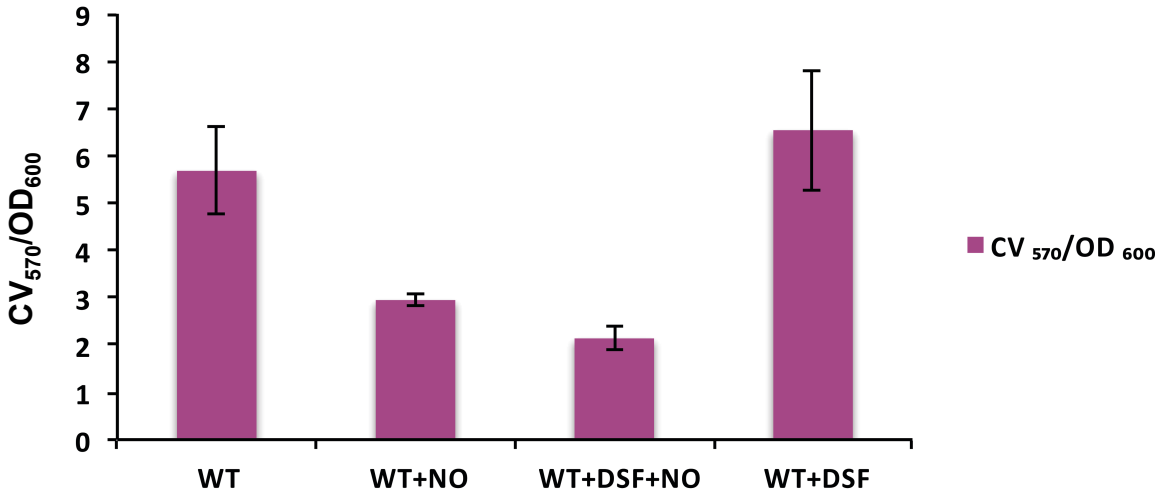

Figure 4-8: Crystal violet quantification of *P. aeruginosa* biofilm formation in the presence of NO and *cis*-2-decenoic acid.

The effect of *cis*–2–decenoic acid has been shown in PAO1 biofilms before, where it was observed to decrease biofilm formation in continuous biofilms grown in flow-cells[82, 88, 100]. Nitric oxide has also been shown to mediate dispersion in PAO1 and PA14 biofilms via a different pathway[20, 21, 53, 91]. Here, we show the combined effect of these two dispersal signals on PAO1 biofilms. Since *P. aeruginosa* forms robust biofilms, we chose a shorter time-point (5 hours) to analyze the effect of NO and *cis*-2-decenoic acid (fig 4-8). Static biofilms grown in the presence of NO were less dense, as expected. However, in the presence of *cis*-2-decenoic acid, we observed a slight increase, as opposed to a decrease observed in earlier studies. This could be due to the shorter time-point, as the earlier studies have been done for longer time points (12-24 hours). To confirm this, we did control experiments to analyze biofilms grown for 24 hours in the presence of *cis*-2-decenoic acid (appendix), and noticed a decrease in biofilm growth. In the presence of both NO and *cis*-2-decenoic acid, the amount of biofilm formed was much lower. This indicates a possible synergistic effect of NO and *cis*-2-decenoic acid on biofilm formation, albeit via different pathways.

Confocal scanning laser microscope (CSLM) imaging of biofilms. Steady-state biofilms for *S. woodyi* and *P. aeruginosa* were grown on microscope slides at the air-liquid interface. The mature biofilms were stained with SYTO9 (green dye; stains live cells) and propidium iodide (red dye, stains dead cells only), and imaged using confocal microscopy (fig 4-9/4-10). This experiment was used to determine the thickness of the biofilm, as well as the density of cells within the biofilm. Most biofilms are known to form uneven structures that can sometimes include large, mushroom shaped macrocolonies. Hence, different spots were selected in the biofilm slide for analyzing the depth and density. Both *P. aeruginosa* and *S. woodyi* form robust biofilms, and hence we selected the time points – 24 hours (*S. woodyi*) and 4 hours (*P. aeruginosa)* to analyze biofilm formation.

For the *P. aeruginosa* biofilms, the cells were fixed with 70% ethanol to avoid contamination. Hence, only the dead cell stain (propidium iodide) could be observed. Comparing the biofilms without any additive, with +NO, + *cis*-2-decenoic acid, and +NO+ *cis*-2-decenoic acid biofilms, we observed decrease in both biofilm thickness and cell density (fig 4-9). The cultures containing +NO+ *cis*-2-decenoic acid showed maximum decrease as compared to *P. aeruginosa* alone (fig 4-10).

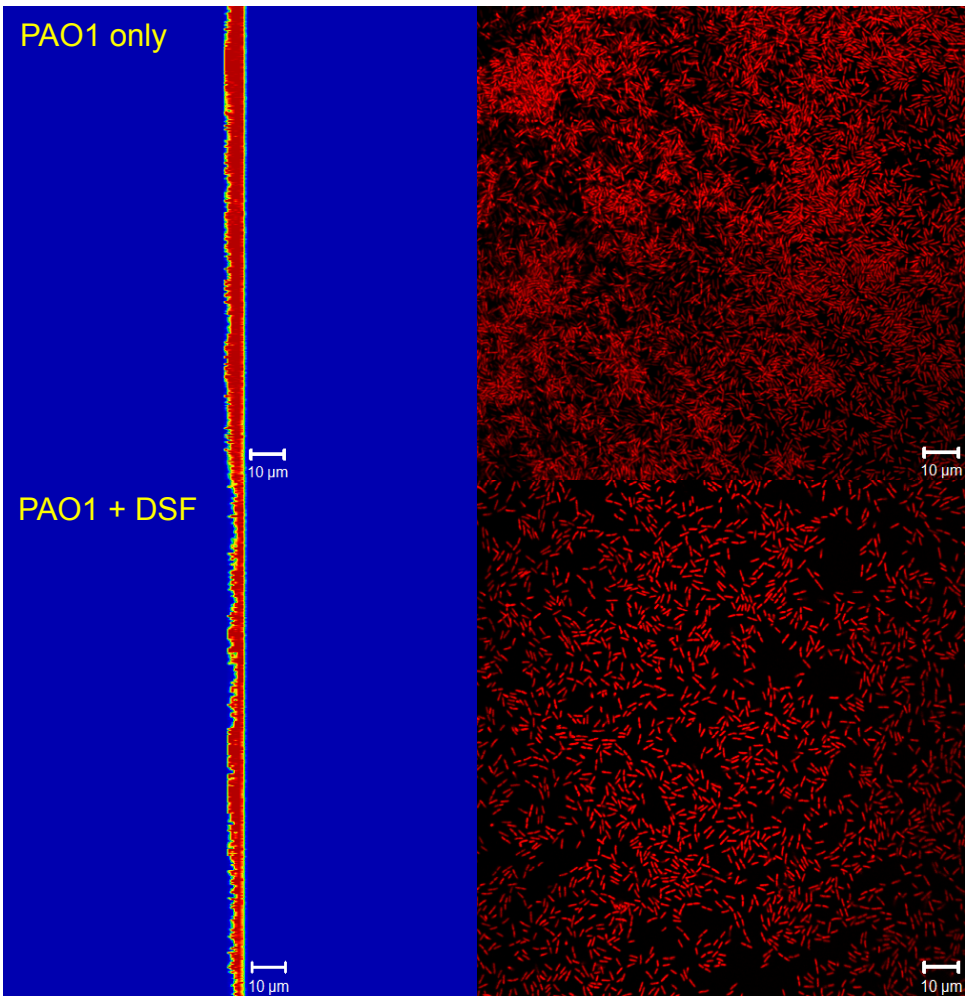

Figure 4-9: CSLM images and z-stack for PAO1 biofilms in the absence and presence of 10 nM *cis*-2-decenoic acid, top-panel; left – PAO1 z-stack, right – PI stained cells; bottom-panel; left – PAO1 + *cis*-2-decenoic acid z-stack, right – PI stained cells.

In the presence of NO, the density of cells decreased only slightly as compared to PAO1 only, but the biofilm was thinner (fig 4-10). These results are similar to the observation for the crystal violet quantification of steady-state biofilms, thus establishing the effect of NO and *cis*-2-decenoic acid in biofilm dispersion in PAO1. The change in biofilm thickness for various cultures grown in the presence of NO or *cis*-2-decenoic acid is shown in fig 4-11.

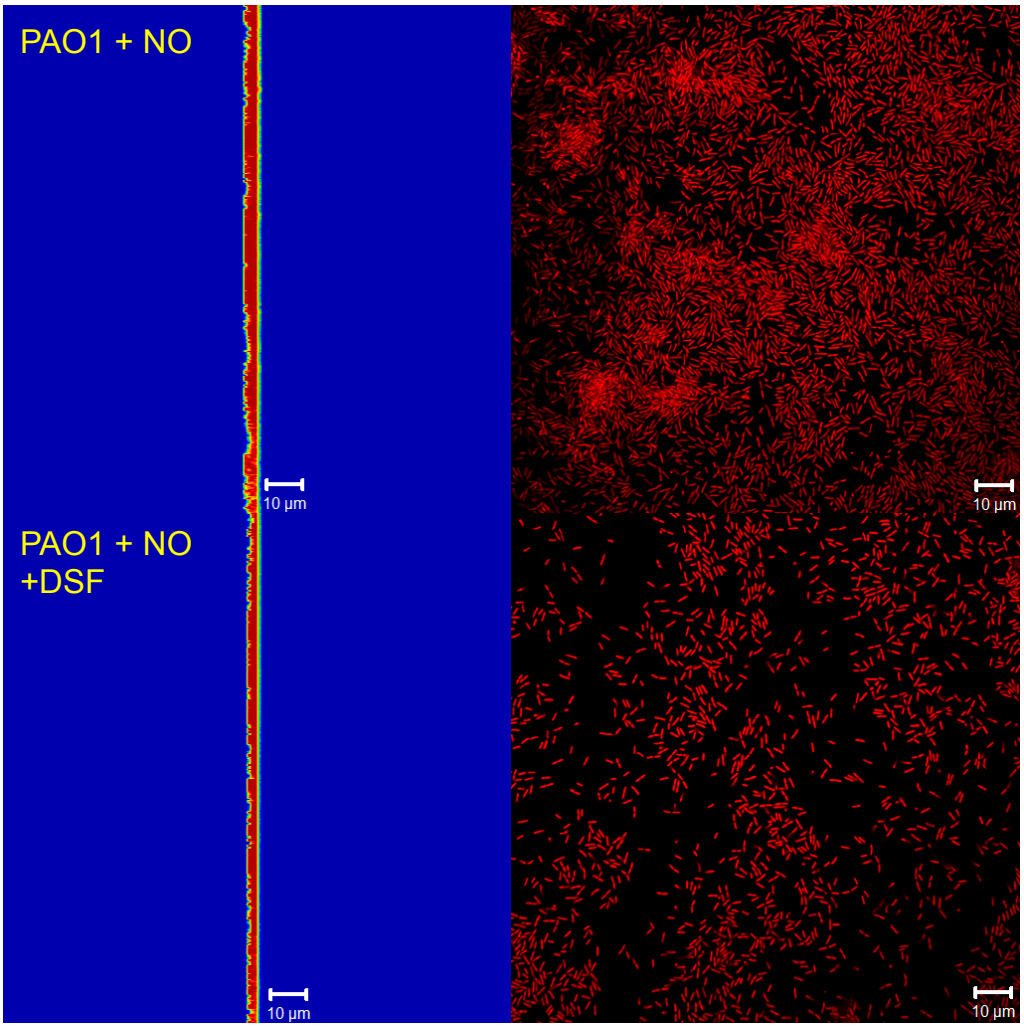

Figure 4-10: CSLM images and z-stack for PAO1 biofilms in the presence of NO only, and NO + *cis*-2-decenoic acid, top-panel; left – PAO1+ NO z-stack, right – PI stained cells; bottom-panel; left – PAO1 + *cis*-2-decenoic acid + NO z-stack, right – PI stained cells.

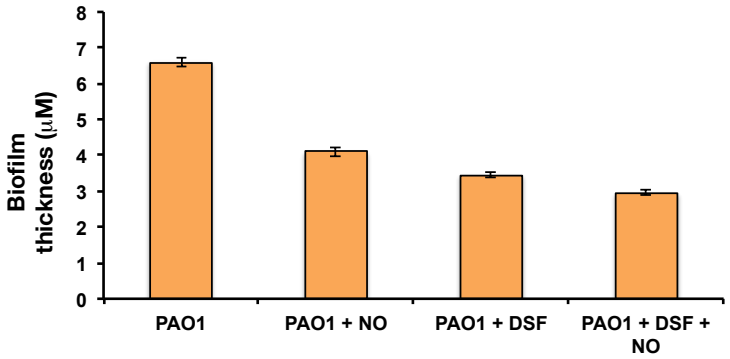

Figure 4-11: Biofilm thickness for PAO1 biofilms, grown without or in the presence of NO, *cis*-2-decenoic acid, and both.

We have previously shown that *S. woodyi* forms robust biofilms, and NO disperses biofilm via an H-NOX regulated pathway, decreasing cyclic-di-GMP levels in the bacteria[13]. Here, we wanted to test the effect of NO + *cis*-2-decenoic acid on biofilms formed by the wild-type strains. Confocal images show that NO decreases both density and biofilm thickness (fig 4-11), as seen before. However, for the culture grown in the presence of *cis*-2-decenoic acid, along with decrease in cell density we also observed long strands, which look like elongated cells. We also observed these elongated cells for NO + *cis*-2-decenoic acid cultures (fig 4-11); however, the density of the cells was higher. These elongated cells have been observed in bacterial biofilms before, and are recognized as a representation of highly efficient swarmer cells that do not biofilm as well as wild-type cells[101]. Swarming is often found to be opposite to biofilm in nature, as swarmer cells glide across surfaces for nutrients, as opposed to a biofilm, where they settle down[18, 102]. Hence, *cis*-2-decenoic acid may affect the cells by inducing swarming phenotype, thus reducing the ability of bacteria to form biofilms.

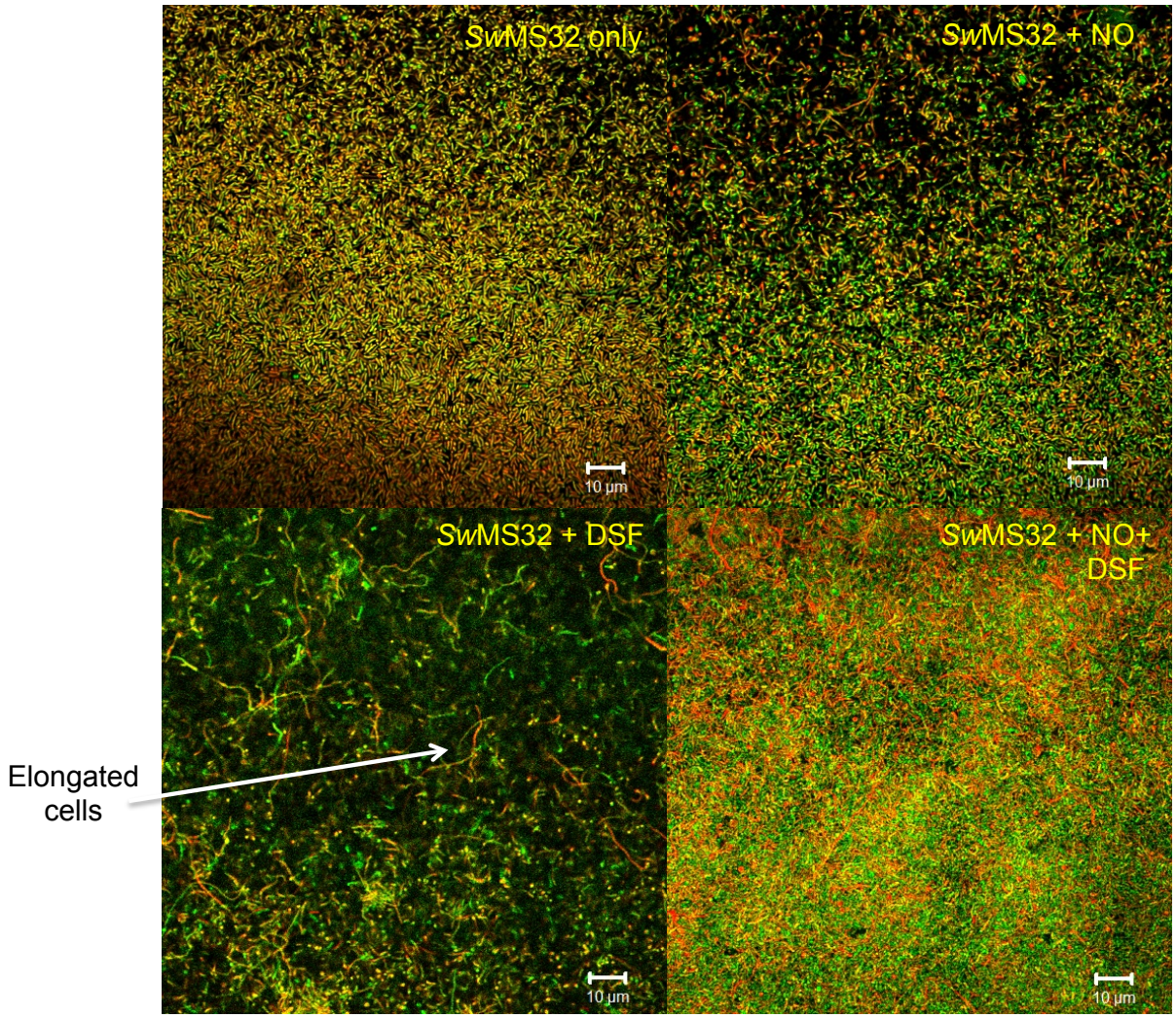

Figure 4-12: CSLM images for *Sw*MS32 (*Shewanella woodyi wild-type)* biofilms; from top-left, clockwise: *Sw*MS32 by itself, *Sw*MS32 + NO, *Sw*MS32 + *cis*-2-decenoic acid, and *Sw*MS32 + NO + *cis*-2-decenoic acid.

4.4 Discussion

Biofilm formation is a dynamic process involving continuous phenotypic changes. This involves changes in the flagellar synthesis, polysaccharide synthesis, and cell-cell communication or quorum sensing. There are various signals that have been identified to affect and control some of these pathways. Bacteria synthesize most of these signals themselves to induce dispersal, and this often offers a method of repopulating different energy sources. Sometimes, dispersal

also provides a way to escape harsher environmental conditions, thereby highlighting a natural defense mechanism used by bacteria for survival[103].

Cis-2-decenoic acid, an unsaturated fatty acid isolated from spent culture of various bacteria, has been shown to disperse biofilms in many bacterial species. Nitric oxide, a diffusible small gaseous signaling molecule, has been shown to diminish biofilm formation in a number of species, and often involves repression of biofilm via reducing intracellular levels of cyclic-di-GMP, an important bacterial secondary messenger. Recently, some proteins involved in the synthesis and degradation of cyclic-di-GMP have been shown to function as *cis*-2-decenoic acid receptors. This indicates a multi-level network of signaling control, regulating various pathways.

In this report, we have analyzed a possible synergistic effect of NO and *cis*-2-decenoic acid, two dispersal agents. Analysis of solid-liquid interface biofilms, and air-liquid interface biofilms grown in the presence of NO and *cis*-2-decenoic acid show marked decrease in cell density and biofilm thickness. We did not observe any change in the growth rate in the presence of these dispersal agents, indicating that the effect in biofilms may be due to a change in cellular function, and not deformed growth.

To conclude, the analysis of these two established dispersal agents, NO and *cis*-2-decenoic acid indicate that they may be acting together to induce dispersion. In nature, most signals participate in a cross talk of networks, which often overlap to favor a particular phenotype. Thus, it is probable that *cis*-2-decenoic acid and NO may function in a synergistic manner to induce dispersal. The pathways through which they function are still being identified, however,

regulation of cyclic-di-GMP concentrations is a probable target. Many signals repress the intracellular levels of this secondary messenger, and it has also been independently reported for NO and *cis*-2-decenoic acid, which negatively regulate cyclic-di-GMP concentration. Other possible targets could include two-component systems, involving kinases and response regulators. Together, this complex network of exogenous, intracellular and interspecies signals control this essential switch from sessile to motile lifestyle.

CHAPTER 5: STRCUTURAL STUDIES AND MODEL DEVELOPMENT OF THE *Shewanella Woodyi* BI-FUNCTIONAL ENZYME HaCE

Abstract: Bi-functional proteins containing GGDEF-EAL domains have been characterized as important players in bacterial signaling pathways. They are functionally responsible for regulating the intracellular cyclic-di-GMP pool. However, the structural characteristics of these enzymes are still being elucidated. Also, it is still being understood how these the activity of these domains is differentially regulated by various signals such as NO, O_2 and blue light. It has been shown that NO-bound H-NOX differentially regulates the dual activities of *Sw*HaCE. In this study, we have some preliminary SAXS studies with *Sw*HaCE by itself, equimolar mixture of *Sw*HaCE and *Sw*H-NOX Fe(II) unligated, and equimolar mixture of *Sw*HaCE and NO-bound *Sw*H-NOX. These experiments offer a structural view of the functional regulation of *Sw*HaCE by NO-bound *Sw*H-NOX. It also hints towards possible domain organization in such multi-domain and multi-functional proteins.

5.1 Introduction

Small-Angle X-ray Scattering (SAXS) studies are used to determine protein conformations in solution. These experiments offer a low-resolution structural model, which is sensitive to the shape and size of the protein[104-106]. The scattering profile of a protein in the presence and absence of a binding partner can provide an idea about the conformational changes associated with the protein-protein interaction.

In our system, we know that *Sw*H-NOX/*Sw*HaCE associate to form a protein complex. We have also shown that NO-bound H-NOX undergoes conformational perturbations and associates differently with *Sw*HaCE as compared to Fe(II)-unligated *Sw*H-NOX. We are currently in the process of doing SAXS experiments to determine a structural model for the *Sw*H-NOX/*Sw*HaCE complex. The experiments are being done for *Sw*HaCE by itself, *Sw*H-NOX Fe(II)-unligated/*Sw*HaCE complex (1:1 molar ratio) and NO-bound *Sw*H-NOX/*Sw*HaCE complex (1:1 molar ratio).

Previous crystal structures and SAXS studies of diguanylate cyclases from other organisms (PleD, *Caulobacter cresentus*; WspR, *Pseudomonas aeruginosa*) provide mechanistic details for this bacterial cyclase domain. The DGC domain, which catalyzed the cyclization of 2 molecules of GTP to form cyclic-di-GMP, has a fold that is similar to the mammalian adenylyl cyclase. Concentration based oligomerization (dimer, tetramer) has been shown to be important for maintaining activity. Structural studies provide evidence that the cyclase domain undergoes major conformational rearrangements upon adding substrate (GTP). Most of these structures indicate a compact structure in the absence of the substrate. However, upon adding GTP, the protein oligomers assume more elongated structures, which catalyze the reaction.

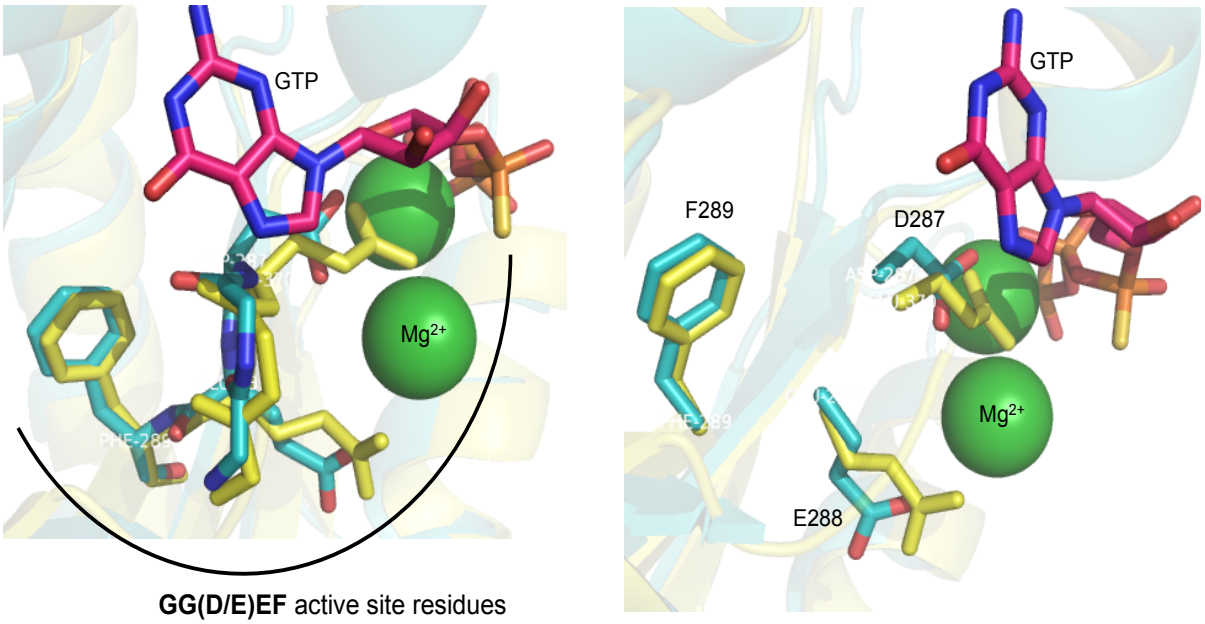

Figure 5-1: Structural alignment of the diguanylate cyclase active site pocket from PleD (PDB ID: 2V0N, yellow) and *Sw*HaCE (cyan). The conserved catalytic residues (GGD/EEF) are highlighted in the stick format. The position of the divalent metal cation (Mg^{2+}, green) is shown with respect to the catalytic residues (D/E, E and F; stick format) and the substrate (GTP; pink).

Another important catalytic feature of GGDEF domains is the allosteric I-site (inhibition site, RxxD motif). Some enzymes containing this conserved motif were found to be inactive upon purification. Upon further analysis, it was found that cyclic-d-GMP purifies bound to the I-site in these protein.

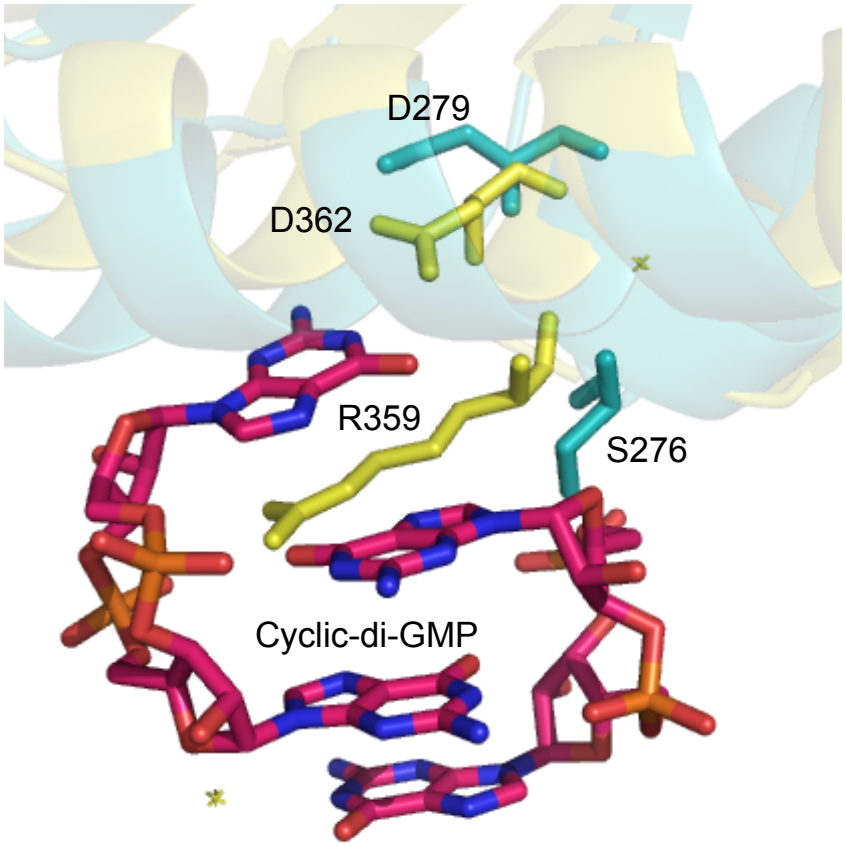

Figure 5-2: Structural alignment of the allosteric inhibition site (I-site) from PleD (PDB ID: 2V0N, yellow) and *Sw*HaCE (cyan). The residues from the I-site motif (RxxD, PleD) are shown in stick format. The corresponding positions in *Sw*HaCE (SxxD) are also shown, along with the bound cyclic-di-GMP (stick; pink).

This allosteric inhibition locks the protein in an elongated and twisted conformation, which is an oligomeric form that renders the enzyme inactive. Treatment with a phosphodiesterase, that catalyzes the hydrolysis of the cyclic-di-GMP, recovers the enzymatic activity. This recovery is also associated with major changes in conformation and oligomerization. WspR was shown to purify as an inactive, cyclic-di-GMP bound tetramer, which undergoes rearrangement to form the active dimer upon hydrolysis of the allosteric cyclic-di-GMP. As per the structural and

sequence alignment, *Sw*HaCE does not contain the conserved RxxD motif, and instead has an SxxD motif. Kinetic studies rule out any allosteric contribution to the cyclase activity.

For *Sw*HaCE, we have shown using sedimentation equilibrium studies that the protein forms a homodimers in solution. The native protein is active as a diguanylate cyclase and a phosphodiesterase, which makes it a bi-functional enzyme.

Hence, we also used the structure of the GGDEF-EAL containing di-domain protein FimX (PDB ID: 4J40) and aligned *Sw*HaCE to generate a structural model. FimX contains a degenerate GGDEF (GDSIF) and an EVL motif. The alignment surface shows that though the ExL domains of these 2 proteins have a similar fold, the cyclase domains are not homologous. This is probably because the cyclase domain from FimX is degenerate, as compared to the active cyclase domain from *Sw*HaCE. In comparison, the surface of PleD (PDB ID: 2V0N) and *Sw*HaCE show similar fold and overlap of the active site. However, this di-domain model proposes an elongated conformation for *Sw*HaCE, similar to other proteins in this class.

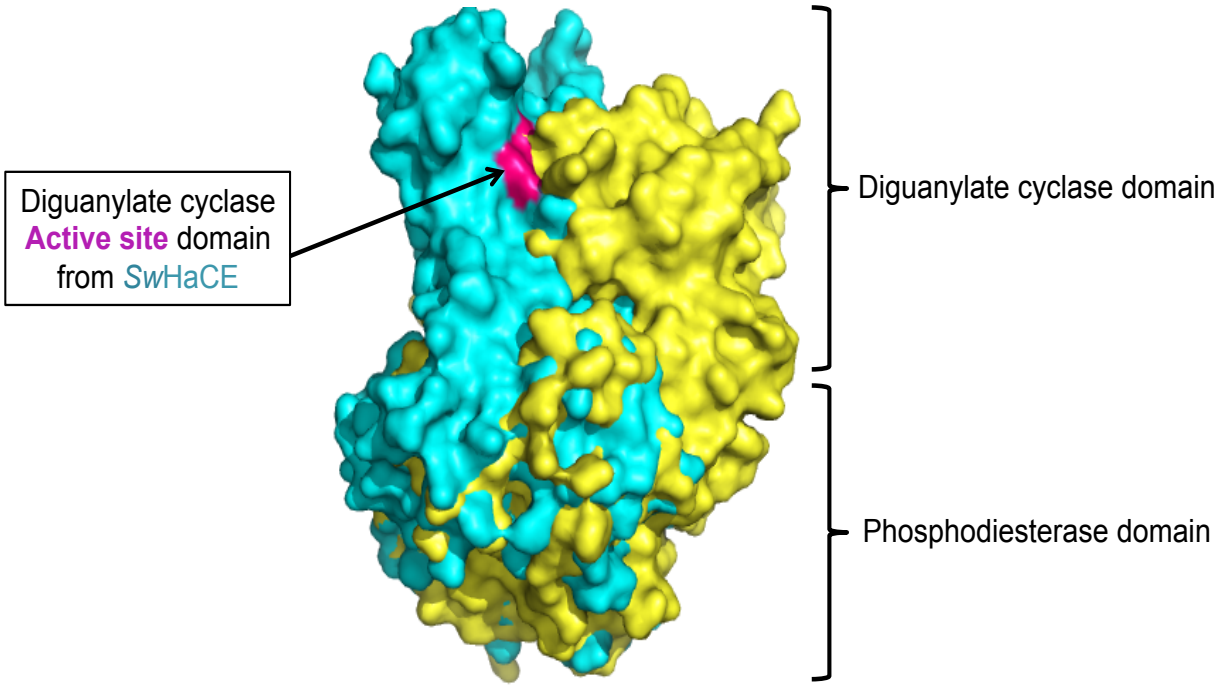

Figure 5-3: Structural alignment of FimX (PDB ID: 4J40) and *Sw*HaCE showing surface overlap. The cyclase active site is indicated in pink.

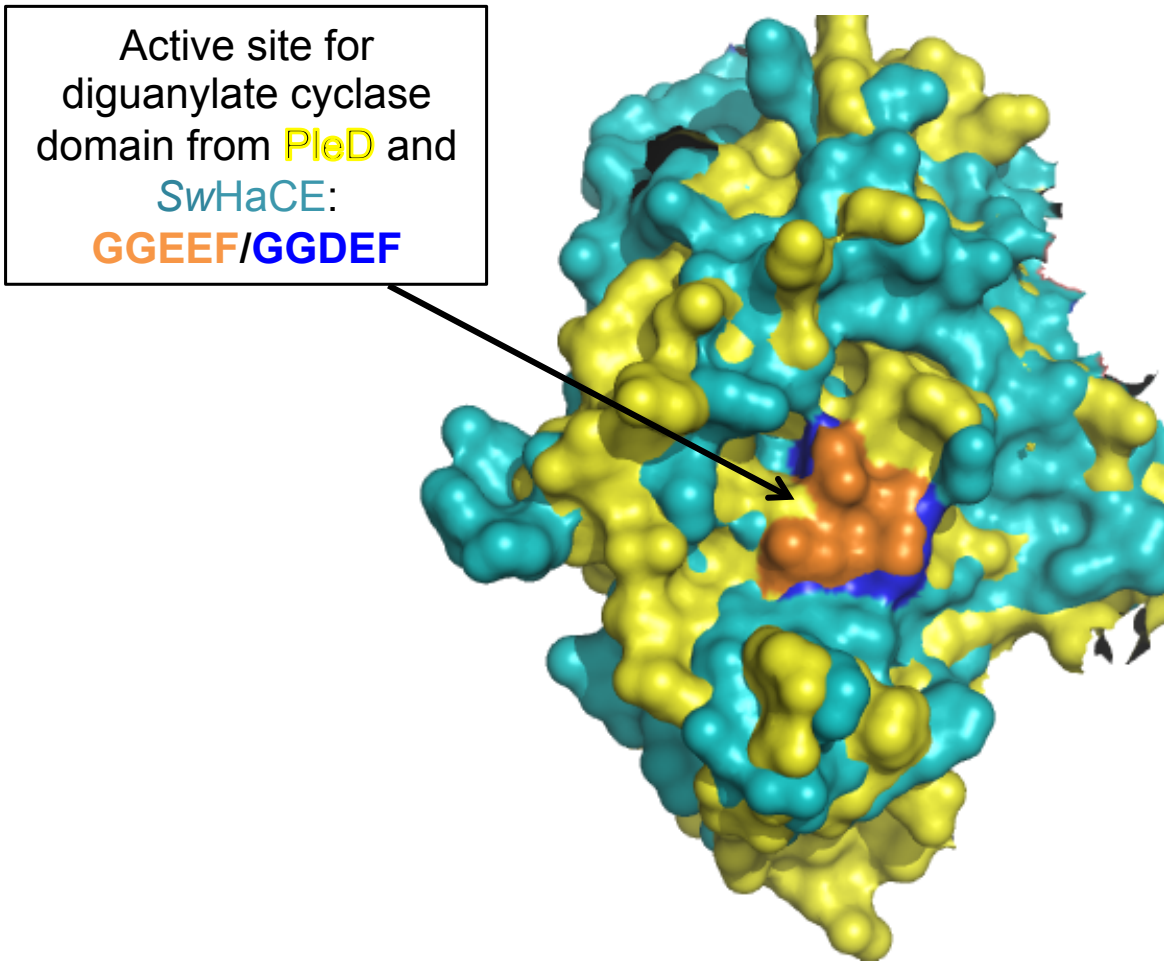

Figure 5-4: Structural alignment of the diguanylate cyclase domain from PleD (PDB ID: 2V0N) and *Sw*HaCE. The surface view shows the position of the active site (PleD, orange; *Sw*HaCE, blue).

This is agreement with our observation, where we followed *Sw*HaCE by analytical gel filtration. The molecular weight determination and elution time indicated a monomeric state. Since analytical gel filtration as a technique for molecular weight determination is shape dependent, it is likely the reason why *Sw*HaCE consistently elutes as a monomer from the column. This also explains our results from sedimentation velocity experiments, which perform shape-dependent analysis of protein molecular weight, and indicate a monomeric state for *Sw*HaCE. All these

experiments, with the concluding dimer estimation from sedimentation equilibrium experiments, indicate an elongated structure for *Sw*HaCE, similar to other known cyclase enzymes.

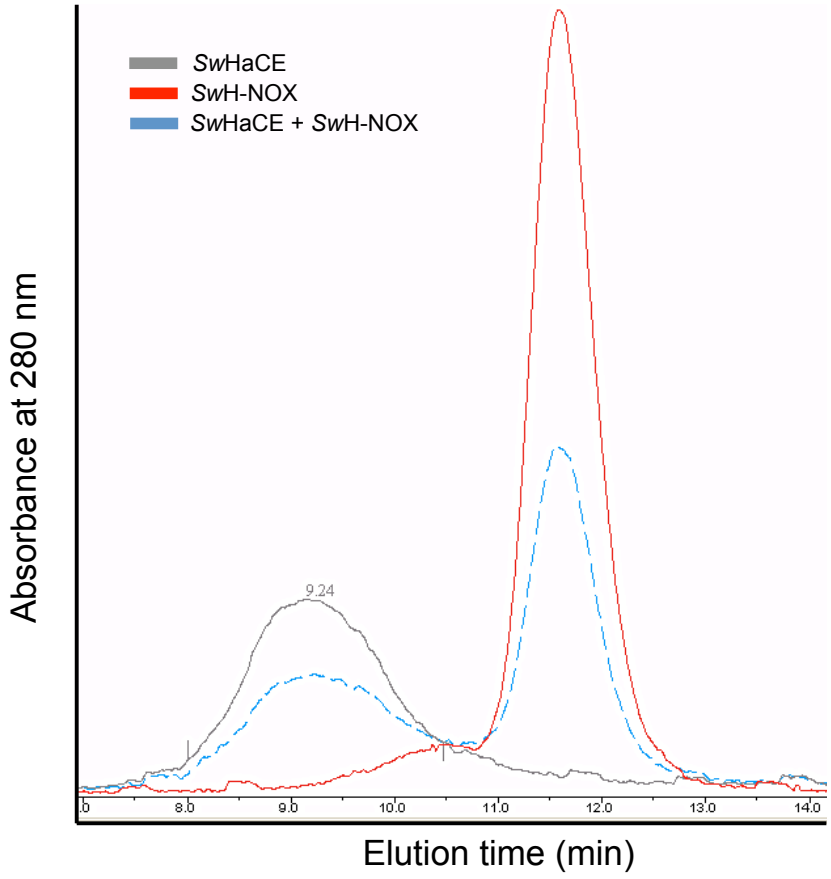

Figure 5-5: Analytical gel filtration experiments indicate monomeric state for *Sw*HaCE and *Sw*H-NOX.

However, sedimentation equilibrium studies indicated a dimeric state at similar concentrations. Since analytical gel filtration is a shape dependent technique for determining molecular weight, we concluded using sedimentation equilibrium results that *Sw*HaCE is a dimer in solution.

Other than the GGDEF and the EAL domain, *Sw*HaCE also has an N-terminal PAS domain. This domain has been shown to mediate protein-protein interactions, and hence, these solution

models add to the understanding of how the individual domains interact with each other, and affect function.

CHAPTER 6: DISCUSSIONS AND CONCLUSIONS

Signaling networks are extremely modular in nature. These modules include sensor-effector pairs, receptors for small molecules and interfaces or domains for protein-protein interactions. The study of signaling networks also provides ample opportunity to recognize new targets for drug discovery, which can either be repressed or enhanced.

Bacterial signaling networks have always been lucrative as many of these have a direct correlation with virulence and human health. Among these, biofilm is an increasingly studied network, as bacteria living in biofilms are shielded from antibiotics, making them resistant, and pathogenic. The signals at the center of biofilm formation are being recognized, and characterized with respect to protein partners, which translate and transduce the message to induce phenotype. Among these signals, NO and cyclic-di-GMP have gained increasing importance. Nitric oxide, a recognized signaling molecule in mammals, was identified as a dispersal agent at sub–lethal concentrations, whereas cyclic-di-GMP is an intracellular secondary messenger molecule that plays a ubiquitous role in various cellular functions. There are a few studies that have shown the correlation between 2 signals, mostly via H-NOX protein (a bacterial NO sensor). These studies indicate a NO/H-NOX based mechanism that controls the intracellular levels if cyclic-di-GMP, and affects biofilm formation.

However, the nuances of these pathways are still being studied. Details at the molecular level of signal transduction including binding of NO to H-NOX, trigger of conformational change, interaction with HaCE, change in function, change in cyclic-di-GMP concentration, finally leading to an output, are not yet fully understood. Given the significance of these initial events with respect to an output at the cellular level, it is imperative to elucidate the mechanism of the signal relay. Details at the molecular level of nitric oxide–induced signal transduction involve binding of NO to HNOX which triggers a conformational change followed by and interaction of HNOX and HACE leading to change in function and cyclic-di-GMP concentration, finally leading to an output which may manifest as an increase or decrease in biofilm/virulence/quorum sensing. These intrinsic changes are not fully understood. Given the significance of these initial events with respect to an output at the cellular level, it is imperative to elucidate the mechanism of the signal relay.

This work addresses some of these questions in *S. woodyi,* which contains an H-NOX/HaCE pathway that participates in biofilm regulation. The role of NO as the signaling molecule has been shown before, however, the mechanistic and molecular details of this protein-protein interaction in the context of biofilm formation has been shown in chapter 2 of this thesis. The H-NOX/HaCE protein complex was found to associate in a 2:2 stoichiometry, the first biophysical evidence for a H-NOX associated functional enzyme. The interface and residues that mediates this interaction has been identified. These residues clustered on the N-terminal helices, providing evidence for the involvement of these helices in transducing the signal-binding event. We also deduced the effect of this interface on enzyme activity, further elucidating how this protein complex results in a functional change within the cell.

The importance of HaCE enzymes is evident in bacterial signaling, and the function of these enzymes can be correlated to a stimulus. Hence, it is important to understand more about the

structure-function relationship of these enzymes, and elucidate the substrate kinetics. In chapter 3, we have experimentally commented upon the PDE function from di-domain enzymes, containing dual functioning GGDEF-EAL domains. Identification of conserved residues in the enzyme active site was corroborated by mutational studies to confirm their role in catalysis. We also determined distinct structural and functional features for these catalytic residues, as compared to stand-alone PDE domains. These results add to the existing knowledge of bi-functional enzymes in bacteria, while presenting interesting questions about domain arrangement, role of intra- and inter-domain interactions in enzyme function, and conformational perturbations upon binding a signal. Some of these questions are being answered using SAXS and crystal structure studies, while others need more detailed experimental design.

Overall, this dissertation provides a structural, biophysical and biochemical view on NO-regulated HaCE enzymes, which have been identified as important players in signal transduction for various pathways, important for both bacteria and humans, especially in the context of diseases. Elucidation of the interaction surface of H-NOX/HaCE protein complex highlights the role of N-terminal helices in regulating this protein complex. This confirms the participation of N-terminal helices in signal transduction. The PDE domain from *Sw*HaCE has also been analyzed to identify the role of different residues in catalysis. This preliminary analysis of a PDE domain from a bi-functional protein contributes to the understanding of enzyme function in di-domain proteins.

Future projects may involved detailed study of other signal-regulated HaCE/HahK enzymes, which can provide an insight into a general mechanism of regulation by NO/H-NOX. These mechanisms also explain the mechanistic details of how NO-bound H-NOX contributes to various pathways by modulating the activity of these enzymes. The effect of sGC (NO-mimicking) activators has been analyzed with respect to upregulation of sGC enzyme activity, it

would be interesting to carry out similar studies in a H-NOX/HaCE protein complex, and determine the functional output. Finally, future studies to elaborate upon the biochemical/biophysical characteristics of signal induced conformational perturbations in H-NOX associated enzymes can comment upon the intrinsic mechanism of signal transduction in these systems.

APPENDIX

We have two H-NOX/HaCE protein complexes available for studies. The H-NOX/HaCE complex from *S. woodyi* has been shown to associate as a heterotetramer in solution. Depending on the ligation state [NO-bound vs. Fe(II)–unligated], H-NOX differentially regulates the two activities of HaCE, diguanylate cyclase and phosphodiesterase. Similarly, in *A. vitis*, the HaCE, which does not have a PAS domain, also associates with H-NOX. We are in the process of determining the stoichiometry for this complex, though it has been established that the *Avi*HaCE, which has an active diguanylate cyclase domain, dimerizes in solution (Dr. Natasha M. Nesbitt).

We are in the process of co-crystallizing the *Avi*H-NOX/HaCE protein complex, in a collaboration with Prof. Miguel Garcia-Diaz. The co-crystal of this complex should offer detailed insight into the mechanism of association and regulation of enzyme function by NO-sensing. This is the first structural evidence of bacterial H-NOX protein that has been elucidated in a regulatory role with an enzyme.

A.1 CD studies to determine fold

We have done circular dichroism (CD) studies to confirm the structural integrity and fold of these proteins. CD ensures that the enzymes and proteins in solution are folded, and not forming

aggregates[107, 108]. CD can also be used to detect changes in secondary structure, if any, to indicate a binding event or conformational change due to protein-protein interactions[109]. For this purpose, we did a set of experiments where we obtained the CD spectra for NO-bound *Sw*H-NOX, a complex of NO-bound *Sw*H-NOX and *Sw*GGAAF (the cyclase-inactive mutant of *Sw*HaCE), and a complex of NO-bound *Sw*H-NOX and *Sw*GGAAF with GTP, the substrate for the cyclase domain. We wanted to determine if the addition of either the binding partner or a substrate-bound binding partner induces any change in the secondary structure of NO-bound *Sw*H-NOX.

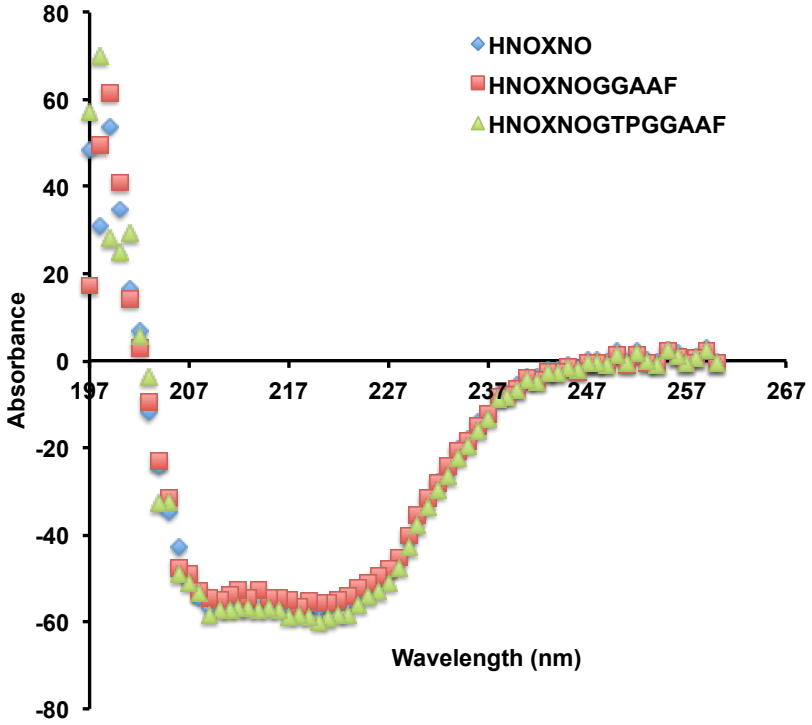

Figure A-1: CD spectra for NO-bound *Sw*H-NOX, complex of NO-bound *Sw*H-NOX and *Sw*GGAAF, and a complex of NO-bound *Sw*H-NOX and *Sw*GGAAF with GTP.

Though the protein was found to be folded, and displayed preserved secondary structure, no drastic change in the structure was observed due to binding.

A.2 ITC studies for thermodynamic analysis

Other than NMR and enzymatic analysis, we have also used chemical cross – linking and Isothermal calorimetry (ITC) to determine the binding interface of this protein complex, as well as determine the thermodynamic parameters of this interaction. However, chemical cross – linking done on full-length HaCE containing PAS, GGDEF and EAL domains was unsuccessful to noisy data. ITC has been used ubiquitously to study the thermodynamic parameters of protein-protein and protein-substrate complexes[110-112]. This includes diguanylate cyclase proteins, as well as cyclic-di-GMP receptors proteins, like PilZ[30], for which the stoichiometry, affinity and ΔH, ΔS has been calculated[113]. The titration curves are shown for different H-NOX complexes [Fe(III), Fe(II) and Fe(II)-NO], the calculated ΔH, ΔS and K_D values are summarized in table 1.

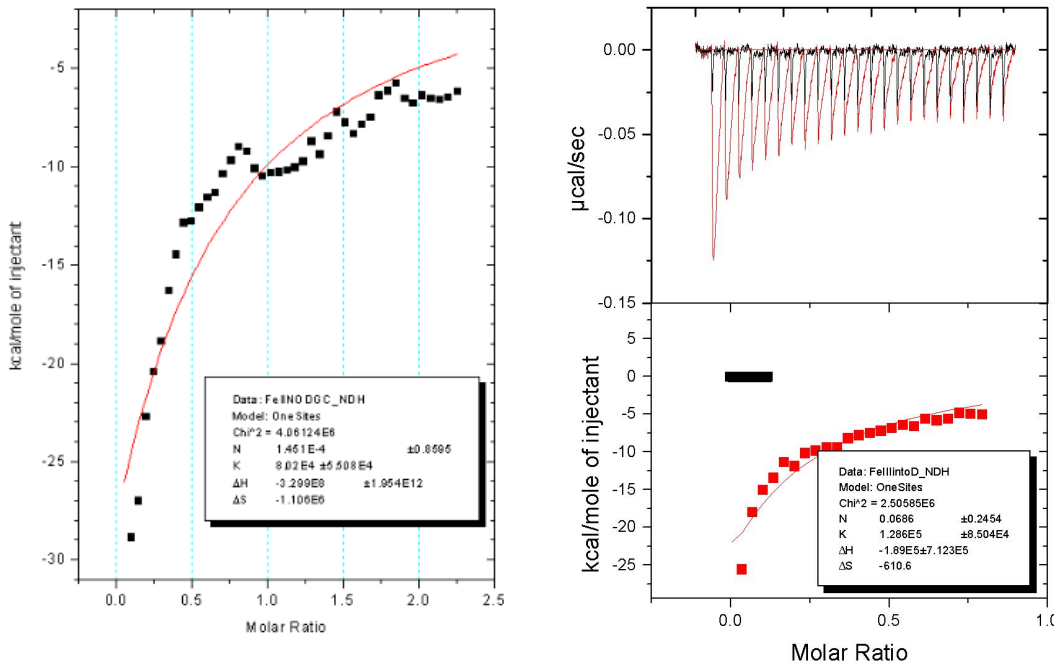

Figure A-2: ITC curves for Fe(II)-NO *Sw*H-NOX *Sw*HaCE (left) and Fe(III) *Sw*H-NOX/*Sw*HaCE (right).

Table A-1: Thermodynamic parameters calculated from ITC titrations of *Sw*HaCE into Fe(III), Fe(II) and Fe(II)-NO *Sw*H-NOX.

H-NOX complex	K_D (μM)	Stoichiometry (N)	ΔH (Kcal/mol)
Fe(III)	2.63	0.843	-5.243 e4
Fe(II)-CO	4.45	1.541	-3.526e5
Fe(II)-NO	12.50	1.450	-3.299e8

Table A-2: Ligand binding properties and NO_{off} kinetics for the E16K, F17A and E20K mutants of *Sw*H-NOX as compared to WT *Sw*H-NOX.

Protein	Fe(II)	Fe(II)-NO	Fe(II)-CO	K_{off}(NO) ($X\ 10^{-4}\ s^{-1}$)	Ref.
WT *Sw*H-NOX	431	399	423	15.2 ± 3.50	1
E16K *Sw*H-NOX	431	399	424	7.97 ± 0.06	This study
F17A *Sw*H-NOX	431	398	423	7.45 ± 0.18	This study
E20K *Sw*H-NOX	431	399	423	7.71 ± 0.15	This study

[1]The experiment was performed as previously described (Liu, N.; Xu, Y.; Hossain, S.; Huang, N.; Coursolle, D.; Gralnick, J. A.; Boon, E. M. *Biochemistry* **2012**, *51*, 2087).

Supporting Table A-1: Ligand binding properties and NO off kinetics for the E16K, F17A and E20K mutants of *Sw*H-NOX as compared to WT *Sw*H-NOX. The dissociation rates for the Fe(II)-NO complexes of each *Sw*H-NOX construct were fit to the following equation: $y = y_0 + a_1*(1 - e^{(-b_1*x)}) + a_2*(1-e^{(b_2*x)})$ using Origin 7.0 software. Each experiment was done thrice for error determination.

Table A-3: Malachite Green Assay; PPi standard curve and IPP control

Reaction	Pi (mM)
0.78 mM PPi + 10 ml IPP	0.00343
1.56 mM PPi + 10 ml IPP	0.00490
3.125 mM PPi + 10 ml IPP	0.01037
6.25 mM PPi + 10 ml IPP	0.04735
12.5 mM PPi + 10 ml IPP	0.06118
25 M mM PPi + 10 ml IPP	0.12349
50 mM PPi + 10 ml IPP	0.27686
25 mM PPi + 10 ml IPP	0.12349
25 mM PPi + 20 ml IPP	0.13303

Supporting Table A-2: PPI concentrations used for the standard curve. The last 2 rows show the controls for IPP. As shown for the PPi standard reaction with IPP, the amount of Pi generated in the reaction does not change when the amount of IPP is doubled (10 U/ml and 20 U/ml). This indicates that for the cyclase reactions of *Sw*HaCE with GTP, IPP is not the rate-limiting enzyme, and does not interfere with the enzyme activity.

Figure A-3: A. Sedimentation equilibrium experiments for WT *Sw*H-NOX conducted using rotor speeds 17,000, 27,000 and 34,000 rpm (g-force of 23,300, 58,700 and 93,000 respectively). The signal at 400 nm was monitored. The molecular weight calculated from HeteroAnalysis is 23.3 kDa. The expected molecular weight for a monomer is 22.5 kDa. B. Sedimentation equilibrium experiments for E16K *Sw*H-NOX in solution. The rotor speeds used were same as for WT *Sw*H-NOX. As calculated from HeteroAnalysis, the molecular weight is 23.8 kDa. The expected molecular weight for a monomer Is 22.5 kDa. Each experiment was performed in triplicate. C. Sedimentation equilibrium experiments for the E16K *Sw*H-NOX mutant in association with *Sw*HaCE complex in solution. Rotor speeds of 9000, 14,000 and 18,000 rpm (g-force of 6500, 15,800 and 26,100 respectively) were used, and the signal at 400 nm was monitored. The molecular weight calculated from HeteroAnalysis is 76 kDa, which does not match the MW of a heterotetrameric complex (197.2 kDa). D. Sedimentation equilibrium experiments for *Sw*WT H-NOX by itself in solution. Rotor speeds of 9000, 14,000 and 18,000 rpm (g-force of 6500, 15,800 and 26,100 respectively; calculated from the molecular weight of *Sw*HaCE) were used, and the signal at 400 nm was followed. The molecular weight calculated from HeteroAnalysis is 75 kDa, which may be a species containing aggregates of H-NOX at higher speeds. This explains the result for E16K *Sw*H-NOX (Figure A3C), where the species detected is not a complex with *Sw*HaCE, but probably aggregates of E16K *Sw*H-NOX.
Figure A3A.

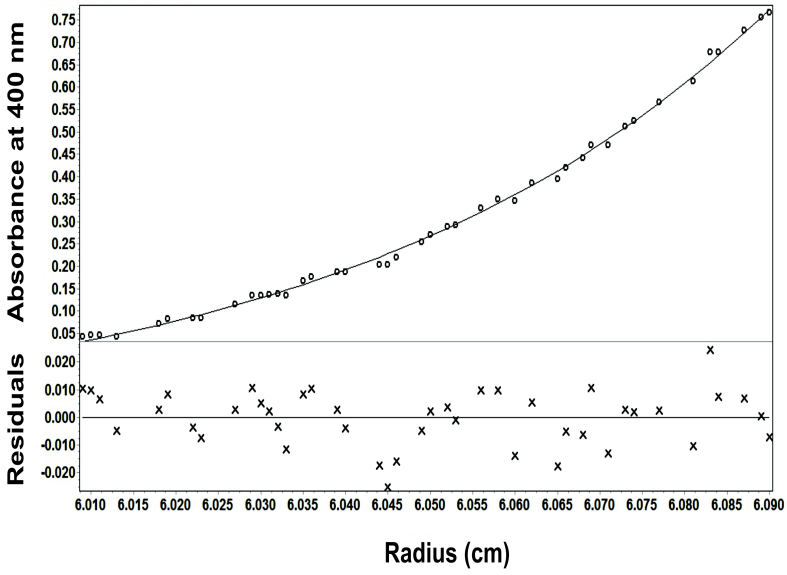

Figure A3B.

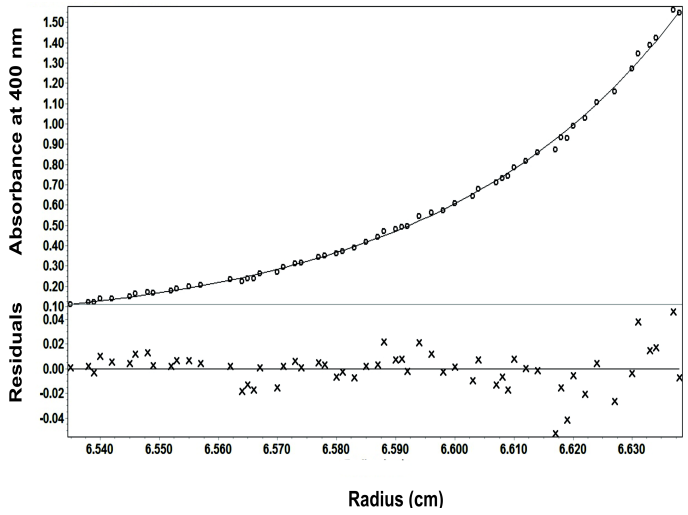

Figure A3C.

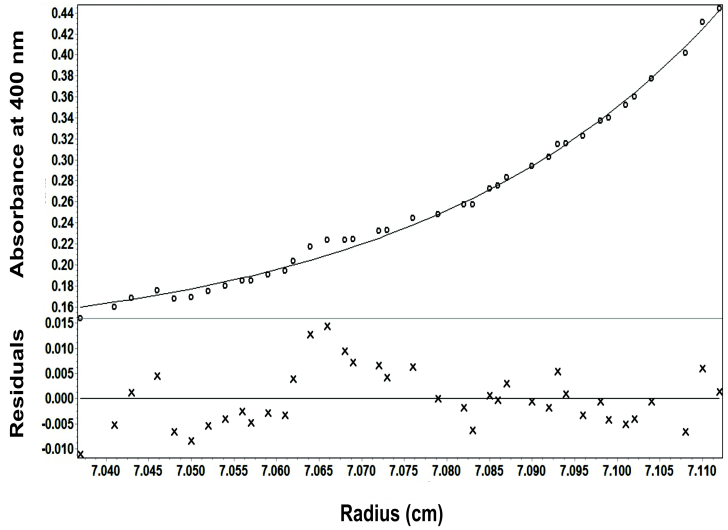

Figure A3D.

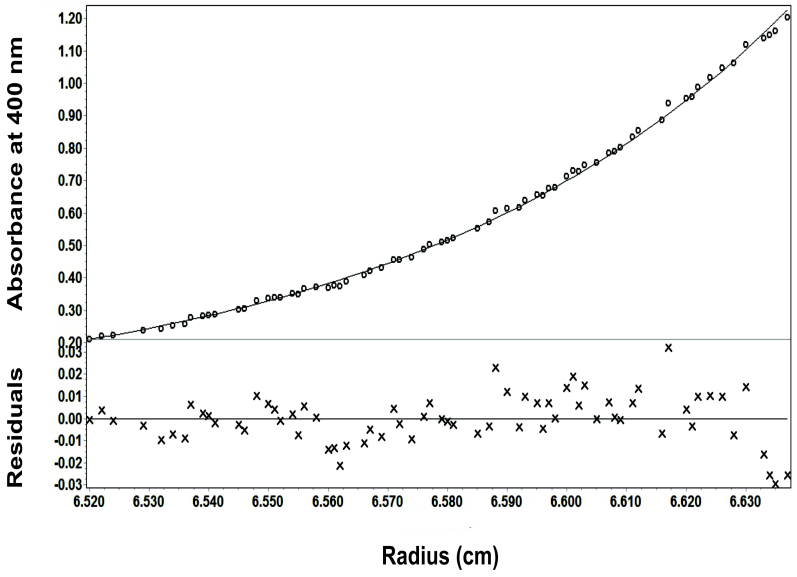
Absorbance at 400 nm
1.20
1.10
1.00
0.90
0.80
0.70
0.60
0.50
0.40
0.30
0.20
Residuals
0.03
0.02
0.01
0.00
-0.01
-0.02
-0.03
6.520
6.530
6.540
6.550
6.560
6.570
6.580
6.590
6.600
6.610
6.620
6.630
Radius (cm)

Figure A-4: A. A standard curve for PPI was generated for the Malachite Green assay, and IPP was used to cleave the PPI. The concentrations used are listed in table 2. The error bars associated with each data point are smaller than the size of the symbol. B. The production of Pi was plotted as a function of increasing *Sw*HaCE concentration. This indicates that *Sw*HaCE is the rate-limiting enzyme, and change in the enzyme concentration changes activity, which is measured by change in the Pi concentration. The error bars for the two data points at the highest concentration are smaller than the size of the symbol.
Figure A4A.

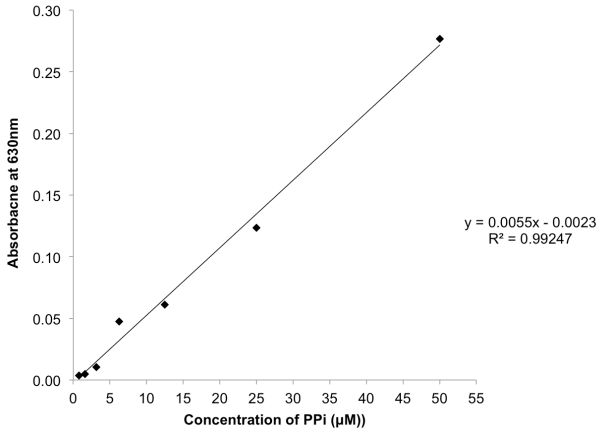

Figure A4B.

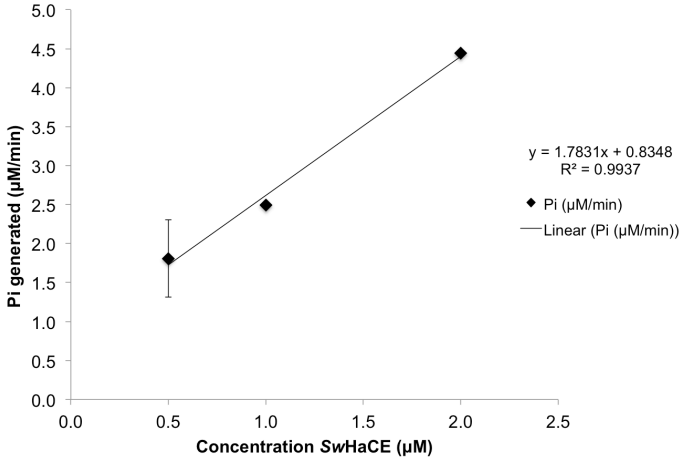

Table A-3: Initial velocity for *Sw*GGAAF (cyclase-silent) using cyclic-di-GMP as the substrate in the presence of *Sw*H-NOX surface mutants.

Reactions[a]	Vi (min-1)
*Sw*GGAAF	0.0725 ± 0.04
*Sw*GGAAF + E16K *Sw*H-NOX	0.5264 ± 0.20
*Sw*GGAAF + F17A *Sw*H-NOX	0.0211 ± 0.01
*Sw*GGAAF + E20K *Sw*H-NOX	0.1191 ± 0.04

[a]All reactions contained 100 mM cyclic-di-GMP, 5 mM $MgCl_2$, and 50 mM Tris-Cl, pH 8.0.

Figure A-5: Initial velocity for PDE activity of *Sw*GGAAF in the presence of *Sw*H-NOX surface mutants.

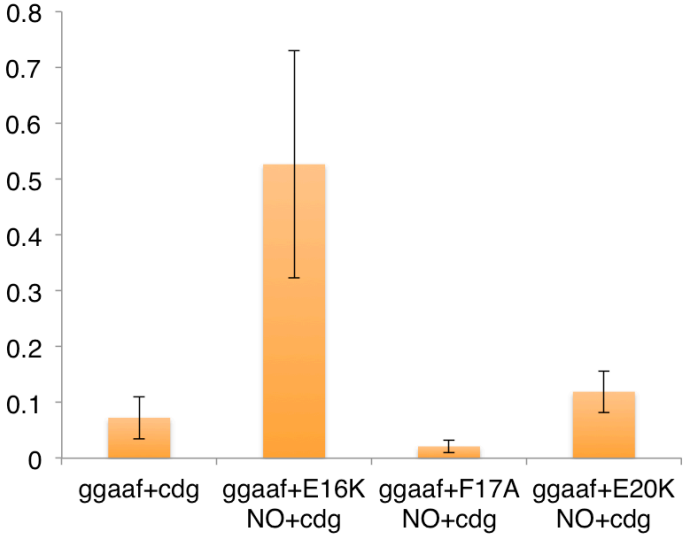

Figure A-6: Representative graph for NO_{off} kinetics (used for E16K, F17A and E20K *Sw*H-NOX mutants).

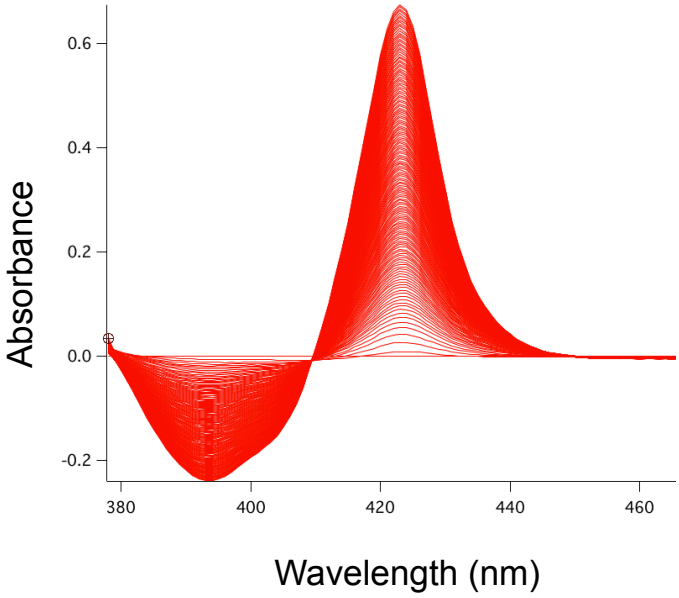

Figure A-7: Representative HPLC traces for other *Sw*HaCE PDE mutants.

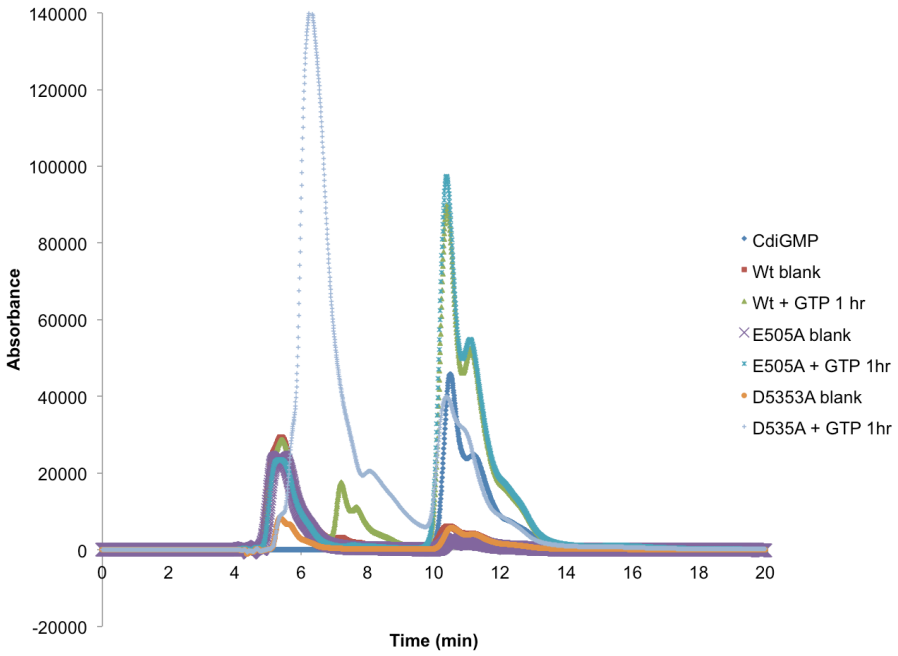

Figure A-8: Representative HPLC traces for control reactions at (0 min and 1 hour time-point) of *Sw*HaCE PDE mutants with cyclic-di-GMP (substrate), as compared to wild-type *Sw*HaCE. For *Sw*HaCE, the pGpG peak appears at 16.5 min in the 1-hour reaction.

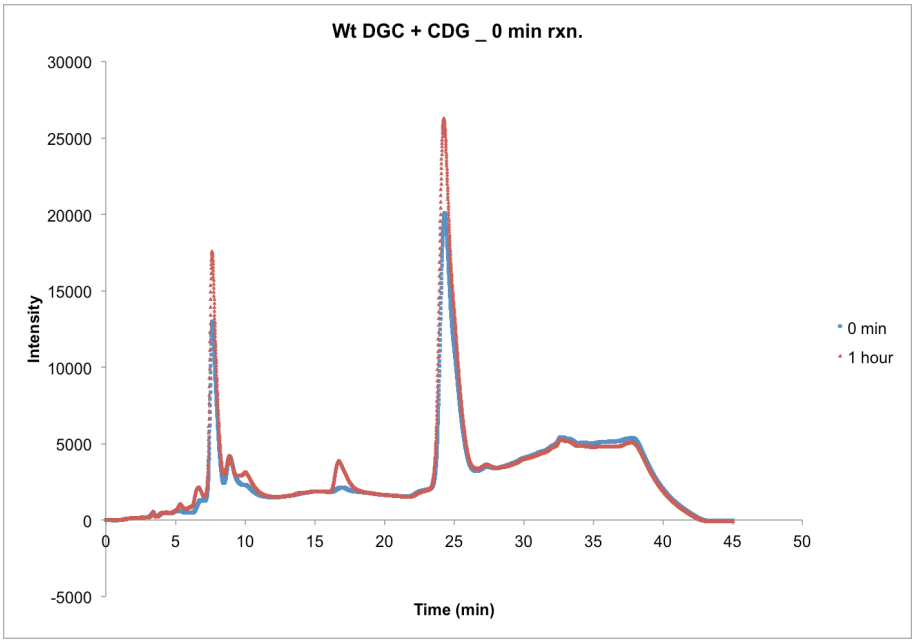

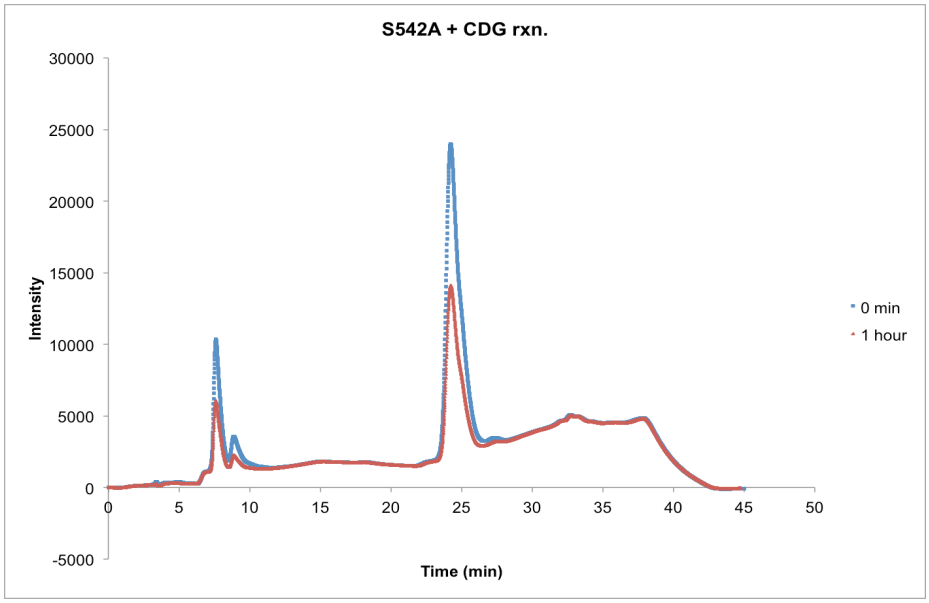

BIBLIOGRAPHY

1. Denninger, J., W. and Marletta, M., A., *Guanylate cyclase and the NO/cGMP signaling pathway.* Biochimica et Biophysica Acta, 1999. 1411: p. 334-350.

2. Boon, E. M., Huang, S. H. and Marletta, M. A., *A molecular basis for NO selectivity in soluble guanylate cyclase.* Nat Chem Biol, 2005. 1(1): p. 53-59.

3. Purohit, R., Weichsel, A. and Montfort, W. R., *Crystal structure of the Alpha subunit PAS domain from soluble guanylyl cyclase.* Protein science : a publication of the Protein Society, 2013. 22(10): p. 1439-44.

4. Underbakke, E. S., Lavarone, A. T. and Marletta, M. A., *Higher-order interactions bridge the nitric oxide receptor and catalytic domains of soluble guanylate cyclase.* Proceedings of the National Academy of Sciences of the United States of America, 2013. 110(17): p. 6777-82.

5. Boon, E. M. and Marletta, M. A., *Ligand discrimination in soluble guanylate cyclase and the H-NOX family of heme sensor proteins*. Current opinion in chemical biology, 2005. 9(5): p. 441-6.

6. Iyer, L., Anantharaman, V. and Aravind, L., *Ancient conserved domains shared by animal soluble guanylyl cyclases and bacterial signaling proteins.* BMC Genomics, 2003. 4(1): p. 1-8.

7. Ma, X., *NO and CO differentially activate soluble guanylyl cyclase via a heme pivot-bend mechanism*. The EMBO Journal 2007. 26: p. 578-588.

8. Plate, L. and Marletta, M. A., *Nitric oxide-sensing H-NOX proteins govern bacterial communal behavior.* Trends in biochemical sciences, 2013. 38(11): p. 566-75.

9. Erbil, W.K., et al., *A structural basis for H-NOX signaling in Shewanella oneidensis by trapping a histidine kinase inhibitory conformation.* Proceedings of the National Academy of Sciences of the United States of America, 2009. 106(47): p. 19753-60.

10. Arora, D. P. and Boon, E. M., *Nitric oxide regulated two-component signaling in Pseudoalteromonas atlantica.* Biochemical and Biophysical Research Communications, 2012. 421(3): p. 521-526.

11. Plate, L. and Marletta, M. A., *Nitric oxide modulates bacterial biofilm formation through a multicomponent cyclic-di-GMP signaling network.* Molecular cell, 2012. 46(4): p. 449-60.

12. Carlson, H. K., Vance, R. E. and Marletta, M. A., *H-NOX regulation of c-di-GMP metabolism and biofilm formation in Legionella pneumophila.* Molecular Microbiology, 2010: p. no-no.

13. Liu, N., et al., *Nitric oxide regulation of cyclic di-GMP synthesis and hydrolysis in Shewanella woodyi*. Biochemistry, 2012. 51(10): p. 2087-99.

14. Wang, Y., Dufour, Y. S., Carlson, H. K., Donohue, T. J., Marletta, M. A., and Ruby, E. G., *H-NOX–mediated nitric oxide sensing modulates symbiotic colonization by Vibrio ˛scheri.* Proc Natl Acad Sci U S A, 2010. 107(18): p. 8375-8380.

15. Henares, B. M., Higgins, K. E. and Boon, E. M., *Discovery of a nitric oxide responsive quorum sensing circuit in Vibrio harveyi.* ACS chemical biology, 2012. 7(8): p. 1331-6.

16. Henares, B. M., Xu, Y. and Boon, E. M., *A nitric oxide-responsive quorum sensing circuit in Vibrio harveyi regulates flagella production and biofilm formation.* International journal of molecular sciences, 2013. 14(8): p. 16473-84.

17. Galperin, M. Y., *Bacterial signal transduction network in a genomic perspective.* Environmental Microbiology, 2004. 6(6): p. 552-67.

18. Verstraeten, N., et al., *Living on a surface: swarming and biofilm formation.* Trends in microbiology, 2008. 16(10): p. 496-506.

19. Xavier, J. B. and Foster, K. R., *Cooperation and conflict in microbial biofilms.* Proceedings of the National Academy of Sciences of the United States of America, 2007. 104(3): p. 876-81.

20. Barraud, N., et al., *Involvement of nitric oxide in biofilm dispersal of Pseudomonas aeruginosa.* Journal of Bacteriology, 2006. 188(21): p. 7344-53.

21. Romeo, T., *When the party is over: a signal for dispersal of Pseudomonas aeruginosa biofilms*. Journal of Bacteriology, 2006. 188(21): p. 7325-7.

22. Karatan, E. and Watnick, P., *Signals, regulatory networks, and materials that build and break bacterial biofilms.* Microbiology and molecular biology reviews : MMBR, 2009. 73(2): p. 310-47.

23. Waters, C. M., et al., *Quorum sensing controls biofilm formation in Vibrio cholerae through modulation of cyclic di-GMP levels and repression of vpsT.* Journal of Bacteriology, 2008. 190(7): p. 2527-36.

24. Ueda, A. and Wood, T. K., *Connecting quorum sensing, c-di-GMP, pel polysaccharide, and biofilm formation in Pseudomonas aeruginosa through tyrosine phosphatase TpbA (PA3885).* Plos Pathogens, 2009. 5(6): p. e1000483.

25. Castiglione, N., Stelitano, V., Rinaldo, S., Giardina, G., Caruso, M., and Cutruzzola, F., *Metabolism of cyclic-di-GMP in bacterial biofilms: From a general overview to biotechnological applications.* Indian Journal of Biotechnology, 2011. 10: p. 423-431.

26. Ma, Q., et al., *Engineering a novel c-di-GMP-binding protein for biofilm dispersal.* Environmental Microbiology, 2011. 13(3): p. 631-42.

27. Newell, P. D., et al., *A c-di-GMP effector system controls cell adhesion by inside-out signaling and surface protein cleavage*. PLoS biology, 2011. 9(2): p. e1000587.

28. An, S., Wu, J. and Zhang, L. H., *Modulation of Pseudomonas aeruginosa biofilm dispersal by a cyclic-di-GMP phosphodiesterase with a putative hypoxia-sensing domain.* Applied and environmental microbiology, 2010. 76(24): p. 8160-73.

29. Hickman, J. W. and Harwood, C. S., *Identification of FleQ from Pseudomonas aeruginosa as a c-di-GMP-responsive transcription factor.* Molecular Microbiology, 2008. 69(2): p. 376-89.

30. Benach, J., Swaminathan, S. S., Tamayo, R., Handelman, S. K., Folta-Stogniew, E., Neely, H., Seetharaman, J., Camilli, A., and Hunt, J. F., *The structural basis of cyclic diguanylate signal transduction by PilZ domains.* The EMBO journal, 2007. 26: p. 5153-5166.

31. Christen, M., et al., *DgrA is a member of a new family of cyclic diguanosine monophosphate receptors and controls flagellar motor function in Caulobacter crescentus.* Proc Natl Acad Sci U S A, 2007. 104(10): p. 4112-7.

32. Cotter, P. A. and Stibitz, S., *c-di-GMP-mediated regulation of virulence and biofilm formation.* Curr Opin Microbiol, 2007. 10(1): p. 17-23.

33. Tamayo, R., Pratt, J. T. and Camilli, A., *Roles of cyclic diguanylate in the regulation of bacterial pathogenesis.* Annu Rev Microbiol, 2007. 61: p. 131-48.

34. Zhang, L. H., *A novel c-di-GMP effector linking intracellular virulence regulon to quorum sensing and hypoxia sensing*. Virulence, 2010. 1(5): p. 391-394.

35. Hengge, R., *Principles of c-di-GMP signalling in bacteria.* Nat Rev Microbiol, 2009. 7(4): p. 263-73.

36. Smith, K. D., et al., *Structural basis of ligand binding by a c-di-GMP riboswitch.* Nature structural & molecular biology, 2009. 16(12): p. 1218-23.

37. Boyd, C. D., et al., *LapG, required for modulating biofilm formation by Pseudomonas fluorescens Pf0-1, is a calcium-dependent protease*. Journal of Bacteriology, 2012. 194(16): p. 4406-14.

38. Malone, J. G., et al., *The structure-function relationship of WspR, a Pseudomonas fluorescens response regulator with a GGDEF output domain*. Microbiology, 2007. 153(Pt 4): p. 980-94.

39. De, N., et al., *Phosphorylation-independent regulation of the diguanylate cyclase WspR*. PLoS Biol, 2008. 6(3): p. e67.

40. Paul, R., et al., *Activation of the Diguanylate Cyclase PleD by Phosphorylation-mediated Dimerization.* Journal of Biological Chemistry, 2007. 282(40): p. 29170-29177.

41. Wassmann, P., et al., *Structure of BeF3- -modified response regulator PleD: implications for diguanylate cyclase activation, catalysis, and feedback inhibition*. Structure, 2007. 15(8): p. 915-27.

42. Kanazawa, T., et al., *Biochemical and Physiological Characterization of a BLUF Protein−EAL Protein Complex Involved in Blue Light-Dependent Degradation of Cyclic Diguanylate in the Purple BacteriumRhodopseudomonas palustris.* Biochemistry, 2010. 49(50): p. 10647-10655.

43. Barends, T. R., et al., *Structure and mechanism of a bacterial light-regulated cyclic nucleotide phosphodiesterase*. Nature, 2009. 459(7249): p. 1015-8.

44. Christen, M., et al., *Identification and characterization of a cyclic di-GMP-specific phosphodiesterase and its allosteric control by GTP*. J Biol Chem, 2005. 280(35): p. 30829-37.

45. tsuyoshi Egawa, A. T., Suematsu, M. and Yonetani, T., *Method for determination of association and dissociation rate constants of reversible biomolecular reactions by isothermal titration calorimeters*. Analytical chemistry, 2007. 79(7): p. 2972-2978.

46. D'Argenio, D. A. and Miller, S. I., *Cyclic di-GMP as a bacterial second messenger.* Microbiology, 2004. 150(Pt 8): p. 2497-502.

47. Jenal, U., *Cyclic di-guanosine-monophosphate comes of age: a novel secondary messenger involved in modulating cell surface structures in bacteria*. Curr Opin Microbiol, 2004. 7(2): p. 185-91.

48. Jenal, U. and Malone, J., *Mechanisms of cyclic-di-GMP signaling in bacteria.* Annu Rev Genet, 2006. 40: p. 385-407.

49. Aldridge, P., et al., *Role of the GGDEF regulator PleD in polar development of Caulobacter crescentus*. Mol Microbiol, 2003. 47(6): p. 1695-708.

50. Ryjenkov, D. A., et al., *Cyclic diguanylate is a ubiquitous signaling molecule in bacteria: insights into biochemistry of the GGDEF protein domain*. J Bacteriol, 2005. 187(5): p. 1792-8.

51. Schmidt, A. J., Ryjenkov, D. A. and Gomelsky, M., *The ubiquitous protein domain EAL is a cyclic diguanylate-specific phosphodiesterase: enzymatically active and inactive EAL domains*. J Bacteriol, 2005. 187(14): p. 4774-81.

52. Ryan, R. P., et al., *Cell-cell signaling in Xanthomonas campestris involves an HD-GYP domain protein that functions in cyclic di-GMP turnover.* Proc Natl Acad Sci U S A, 2006. 103(17): p. 6712-7.

53. Barraud, N., et al., *Nitric oxide signaling in Pseudomonas aeruginosa biofilms mediates phosphodiesterase activity, decreased cyclic di-GMP levels, and enhanced dispersal*. Journal of Bacteriology, 2009. 191(23): p. 7333-42.

54. Yukl, E. T., et al., *Nitric oxide dioxygenation reaction in DevS and the initial response to nitric oxide in Mycobacterium tuberculosis*. Biochemistry, 2011. 50(6): p. 1023-8.

55. Liu, N., Pak, T. and Boon, E. M., *Characterization of a diguanylate cyclase from Shewanella woodyi with cyclase and phosphodiesterase activities*. Mol Biosyst, 2010. 6(9): p. 1561-4.

56. Bradford, M. M., *A rapid and sensitive method for the quantitation of microgram quantities of protein utilizing the principle of protein-dye binding*. Anal Biochem, 1976. 72: p. 248-54.

57. Delaglio, F.e.a., *NMRPipe- A multidimensional spectral processing system based on UNIX pipes. Journal of Biomolecular NMR,* 1995. 6: p. 277-293.

58. Goddard, T. D. and Kneller, D. G., *SPARKY 3.* University of Calfornia, San Francisco.

59. Schuck, P., *Size-Distribution Analysis of Macromolecules by Sedimentation Velocity Ultracentrifugation and Lamm Equation Modeling*. Biophysical Journal, 2000. 78: p. 1606-1619.

60. Boon, E. M., et al., *Nitric oxide binding to prokaryotic homologs of the soluble guanylate cyclase beta1 H-NOX domain*. The Journal of biological chemistry, 2006. 281(31): p. 21892-902.

61. Cole, J. L., et al., *Analytical Ultracentrifugation: Sedimentation Velocity and Sedimentation Equilibrium*. Methods Cell Biology, 2008. 84: p. 143-179.

62. Chan, C., et al., *Structural basis of activity and allosteric control of diguanylate cyclase.* Proc Natl Acad Sci U S A, 2004. 101(49): p. 17084-9.

63. Upson, R. H. e.a., *A Spectrophotometric Method to Measure Enzymatic Activity in Reactions That Generate Inorganic Pyrophosphate*. Anal Biochem, 1996. 243(1): p. 41-45.

64. Carter, S. G. and D. W. Karl, *Inorganic phosphate assay with malachite green: An improvement and evaluation.* Journal of Biochemical and Biophysical Methods, 1982. 7(1): p. 7-13.

65. Mills, E., et al., *The bacterial second messenger c-di-GMP: mechanisms of signalling*. Cell Microbiol, 2011. 13(8): p. 1122-9.

66. Krasteva, P. V., Giglio, K. M. and Sondermann, H., *Sensing the messenger: the diverse ways that bacteria signal through c-di-GMP.* Protein science : a publication of the Protein Society, 2012. 21(7): p. 929-48.

67. McDougald, D., et al., *Should we stay or should we go: mechanisms and ecological consequences for biofilm dispersal*. Nature reviews. Microbiology, 2012. 10(1): p. 39-50.

68. Pellicena, P., et al., *Crystal structure of an oxygen-binding heme domain related to soluble guanylate cyclases.* Proceedings of the National Academy of Sciences of the United States of America, 2004. 101(35): p. 12854-9.

69. Olea, C., et al., *Probing the function of heme distortion in the H-NOX family.* ACS chemical biology, 2008. 3(11): p. 703-10.

70. Muralidharan, S. and Boon, E. M., *Heme flattening is sufficient for signal transduction in the H-NOX family.* Journal of the American Chemical Society, 2012. 134(4): p. 2044-6.

71. Ross, P., Weinhouse, H., Aloni, Y., Michaeli, D., Weinberger-ohana, P. mayer, R., Braun, S., de vroom, E., van der Marel, G. A., van Boom, J. H., and Benziman, M., *Regulation of cellulose synthesis in Acetobacter xylinum by cyclic diguanylic acid.* Nature, 1987. 325(6101): p. 279-281.

72. Sondermann, H., Shikuma, N. J. and Yildiz, F. H., *You've come a long way: c-di-GMP signaling.* Current opinion in microbiology, 2012. 15(2): p. 140-6.

73. Galperin, M. Y., *Diversity of structure and function of response regulator output domains.* Current opinion in microbiology, 2010. 13(2): p. 150-9.

74. Yang, C. Y., et al., *The structure and inhibition of a GGDEF diguanylate cyclase complexed with (c-di-GMP)(2) at the active site.* Acta crystallographica. Section D, Biological crystallography, 2011. 67(Pt 12): p. 997-1008.

75. Rao, F., et al., *Catalytic Mechanism of Cyclic Di-GMP-Specific Phosphodiesterase: a Study of the EAL Domain-Containing RocR from Pseudomonas aeruginosa*. Journal of Bacteriology, 2008. 190(10): p. 3622-3631.

76. Minasov, G., et al., *Crystal Structures of YkuI and Its Complex with Second Messenger Cyclic Di-GMP Suggest Catalytic Mechanism of Phosphodiester Bond Cleavage by EAL Domains*. Journal of Biological Chemistry, 2009. 284(19): p. 13174-13184.

77. Chen, M. W., et al., *Structural Insights into the Regulatory Mechanism of the Response Regulator RocR from Pseudomonas aeruginosa in Cyclic Di-GMP Signaling*. J Bacteriol, 2012. 194(18): p. 4837-46.

78. Vu, B., et al., *Bacterial extracellular polysaccharides involved in biofilm formation*. Molecules, 2009. 14(7): p. 2535-54.

79. Estrela, A. B. and Abraham, W.-R., *Combining Biofilm-Controlling Compounds and Antibiotics as a Promising New Way to Control Biofilm Infections*. Pharmaceuticals, 2010. 3(5): p. 1374-1393.

80. Monds, R. D. and O'Toole, G. A., *The developmental model of microbial biofilms: ten years of a paradigm up for review.* Trends in microbiology, 2009. 17(2): p. 73-87.

81. Kaplan, J. B., *Biofilm dispersal: mechanisms, clinical implications, and potential therapeutic uses.* Journal of dental research, 2010. 89(3): p. 205-18.

82. Fernandez-Pinar, R., et al., *Fatty acid-mediated signalling between two Pseudomonas species.* Environmental microbiology reports, 2012. 4(4): p. 417-23.

83. Toyofuku, M., H. Uchiyama, and N. Nomura, *Social Behaviours under Anaerobic Conditions in Pseudomonas aeruginosa.* International journal of microbiology, 2012. 2012: p. 405191.

84. Schreiber, F., et al., T*he role of nitric-oxide-synthase-derived nitric oxide in multicellular traits of Bacillus subtilis 3610: biofilm formation, swarming, and dispersal*. BMC microbiology, 2011. 11: p. 111.

85. Ryan, R. P. and Dow, J. M., *Communication with a growing family: diffusible signal factor (DSF) signaling in bacteria*. Trends in microbiology, 2011. 19(3): p. 145-52.

86. Deng, Y., et al., *Listening to a New Language- DSF-Based Quorum Sensing in Gram-Negative Bacteria*. Chemical Reviews, 2011(111): p. 160-173.

87. Dow, J. M., et al., *Biofilm dispersal in Xanthomonas campestris is controlled by cell-cell signaling and is required for full virulence to plants.* Proceedings of the National Academy of Sciences of the United States of America, 2003. 100(19): p. 10995-1000.

88. Davies, D. G. and Marques, C. N., *A fatty acid messenger is responsible for inducing dispersion in microbial biofilms.* Journal of Bacteriology, 2009. 191(5): p. 1393-403.

89. Jennings, J. A., Courtney, H. S. and Haggard, W. O., *Cis-2-decenoic acid inhibits S. aureus growth and biofilm in vitro: a pilot study.* Clinical orthopaedics and related research, 2012. 470(10): p. 2663-70.

90. Deng, Y., et al., *Cis-2-dodecenoic acid receptor RpfR links quorum-sensing signal perception with regulation of virulence through cyclic dimeric guanosine monophosphate turnover*. Proceedings of the National Academy of Sciences of the United States of America, 2012. 109(38): p. 15479-84.

91. de la Fuente-Nunez, C., Reffuveille, F., Fairfull-Smith, K. E., and Hancock, R. E. W., *Effect of Nitroxides on Swarming Motility and Biofilm Formation, Multicellular Behaviors in*

Pseudomonas aeruginosa. Antimicrobial agents and chemotherapy, 2013. 57(10): p. 4877-4881.

92. Park, J.W., J. C., *Reactions of nitric oxide and nitrogen dioxide with functionalised alkenes and dienes.* Journal of Chemical Society, 1997(Perkin Transactions): p. 2579-2583.

93. Geisler, A. C. and Rudolph, T. K., *Nitroalkylation--a redox sensitive signaling pathway.* Biochimica et Biophysica Acta, 2012. 1820(6): p. 777-84.

94. Rudolph, V., et al., *Nitro-fatty acid metabolome: saturation, desaturation, beta-oxidation, and protein adduction*. The Journal of biological chemistry, 2009. 284(3): p. 1461-73.

95. Pratt, L. A. and Kolter, R., *Genetic analysis of Escherichia coli biofilm formation- roles of flagella, motility, chemotaxis and type I pili*. Molecular Microbiology, 1998. 30(2): p. 285-293.

96. Liang, Y., et al., *Pellicle formation in Shewanella oneidensis.* BMC microbiology, 2010. 10: p. 291.

97. Friedman, L. and Kolter, R., *Genes involved in matrix formation in Pseudomonas aeruginosa PA14 biofilms.* Molecular Microbiology, 2003. 51(3): p. 675-690.

98. Kobayashi, K., *Bacillus subtilis pellicle formation proceeds through genetically defined morphological changes*. Journal of Bacteriology, 2007. 189(13): p. 4920-31.

99. Armitano, J., Mejean, V. and Jourlin-Castelli, C., *Aerotaxis governs floating biofilm formation in Shewanella oneidensis.* Environmental Microbiology, 2013.

100. Twomey, K. B., et al., *Bacterial cis-2-unsaturated fatty acids found in the cystic fibrosis airway modulate virulence and persistence of Pseudomonas aeruginosa.* The ISME journal, 2012. 6(5): p. 939-50.

101. van Ditmarsch, D., et al., *Convergent evolution of hyperswarming leads to impaired biofilm formation in pathogenic bacteria*. Cell reports, 2013. 4(4): p. 697-708.

102. de la Fuente-Nunez, C., et al., *Inhibition of bacterial biofilm formation and swarming motility by a small synthetic cationic peptide.* Antimicrobial agents and chemotherapy, 2012. 56(5): p. 2696-704.

103. Kostakioti, M., Hadjifrangiskou, M. and Hultgren, S. J., *Bacterial biofilms: development, dispersal, and therapeutic strategies in the dawn of the postantibiotic era.* Cold Spring Harbor perspectives in medicine, 2013. 3(4): p. a010306.

104. Guinier, A. F., G., *Small angle scattering of X-rays.* Journal of Polymer Science, 1955. 19(93): p. 594.

105. Lipfert, J.D., S., *Small-Angle X-Ray Scattering from RNA, Proteins, and Protein Complexes.* Annual Review of Biophysics and Biomolecular Structure, 2007. 36: p. 307-327.

106. Blanchet, C.E., D. I., *Small-Angle X-Ray Scattering on Biological Macromolecules and Nanocomposites in Solution.* Annual Review of Physcial Chemistry, 2013. 64: p. 37-54.

107. Kelly, S. M., Jess, T. J. and Price, N. C., *How to study proteins by circular dichroism.* Biochimica et Biophysica Acta, 2005. 1751(2): p. 119-39.

108. Greenfield, N. J., *Using circular dichroism spectra to estimate protein secondary structure.* Nature Protocols, 2007. 1: p. 2876-2890.

109. Kelly, S.M., N. C., *The application of circular dichroism to studies of protein folding and unfolding.* Biochimica et Biophysica Acta, 1997. 1338: p. 161-185.

110. Freyer, M. W. and Lewis, E. A., I*sothermal Titration Calorimetry: Experimental Design, Data Analysis, and Probing Macromolecule/Ligand Binding and Kinetic Interactions*. 2008. 84: p. 79-113.

111. Liang, Y., *Applications of isothermal titration calorimetry in protein science.* Acta Biochimica Et Biophysica Sinica, 2008. 40(7): p. 565-576.

112. Pierce, M. M., Raman, C. S. and Nall, B. T., *Isothermal Titration Calorimetry of Protein–Protein Interactions.* Methods, 1999. 19: p. 213-221.

113. Qi, Y., et al., *Binding of cyclic diguanylate in the non-catalytic EAL domain of FimX induces a long-range conformational change*. The Journal of biological chemistry, 2011. 286(4): p. 2910-7.